Technische Universität München

Fakultät für Medizin

Institut für Diagnostische und Interventionelle Neuroradiologie

Quantitative Magnetic Resonance Imaging and Spectroscopy of Vertebral Bone Marrow: Addressing Confounding Effects in the Measurement of Fat Fraction and Apparent Diffusion Coefficient

Michael Dieckmeyer

Vollständiger Abdruck der von der Fakultät für Medizin der Technischen Universität München zur Erlangung des akademischen Grades eines

Doktors der Medizinischen Wissenschaft (Dr. med. sci.)

genehmigten Dissertation.

Vorsitzender:	Prof. Dr. Ernst J. Rummeny
Prüfer der Dissertation:	1. Priv.-Doz. Dr. Thomas Baum
	2. Priv.-Doz. Dimitrios C. Karampinos, Ph.D.
	3. apl. Prof. Dr. Jan S. Kirschke

Die Dissertation wurde am 21.03.2019 bei der Technischen Universität München eingereicht und durch die Fakultät für Medizin am 14.08.2019 angenommen.

Abstract

Bone marrow is a tissue mainly comprising of three macroscopic components: water, fat and trabecular bone. All three components play important physiologic and pathophysiologic roles, some already well-established and others topic of current research. As of today a significant number of medical conditions of the musculoskeletal system, e.g. osteoporosis, and the metabolic system, e.g. metabolic syndrome, are still insufficiently understood. On the one hand, this hampers their accurate diagnosis and, on the other hand, is a missing prerequisite for effective treatment and prevention strategies. Magnetic resonance (MR) represents a diagnostic tool to non-invasively measure biomarkers of bone marrow, such as proton density fat fraction (PDFF) and apparent diffusion coefficient (ADC). Therefore, the advancement of quantification of MR-based bone marrow parameters can be an important step en route to a deeper understanding of the underlying mechanisms of bone marrow physiology in health and disease as well as contribute to the improvement of diagnostic performance, treatment and prevention of mentioned medical conditions.

Magnetic resonance imaging (MRI) is a biomedical imaging modality highly valued for its ability to produce excellent soft tissue contrast as well as the absence of considerable adverse effects as it is not relying on ionizing radiation. It is capable of generating images with high spatial resolution. In contrast, single-voxel magnetic resonance spectroscopy (MRS) acquires data only from a single predefined volume in favor of high spectral resolution enabling a more precise analysis of the individual signal components.

The present cumulative thesis is based upon two journal publications within the field of quantitative MR of vertebral bone marrow. It addresses confounding factors in the measurement of (i) MRS-based PDFF, with an emphasis on correction of T_2 decay effects, and (ii) diffusion weighted imaging (DWI)-based ADC, correcting the biasing effect of unsuppressed fat signal.

The first journal publication describes a data acquisition and postprocessing method to quantify vertebral bone marrow fat using single-voxel multiple echo time (multi-TE) MRS. Two confounding factors were addressed: the superposition of water-fat peaks and the difference in T_2 relaxation time between water and fat components. The purpose of this work was twofold. Firstly, it was aimed to correct the effects of both confounding factors for quantification of the PDFF. Secondly, investigate the implications of the implemented correction method in the context of PDFF age dependence. It was demonstrated that T_2-weighted fat fraction significantly overestimates fat content and exaggerates its age dependence in comparison to PDFF. The findings suggest that, wherever possible,

PDFF should be the parameter of choice when it comes to bone marrow fat quantification using single-voxel MRS.

The ADC of water can be quantified using DWI. In order that the measured quantity purely represents the ADC of the water component fat suppression is applied. However, spectrally selective suppression techniques do not suppress all fat signal components perfectly. The purpose of the second journal publication was to remove the confounding effect of unsuppressed fat on ADC quantification. The developed method using additional quantitative MRI measurements was compared and validated against diffusion-weighted MRS (DW-MRS). A good agreement of vertebral bone marrow water ADC as a result of DWI-based and DW-MRS-based quantification strategies could be demonstrated.

The developed methods described in the two publications were and are being applied in clinical studies and ongoing research within the fields of bone marrow physiology, osteoporosis, metabolic studies and treatment monitoring.

List of Incuded Journal Publications

Te present dissertation is based on the following two journal publications:

[JP-I] **M. Dieckmeyer**, S. Ruschke, H. Eggers, H. Kooijman, E. J. Rummeny, J. S. Kirschke, T. Baum, and D. C. Karampinos. "ADC Quantification of the Vertebral Bone Marrow Water Component: Removing the Confounding Effect of Residual Fat". In: *Magn Reson Med (**Editor's Pick**)* 78.4 (Oct. 2017), pp. 1432–1441.

[JP-II] **M. Dieckmeyer**, S. Ruschke, C. Cordes, S. P. Yap, H. Kooijman, H. Hauner, E. J. Rummeny, J. S. Bauer, T. Baum, and D. C. Karampinos. "The need for T_2 correction on MRS-based vertebral bone marrow fat quantification: implications for bone marrow fat fraction age dependence". In: *NMR Biomed* 28.4 (Apr. 2015), pp. 432–439.

The above two journal publications are referred to as JP-I and JP-II, respectively.
Please refer to section 8 for a summary of the two journal publications.

List of Related Publications

I contributed also to the following subject-related journal publications (ordered by year of appearance):

[J1] T. Baum, A. Rohrmeier, J. Syvari, M. N. Diefenbach, D. Franz, **M. Dieckmeyer**, A. Scharr, H. Hauner, S. Ruschke, J. S. Kirschke, and D. C. Karampinos. "Anatomical Variation of Age-Related Changes in Vertebral Bone Marrow Composition Using Chemical Shift Encoding-Based Water-Fat Magnetic Resonance Imaging". In: *Front Endocrinol (Lausanne)* 9 (2018), p. 141.

[J2] D. C. Karampinos, S. Ruschke, **M. Dieckmeyer**, M. Diefenbach, D. Franz, A. S. Gersing, R. Krug, and T. Baum. "Quantitative MRI and spectroscopy of bone marrow". In: *J Magn Reson Imaging* (June 2017).

[J3] C. Cordes, T. Baum, **M. Dieckmeyer**, S. Ruschke, M. N. Diefenbach, H. Hauner, J. S. Kirschke, and D. C. Karampinos. "MR-Based Assessment of Bone Marrow Fat in Osteoporosis, Diabetes, and Obesity". In: *Front Endocrinol (Lausanne)* 7 (2016), p. 74.

[J4] T. Baum, S. Inhuber, **M. Dieckmeyer**, C. Cordes, S. Ruschke, E. Klupp, P. M. Jungmann, R. Farlock, H. Eggers, H. Kooijman, E. J. Rummeny, A. Schwirtz, J. S. Kirschke, and D. C. Karampinos. "Association of Quadriceps Muscle Fat With Isometric Strength Measurements in Healthy Males Using Chemical Shift Encoding-Based Water-Fat Magnetic Resonance Imaging". In: *J Comput Assist Tomogr* 40.3 (2016), pp. 447–451.

[J5] T. Baum, C. Cordes, **M. Dieckmeyer**, S. Ruschke, D. Franz, H. Hauner, J. S. Kirschke, and D. C. Karampinos. "MR-based assessment of body fat distribution and characteristics". In: *Eur J Radiol* 85.8 (Aug. 2016), pp. 1512–1518.

[J6] D. C. Karampinos, S. Ruschke, **M. Dieckmeyer**, H. Eggers, H. Kooijman, E. J. Rummeny, J. S. Bauer, and T. Baum. "Modeling of T2* decay in vertebral bone marrow fat quantification". In: *NMR Biomed* 28.11 (Nov. 2015), pp. 1535–1542.

[J7] C. Cordes, **M. Dieckmeyer**, B. Ott, J. Shen, S. Ruschke, M. Settles, C. Eichhorn, J. S. Bauer, H. Kooijman, E. J. Rummeny, T. Skurk, T. Baum, H. Hauner, and D. C. Karampinos. "MR-detected changes in liver fat, abdominal fat, and vertebral bone marrow fat after a four-week calorie restriction in obese women". In: *J Magn Reson Imaging* 42.5 (Nov. 2015), pp. 1272–1280.

[J8] T. Baum, S. P. Yap, **M. Dieckmeyer**, S. Ruschke, H. Eggers, H. Kooijman, E. J. Rummeny, J. S. Bauer, and D. C. Karampinos. "Assessment of whole spine vertebral bone marrow fat using chemical shift-encoding based water-fat MRI". In: *J Magn Reson Imaging* 42.4 (Oct. 2015), pp. 1018–1023.

I contributed also to the following subject-related conference abstracts (ordered by year of appearance):

[C1] **M. Dieckmeyer**, S. Ruschke, C. Cordes, S. P. Yap, H. Kooijman, H. Hauner, E. J. Rummeny, J. S. Bauer, T. Baum, and D. C. Karampinos. "MRS-Based Vertebral Bone Marrow Fat Quantification Using Prior Fat Spectrum Characterization and T2 Correction". In: *Proc. of the 23rd Scientific Meeting of ISMRM* (May 30–June 5, 2015). (oral presentation, ISMRM Merit Award ***magna cum laude***). Toronto, Canada, 2015, p. 0939.

[C2] **M. Dieckmeyer**, S. Ruschke, H. Eggers, H. Kooijman, H. Kooijman, E. J. Rummeny, J. S. Bauer, T. Baum, and D. C. Karampinos. "Removing the Confounding Effect of the Fat Component in ADC Quantification of the Vertebral Bone Marrow Water Component". In: *Proc. of the 23rd Scientific Meeting of ISMRM* (May 30–June 5, 2015). (oral presentation, ISMRM Merit Award ***magna cum laude***). Toronto, Canada, 2015, p. 0314.

[C3] S. Ruschke, **M. Dieckmeyer**, H. Kooijman, A. Haase, E. J. Rummeny, J. S. Bauer, T. Baum, and D. C. Karampinos. "Separating Water and Olefinic Fat Peaks Using Diffusion-Weighted MRS and Diffusion Constraint Fitting to Measure Vertebral Bone Marrow Fat Unsaturation". In: *Proc. of the 23rd Scientific Meeting of ISMRM* (May 30–June 5, 2015). (oral presentation, ISMRM Merit Award ***magna cum laude***). Toronto, Canada, 2015, p. 0618.

[C4] C. Cordes, **M. Dieckmeyer**, B. Ott, J. Shen, S. Ruschke, M. Settles, C. Eichhorn, J. S. Bauer, H. Kooijman, E. J. Rummeny, T. Skurk, T. Baum, H. Hauner, and D. C. Karampinos. "Bone Marrow Fat Behaves Differently from Abdominal Fat, Liver Fat and Serum Lipids After a Four-Week Calorie Restriction in Obese Women". In: *Proc. of the 23rd Scientific Meeting of ISMRM* (May 30–June 5, 2015). (electronic poster). Toronto, Canada, 2015, p. 4117.

[C5] D. C. Karampinos, S. Ruschke, **M. Dieckmeyer**, H. Eggers, H. Kooijman, E. J. Rummeny, J. S. Bauer, and T. Baum. "Comparison of T2* Correction Methods for Vertebral Bone Marrow Fat Quantification Using Chemical Shift Encoding-Based Water-Fat Imaging". In: *Proc. of the 23rd Scientific Meeting of ISMRM* (May 30–June 5, 2015). (oral presentation). Toronto, Canada, 2015, p. 0338.

[C6] T. Baum, S. P. Yap, **M. Dieckmeyer**, S. Ruschke, H. Eggers, H. Kooijman, E. J. Rummeny, J. S. Bauer, and D. C. Karampinos. "Whole Spine Vertebral Bone Marrow Proton Density Fat Fraction Mapping: Anatomical Variation and Gender-Specific Reference Database". In: *Proc. of the 23rd Scientific Meeting of ISMRM* (May 30–June 5, 2015). (traditional poster). Toronto, Canada, 2015, p. 1216.

[C7] **M. Dieckmeyer**, S. Ruschke, H. Kooijman, E. J. Rummeny, J. S. Kirschke, T. Baum, and D. C. Karampinos. "Comparison of Vertebral Bone Marrow Water ADC Between Young and Old Subjects: DW-MRS Versus DWI". In: *Proc. of the 24th Scientific Meeting of ISMRM* (May 7–13, 2016). (electronic poster). Singapore, Singapore, 2016, p. 4463.

[C8] T. Baum, S. Inhuber, **M. Dieckmeyer**, C. Cordes, S. Ruschke, E. Klupp, H. Eggers, H. Kooijman, E. J. Rummeny, A. Schwirtz, J. S. Kirschke, and D. C. Karampinos. "Association of Quadriceps Muscle Fat with Isometric Strength Measurements in Healthy Males Using Chemical Shift Encoding-Based Water-Fat MRI". In: *Proc. of the 24th Scientific Meeting of ISMRM* (May 7–13, 2016). (oral presentation). Singapore, Singapore, 2016, p. 0759.

[C9] C. Cordes, T. Baum, J. Clavel, S. Ruschke, **M. Dieckmeyer**, D. Franz, H. Kooijman, E. J. Rummeny, H. Hauner, and D. C. Karampinos. "Subcutaneous Fat Unsaturation Is Negatively Associated with Liver Fat Fraction". In: *Proc. of the 24th Scientific Meeting of ISMRM* (May 7–13, 2016). (electronic poster). Singapore, Singapore, 2016, p. 3913.

[C10] F. Freitag, T. Baum, **M. Dieckmeyer**, J. S. Kirschke, H. Eggers, C. Buerger, C. Lorenz, and D. C. Karampinos. "Automated Assessment of Paraspinal Muscles Fat Composition Based on the Segmentation of Chemical Shift Encoding-Based Water/fat-Separated Images". In: *Proc. of the 25th Scientific Meeting of ISMRM* (Apr. 22–27, 2017). (electronic poster). Honolulu, Hawaii, USA, 2017, p. 4994.

[C11] T. Baum, A. Rohrmeier, J. Syväri, M. Diefenbach, D. Franz, **M. Dieckmeyer**, A. Scharr, H. Hauner, S. Ruschke, J. Kirschke, and D. C. Karampinos. "Anatomical variation of age-related changes in vertebral bone marrow composition using chemical shift encoding-based water-fat MRI". In: *Proc. of the 26th Scientific Meeting of ISMRM* (June 16–21, 2018). (oral presentation). Paris, France, 2018, p. 1243.

[C12] T. Baum, S. Schlaeger, S. Inhuber, F. Kreuzpointer, **M. Dieckmeyer**, F. Freitag, E. Klupp, B. Cervantes, A. Schwirtz, J. Kirschke, and D. C. Karampinos. "Association of thigh muscle fat infiltration with isometric strength measurements based on chemical shift encoding-based water–fat MRI". In: *Proc. of the 26th Scientific Meeting of ISMRM* (June 16–21, 2018). (electronic poster). Paris, France, 2018, p. 5080.

[C13] J. Syväri, S. Ruschke, **M. Dieckmeyer**, D. Franz, H. Hauner, J. Kirschke, T. Baum, and D. C. Karampinos. "Estimating vertebral bone marrow triglyceride unsaturation based on the extraction of the olefinic peak in short-TE STEAM MRS using a constrained fitting model". In: *Proc. of the 26th Scientific Meeting of ISMRM* (June 16–21, 2018). (electronic poster). Paris, France, 2018, p. 5162.

[C14] E. Klupp, B. Cervantes, S. Schlaeger, S. Inhuber, F. Kreuzpointer, **M. Dieckmeyer**, F. Freitag, E. Rummeny, C. Zimmer, J. Kirschke, D. C. Karampinos, and T. Baum. "Relationship of paraspinal muscle DTI metrics to isometric strength measurements". In: *Proc. of the 26th Scientific Meeting of ISMRM* (June 16–21, 2018). (power pitch). Paris, France, 2018, p. 0329.

[C15] J. Syväri, S. Ruschke, **M. Dieckmeyer**, D. Franz, H. Hauner, J. Kirschke, T. Baum, and D. C. Karampinos. "Sex dependence of age-related vertebral bone marrow PDFF and T2 relaxation time changes in a cohort of nearly 200 subjects using multi-TE single-voxel MR spectroscopy". In: *Proc. of the 26th Scientific Meeting of ISMRM* (June 16–21, 2018). (electronic poster). Paris, France, 2018, p. 5163.

[C16] **M. Dieckmeyer**, S. Ruschke, D. Anitha, J. Kirschke, D. C. Karampinos, S. Karupppasamy, and T. Baum. "What is the role of MRS-based bone marrow fatty acid unsaturation level compared to fat fraction in predicting vertebral bone strength?" In: *Proc. of the 26th Scientific Meeting of ISMRM* (June 16–21, 2018). (electronic poster). Paris, France, 2018, p. 5164.

Contents

1 Introduction

Nuclear magnetic resonance (NMR) was first described by Rabi in 1938 [1]. Since then, a lot of theoretical and technical advancements were made, including remarkable contributions from Bloch, Purcell, Mansfield and Lauterbur among others, in order to exploit this phenomenon for imaging the human body. Magnetic resonance imaging (MRI) nowadays is considered the most versatile imaging modality offering a wide range of contrast mechanisms and parameter choices that enable its application in almost all body parts and tissues. In clinical applications, the MR signal usually originates from ^{1}H nuclei, or protons, that are either bound in water or fat molecules. The different molecular environments of the bound protons give rise to a difference in resonant frequencies of water and fat components, also expressed as chemical shift. The microscopic surroundings of the protons together with the tissue architecture and microanatomy are also responsible for characteristic relaxation times T_1 and T_2 and diffusion properties.

In contrast to MRI, magnetic resonance spectroscopy (MRS) acquires and averages the signal of a localized region with high spectral resolution. Therefore it enables a more detailed data analysis in the chemical shift dimension. However, the application is limited to body regions that offer a sufficiently large volume of homogeneous tissue.

Particularly interesting for research applications is quantitative MRI and MRS allowing the in-vivo measurement of tissue-specific parameters, such as T_1 and T_2, proton density fat fraction (PDFF) and apparent diffusion coefficient (ADC).

Bone marrow is an important organ of the human organism since it fulfills essential functions. It is the main hematopoietic organ, plays an important role in the pathomechanism of several medical conditions, for example osteoporosis and multiple myeloma, and is affected by such medical conditions or their treatment, such as in bone fractures, metabolic syndrome, anorexia nervosa or radio- and chemotherapy.

However, quantitative measurements in vertebral bone marrow are complicated by the tissue anatomy and composition. As suggested above the difference in relaxation times and ADC between the water and fat component can be significant biasing quantitative measurements if not taken into account correctly. Particularly in ADC quantification of the water component, the presence of an incompletely suppressible fat component represents a significant confounding factor. Therefore, in order to achieve robust and accurate quantification these effects have to be addressed.

1.1 Scientific and Clinical Relevance

Over the last decade, evidence has been growing that the clinical relevance of bone marrow goes way beyond hematological diseases like multiple myeloma. Arguably the most evidence for bone marrow as a key pathogenetic factor has been found in osteoporosis, a disease exhibiting increased bone loss. Apart from the close anatomical relationship between bone and bone marrow, there is also an important functional relationship between these two tissues. In this regard, mesenchymal stem cells found in bone marrow are a key player. Depending on biological, chemical and physical factors and regulated through complex signaling pathways, these progenitor cells can differentiate into osteoblasts or adipocytes. The dysregulation of the differentiation of bone marrow stem cells thus contributes to the pathogenesis of both bone diseases and metabolic diseases, like metabolic syndrome and anorexia nervosa. Furthermore, the predominant occurence of bone metastases in the axial skeleton suggests that bone marrow, in particular hematopoietically active red marrow, plays a crucial role in metastatic bone disease by increasing the susceptibility for the adhesion of malignant cells.

Osteoporosis is a medical condition predominantly found in postmenopausal aging women characterized by demineralization and structural deterioration of the bone leading to an increased fracture risk [2]. Most common locations of osteoporotic fractures are the vertebral bodies and the proximal femur. Apart from a decreased quality of life and increased mortality [3], osteoporosis, in particular osteoporotic fractures, are associated with an enormous socioeconomic burden. Problems that are expected to increase in the future due to the global demographic development [4]. Prevention of fractures is one of the key aspects in osteoporosis treatment making the early diagnosis very important. However, the current diagnostic gold standard, dual energy X-ray absorptiometry (DEXA)-based bone mineral density (BMD) measurement, suffers from limited precision in the prediction of fracture risk [5, 6, 7] that can lead to overtreatment or undertreatment and increased health care costs. Overtreatment implies unnecessary adverse drug effects while undertreatment of osteoporosis entails preventible fractures and associated complications. Numerous studies demonstrated an increased vertebral bone marrow fat fraction in osteoporotic subjects measured by quantitative MRI [8] and MRS [9, 10, 11, 12]. More recently, vertebral fat fraction has also been shown to be negatively associated with prevalent vertebral fractures [13] and failure load [14], respectively. Interestingly, MRS-based measurements of vertebral bone marrow fat composition were shown to be associated with prevalent fractures as well [15]. Bone marrow diffusion properties have been shown to be altered in osteoporosis [16, 17], although with less evidence so far.

Metabolic syndrome is a medical condition characterized by abdominal obesity, hypertension, dyslipidemia and insulin resistance [18, 19, 20], the latter commonly resulting in type 2 diabetes mellitus. It has a rapidly growing prevalence in the industrial nations and is a major risk factor for cardiovascular disease [21] and kidney disease, among other medical conditions, contributing substantially to all-cause mortality. Triglyceride stor-

age, lipid deposition and fatty degeneration of tissue are known to play an important role in metabolic syndrome [22]. This predominantly involves visceral adipose tissue (VAT) [23, 24], but also subcutaneous adipose tissue (SAT) [25] as well as intramuscular fat [26] and intrahepatic fat [27, 28]. In recent years there has also been growing evidence for a relationship between metabolic syndrome and vertebral bone marrow [29, 30].

Paradoxically, there has been shown an increased vertebral bone marrow fat fraction in women suffering from anorexia nervosa [31].

Vertebral fractures can be caused by malignant disease, most commonly in the form of bone metastases. The differentiation between benign and malignant fractures is of high clinical importance because it can imply completely different treatments. Sensitivity and specificity of fracture classification may be increased by the use of quantitative MR-based biomarkers and thus assist in making the right treatment decisions. In particular, PDFF [32, 33] and ADC [16, 34] of vertebral bone marrow have been reported to have the highest potential for this application.

Multiple myeloma is a malignant disease, more precisely a B-cell non-Hodgkin lymphoma, characterized by a monoclonal proliferation of plasma cells in the bone marrow. While morphological MRI is the most sensitive imaging modality for the early detection of bone marrow infiltration [35] the application of quantitative MRI can have additional value. ADC is associated with bone marrow cellularity and may therefore serve as a treatment response parameter [36, 37, 38] as well as increase the sensitivity of bone marrow infiltration [39].

Quantitative MRI of vertebral bone marrow can serve various purposes. Its ability of in-vivo measurements of tissue-specific properties in a non-invasive manner is almost unique. Thereby it may help to advance the understanding of the complex pathophysiology in multifactorial diseases like osteoporosis, metabolic syndrome and multiple myeloma. Furthermore, it may improve diagnostic accuracy in the prediction and differentiation of vertebral fractures. This underlines the scientific and clinical relevance to refine the utilized quantification methodology.

1.2 Thesis Purpose

The overall purpose of the present dissertation was twofold. Firstly, the development and refinement of MRI- and MRS-based methods to improve the accuracy of the quantification of the tissue-specific parameters PDFF and ADC in vertebral bone marrow. This was realized by implementing more complex quantification models in order to take into account the considerable differences between bone marrow water and fat with respect to relaxation times and diffusion properties. Secondly, the developed methods were applied in in-vivo studies, compared to existing quantification methods and analyzed in terms of feasibility, robustness and systematic bias.

1.3 Thesis Structure

In the present cumulative dissertation, the technical and clinical background of the two embedded journal publications and the corresponding methodology is described. Furthermore, it intends to give an overview of the existing literature and discuss the findings of the publications in this context.

Chapter 2 briefly recapitulates the most important aspects of MR physics while section 3 focuses on MR hardware. A short overview of the relevant magnetic resonance spectroscopy techniques is provided in chapter 4 followed by the most important aspects of MR-based fat quantification in chapter 5. Fundamentals of bone marrow anatomy and physiology are presented in chapter 6. The two embedded journal publication are summarized in chapter 8. At the end, a review of the current literature as well as a comprehensive discussion of the present work are given in chapter 9.

2 Magnetic Resonance in Medicine

This chapter contains an overview of the physical and technical basics of magnetic resonance in medicine in general as well as used in the present thesis.

2.1 MR Physics

The in-vivo visualization of the human body ranks among the most fascinating capabilities of modern-day medicine. It all starts with the phenomenon of nuclear magnetic resonance (NMR) in which nuclei in a constant magnetic field absorb and re-emit electromagnetic radiation. In medicine, the nucleus of interest is the one of the hydrogen atom (^{1}H), because of its abundance in the human body. The ^{1}H nucleus is a single positively charged proton spinning on its own axis and thus representing a constantly moving charge generating its own magnetic field, known as its magnetic moment.

2.1.1 Nuclear Magnetic Resonance

To explain NMR in detail, especially on the atomic scale, quantum mechanics is needed. However, magnetic resonance in medicine involves large numbers of nuclei, also referred to as spin ensembles, so that the classical mechanical description is considered sufficient in the context of the present work. From particle physics we know that every proton has an intrinsic angular moment, called spin. Analogously, a spin ensemble has an intrinsic angular moment A. The relation between the induced magnetic moment M and A is described by the gyromagnetic ratio gamma:

$$M = \gamma A. \tag{2.1.1}$$

In the case of ^{1}H nuclei $\gamma/(2\pi) = 42.58$ MHz T^{-1}. In the presence of an external magnetic field B the magnetic moment M experiences a torque τ,

$$\tau = M \times B = \frac{dA}{dt}, \tag{2.1.2}$$

which makes it precess around the direction of B. The frequency ω of this precession is proportional to the external magnetic field B_0 and given by the Larmor equation

$$\omega_0 = -\gamma B_0. \tag{2.1.3}$$

This represents one of the most important relationships in magnetic resonance imaging. For ^{1}H nuclei at a field strength of 3 T, $\omega = 42.58$ MHz T^{-1} $\cdot$ 3T $= 127.74$ MHz.

2.1.2 Measuring the Magnetic Moment

Since the net magnetization M_0 in the body is very small (in the order of 1 μT) compared to the main magnetic field B_0 (e.g. 3 T), it is impossible to measure it while being parallel to B_0. However, by tipping it away from the z-direction, M_0 can be measured using a detector which is only sensitive to magnetic fields in the x-y-plane, also referred to as the transverse plane. To flip M_0 away from the z-direction, an RF pulse, also referred to as the B_1 field, oscillating at the Larmor frequency ω_0, is used. An RF pulse that tips M_0 exactly into the x-y-plane is called a 90° pulse. Right after being tipped into the x-y-plane all spins are in phase coherence. Now the receiver coil can measure the voltage induced by M_0 precessing in the transverse plane. This signal is called free induction decay (FID) and its amplitude decays rapidly because of the dephasing of the protons. In clinical MR imaging, echoes are used rather than measuring the FID directly.

2.1.3 Relaxation

There are two types of relaxation mechanisms to explain the process of a spin ensemble, represented by the magnetization vector M, transitioning from a non-equilibrium state to an equilibrium state:

- T_1 relaxation, also referred to as longitudinal relaxation or spin-lattice relaxation, describes the mechanism of the longitudinal component of the magnetization exponentially recovering towards thermodynamic equilibrium with its surroundings. It is characterized by the relaxation time T_1 or relaxation rate $R_1 = T_1^{-1}$. Assuming that the magnetization vector is in the x-y-plane at $t = 0$, the longitudinal component of the magnetization can be described as

$$M_z(t) = M_0(1 - e^{-\frac{t}{T_1}}). \tag{2.1.4}$$

- T_2 relaxation, also referred to as transverse relaxation or spin-spin relaxation, describes the mechanism of the transverse component of the magnetization exponentially decaying to equilibrium. It is characterized by the relaxation time T_2 or relaxation rate $R_2 = T_2^{-1}$,

$$M_{xy}(t) = M_{xy}(0)e^{-\frac{t}{T_2}}. \tag{2.1.5}$$

In effectively any MR experiment, spins in the x-y-plane are exposed to magnetic field inhomogeneities as well as spin-spin interactions causing them to dephase. To describe the signal loss caused by this dephasing the composite time constant T_2^* or relaxation rate R_2^*, respectively, is used: $T_2^{*-1} = T_2^{-1} + T_2'^{-1}$. By definition, T_2^* is always shorter or equal to T_2. In practice, the most important characteristic distinguishing T_2' from T_2 is that the signal loss described by T_2' relaxation, and hence caused by magnetic

field inhomogeneities, is recoverable while signal loss caused by T_2 relaxation is non-recoverable.

2.1.4 Chemical Shift

Due to different chemical environments the same nucleus, usually ^{1}H in clinical imaging, can have different resonant frequencies. That phenomenon is caused by the shielding effect of surrounding electrons resulting in a slightly lower static magnetic field experienced by a certain nucleus. This implies that the resonant frequency of a nucleus contains information about the chemical structure it is bound in. The chemical shift of a nucleus is given relative to the reference resonant frequency of the ^{1}H nuclei in tetramethylsilane (TMS) in the unit parts per million (ppm). It is defined as

$$\delta_{ppm} = \frac{f - f_{\mathrm{TMS}}}{f_{\mathrm{TMS}}} 10^6. \tag{2.1.6}$$

The chemical shifts of ^{1}H nuclei bound in water molecules and methylene environments of triglycerides, which account for the main part of the fat signal, are 4.67 ppm and 1.3 ppm, respectively. The difference in resonant frequencies resulting from chemical shift differences is proportional to the field strength of the main magnetic field. Thus higher field strength results in higher spectral dispersion.

2.2 From Echoes to Images

There are two major types of echoes used in MRI, spin echo (SE) and gradient echo (GE).

2.2.1 Spin echo

A SE sequence (Fig. 2.1) is initiated by a 90° RF pulse tipping the magnetization into the x-y-plane. Due to B_0 inhomogeneities and differences in tissue susceptibilities the spins start to dephase. After a certain time TE/2 a 180° RF pulse, also referred to as refocusing pulse, is applied, reversing the phase angles of the spins. After the same time TE/2 experiencing the same field inhomogeneities as before the spins meet at the same direction in the x-y-plane and are rephased again generating an echo. Due to the phase reversal dephasing caused by B_0 inhomogeneities and differences in tissue susceptibilities can be completely recovered and the signal amplitude of the spin echo depends only on transverse relaxation and diffusion. When no diffusion sensitization is introduced into the sequence the effect of diffusion on the signal is relatively small compared to the effect of transverse relaxation. The spin echo signal can thus be simplified as

$$S_{\mathrm{SE}} = S_0 e^{-\frac{TE}{T_2}}. \tag{2.2.1}$$

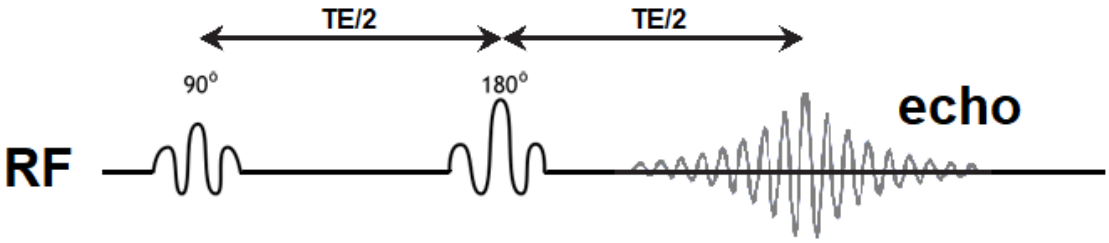

Figure 2.1: Spin echo sequence.

2.2.2 Gradient echo

A GE sequence (Fig. 2.2) starts with an initial small flip angle (f.e. 3°) RF pulse immediately followed by a magnetic field gradient causing rapid dephasing of the transverse magnetization. Thereafter a gradient of opposite polarity is applied reversing the dephasing effect of the first gradient and causing the spins to rephase again generating an echo. The second gradient compensates only for dephasing caused by the first dephasing gradient. Dephasing caused by B_0 inhomogeneities does not get recovered. Therefore, the amplitude of the echo signal, i.e. the envelope of the FID curve, is determined by T_2^*.

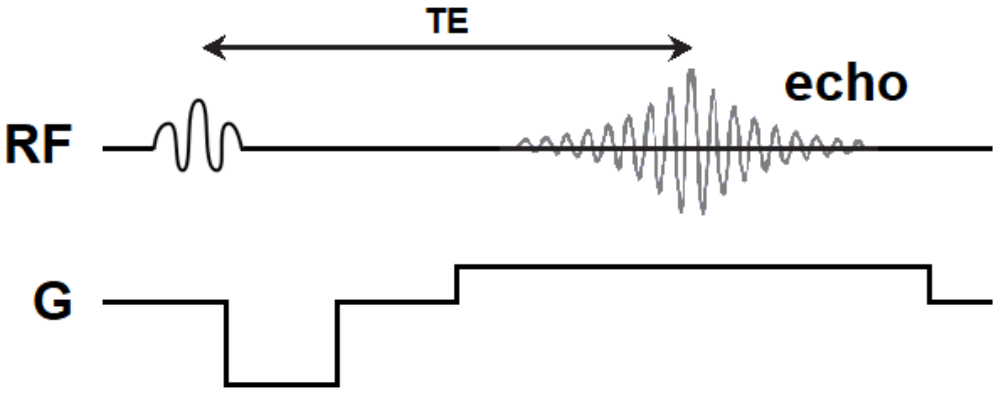

Figure 2.2: Gradient echo sequence.

2.2.3 MR Pulse Sequences

Due to the immense variety in pulse sequence design, MRI is a very versatile imaging modality. Every MR experiment comprises RF pulses and magnetic field gradients that

are combined in a specific manner to serve a certain application. The most important characteristics of a clinical pulse sequence include image contrast, total scan time, signal-to-noise-ratio (SNR) and insensitivity to motion. But pulse sequence design can achieve much more, such as quantitative imaging, functional imaging or spectroscopy. Regardless of the application there is always a trade-off between scan time on one side and desired image quality, spectral quality or quantitative accuracy on the other requiring the designer to take into account the exact purpose of the pulse sequence. A pulse sequence is presented as a pulse sequence diagram containing five horizontal axes - one for RF transmission, one for signal acquisition and one for each gradient direction (Fig. 2.3). The pulse sequence is repeated with a constant timing. The number of repetitions depends on the desired field of view (FOV), voxel size and SNR among others. The duration between two consecutive repetitions is termed time of repetition (TR). Every common MR pulse sequence generates one or multiple echoes and the echo time (TE) is defined as the duration from the center of the RF excitation pulse to the center of the echo which, in conjunction with TR, is one of the major determinators of image contrast, f.e. T_1-weighted, T_2-weighted or proton density-weighted.

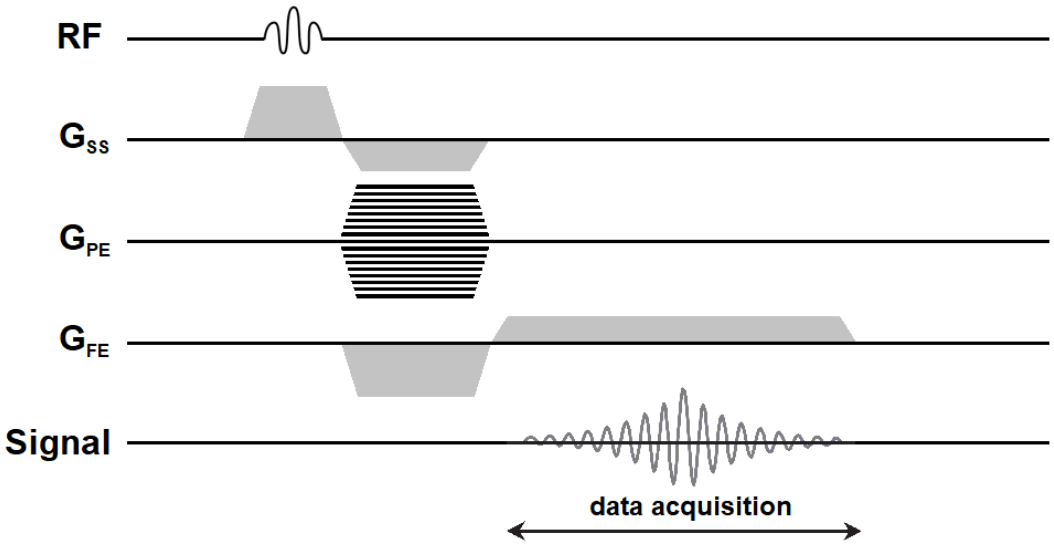

Figure 2.3: Basic gradient echo pulse sequence. G_{SS}: Slice-selective gradient, G_{PE}: Phase-encoding gradient, G_{FE}: Frequency-encoding gradient

2.2.4 k-Space

The MR signal is sampled in the frequency domain with the sampling points $k = [k_x, k_y, k_z]$, that are determined by amplitude and duration of the gradients G_x, G_y and G_z, forming the so-called k-space. The k-space representation of the image $S(k_{\mathrm{FE}}, k_{\mathrm{PE}})$ and the image domain representation $\rho(x, y)$ are related to each other by means of the Fourier transform:

$$S(k_{\mathrm{FE}}, k_{\mathrm{PE}}) = \int_{-\infty}^{\infty} \int_{-\infty}^{\infty} \rho(x, y) e^{-i2\pi(xk_{\mathrm{FE}} + yk_{\mathrm{PE}})} dxdy. \tag{2.2.2}$$

2.2.5 Spatial Encoding

Until now basic physical principles and experimental fundamentals contributing to the generation of an MR signal have been described. In order to create an actual image composed of voxels the location of the signal source, i.e. the protons, has to be encoded. For this purpose three pairs of gradient coils, one for each axis, are used to add spatially varying magnetic fields, also referred to as gradient fields, to the main magnetic field. This causes the resonant frequency of the protons to also be location-dependent and enables spatial encoding.

There are different options to encode the x-, y- and z-components of a spatial location. In 2D or multislice imaging an RF excitation pulse of limited bandwidth and a gradient field in the z-direction are applied simultaneously to selectively excite a single slice of the imaging volume. Slice position and thickness are determined by the RF carrier frequency and bandwidth, respectively. The gradient field in the z-direction is also called slice-selective gradient or G_z. Spatial encoding of the x- and y-dimension is then achieved by means of phase and frequency encoding using the remaining two perpendicular gradient fields G_x and G_y. Phase encoding is realized by briefly turning on a gradient G_{PE} in the x-direction after the excitation pulse (Fig. 2.3). For the duration of G_{PE} spins accumulate phase resulting in a phase angle that is linearly dependent on the location in the x-dimension. Finally, frequency encoding is achieved by applying the frequency-encode or readout gradient G_{FE} and acquiring the generated echo for a continuous set of frequencies (Fig. 2.3). For each repetition of the pulse sequence the amplitude of G_{PE} is changed and the readout gradient remains constant in order to cover k-space line by line. A two-dimensional Fourier transform is used to convert the sampled data into an actual 2D image.

The second option is 3D imaging where the slice selection step is replaced by a second phase encoding step. This implies that in each repetition of the sequence the complete volume is excited and allows for high-quality multiplanar reconstructions. To convert the k-space data into the image domain a three-dimensional Fourier transform has to be applied. Defining the phase encoding gradient in y-direction and the readout gradient in x-direction is by no means mandatory. Depending on the application and imaged body

region the directions can be transposed. Moreover, the three perpendicular gradient fields can be linearly combined allowing the generation of any desired slice orientation, f.e. coronary, sagittal or oblique.

2.3 Diffusion Weighted MR

Protons within a liquid are subject to random molecular motion which causes random displacement of protons over time and can be exploited to make MR signals sensitive to diffusion. By inserting pulsed field gradients, also referred to as diffusion encoding gradients, into a spin echo sequence (Fig. 2.4) or other appropriate sequence, the displacement of protons causes imperfect rephasing of the spins since diffusing protons have changed location and hence experience different magnetic fields before and after the refocusing pulse. This results in a loss of signal that depends on two factors. The degree of diffusion, quantified by means of the diffusion coefficient D, as well as amplitude, duration and timing of the diffusion encoding gradients, subsumed by the so-called b-factor b. The diffusion weighted signal shows an exponential behavior, also known as the Stejskal-Tanner equation:

$$S = S_0 e^{-bD}, \tag{2.3.1}$$

where S_0 denotes the signal intensity without diffusion weighting.

Diffusion is not the only cause of proton displacement and the consequent signal attenuation in diffusion weighted sequences. For example, flow of blood or other body fluids as well as microcirculation can contribute to the loss of signal caused by adding diffusion encoding gradients to the MR sequence. Therefore, in practice the term apparent diffusion coefficient (ADC) is used instead of D.

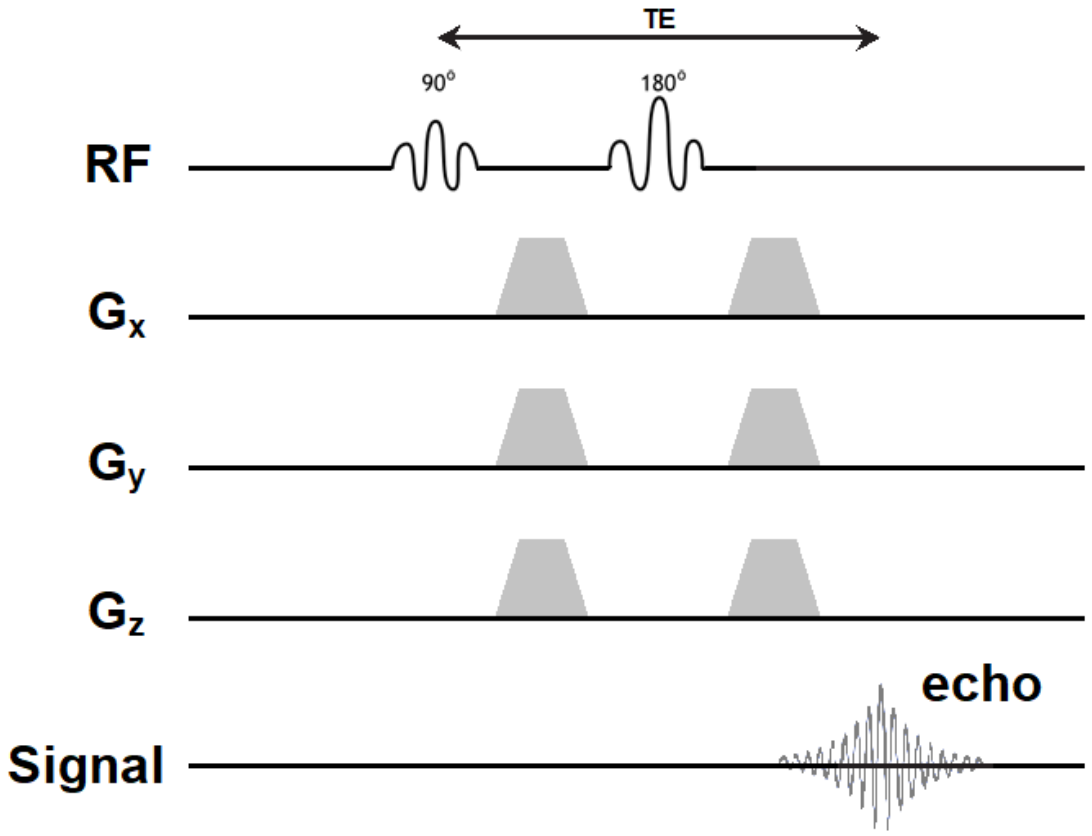

Figure 2.4: Basic pulsed gradient spin echo sequence with equal diffusion weighting in each gradient direction. $G_{x,y,z}$: Gradient in x- y- and z-direction, respectively.

3 Clinical MR Equipment

Most modern MR systems that are used in a clinical setting have a main magnetic field strength of 1.5 T or 3 T, some even up to 7 T. The main components of these systems comprise the magnet, the gradient coils, the radio frequency coils as well as a high-performance computer for hardware control and image reconstruction. In addition, the MR scanner has to be installed in a dedicated room featuring a cooling system and electromagnetic shielding to ensure a constant temperature and minimize electromagnetic interference with the environment.

3.1 Magnet

The magnet is the heart of the MR system and creates a static magnetic field B_0. Every magnet has a constant magnetic field strength, or flux density, which is measured in tesla [T]. Nowadays clinical whole-body MR systems usually have a field strength of 1.5 T or 3 T. Higher field strengths have the advantage of improved signal-to-noise ratio (SNR) which can be used to increase spatial resolution or reduce the imaging time. In addition, the chemical shift-induced frequency offset is linearly dependent on the magnetic field strength which can be advantageous, e.g. for spectral fat suppression or MR spectroscopy, but also aggravate problems in certain applications, e.g. chemical shift artifacts. In the history of MRI systems, different types of magnets have been used, including air-cored resistive magnets, iron-cored electromagnets, permanent magnets and superconducting magnets. However, in modern MRI systems superconducting magnets are the technology of choice. They enable the design of whole-body systems featuring high fields in combination with good field homogeneity. These magnets utilize the superconducting properties that certain materials show at extremely low temperatures, close to absolute zero (-273.16° C, 0 K). This requires a cooling system usually using liquid helium as cryogen raising the weight of a modern superconducting magnet and its cryogen to 3000 - 4000 kg. Besides the field strength, field homogeneity is what determines the performance of a magnet. Shimming is performed to minimize inhomogeneities. Fixed shimming refers to the attachment of small metal plates to the magnet during the installation in order to reduce field distortions from nearby ferromagnetic structures and improve the overall field homogeneity. Dynamic shimming is implemented by the addition of small shim coils to the MR system that optimize the local magnetic field on a per-patient basis.

3.2 Gradient System

In a standard cylindrical magnet, three sets of gradient coils are mounted just inside the bore. They produce orthogonal gradient fields along the x-, y- and z-direction of the magnet that are essential for spatial encoding of the MR signal. There are other purposes of gradient fields, such as the generation of gradient echoes and diffusion encoding. In conventional MR pulse sequences, gradient waveforms have a trapezoid shape being defined by the amplitude, rise time and fall time. The maximum gradient amplitude and speed at which it can be reached, referred to as slew rate, are the main parameters determining the performance of a gradient system. Ideally gradient fields are linear. In reality, gradient linearity decreases towards the edge of the imaging volume which can lead to geometric distortions of the image. Another practical problem, in particular in high slew rate systems, are eddy currents that are induced in nearby conducting components and cause gradient waveform distortions resulting in artifacts and signal loss.

3.3 Radio Frequency System

The radio frequency system comprises three components: coil, transmitter and receiver. The transmitter together with the coil produce the B_1 field used for excitation. In combination with the coil, the receiver is used for detection and demodulation of the MR signal. A body coil, built into the gantry of the MR scanner, generally is used for excitation where as surface coil arrays, positioned close to the imaged region, such as a built-into-the-table spine coil or shoulder coil, are used for signal detection. For some applications, dedicated transmit and receive coils with a built-in T/R switch are used, e.g. knee, head.

3.4 Experimental MR system

All MR experiments and examinations of study participants in the context of the present thesis were carried out on a clinical whole-body 3 T MR scanner (Ingenia, Philips Healthcare, The Netherlands) at the university hospital Klinikum rechts der Isar of the Technical University of Munich in Munich (Germany).

4 Single-voxel Magnetic Resonance Spectroscopy

In-vivo ^{1}H-MRS allows for the differentiation and quantification of protons based on their chemical shift and thus quantitative assessment of tissue composition as well as relative concentrations of certain metabolites. To analyze a well-defined, preferably homogeneous, volume of interest (VOI, Fig. 4.1), also referred to as voxel, a localization technique is applied. There are two localization techniques that are routinely used in single-voxel MRS: STEAM and PRESS.

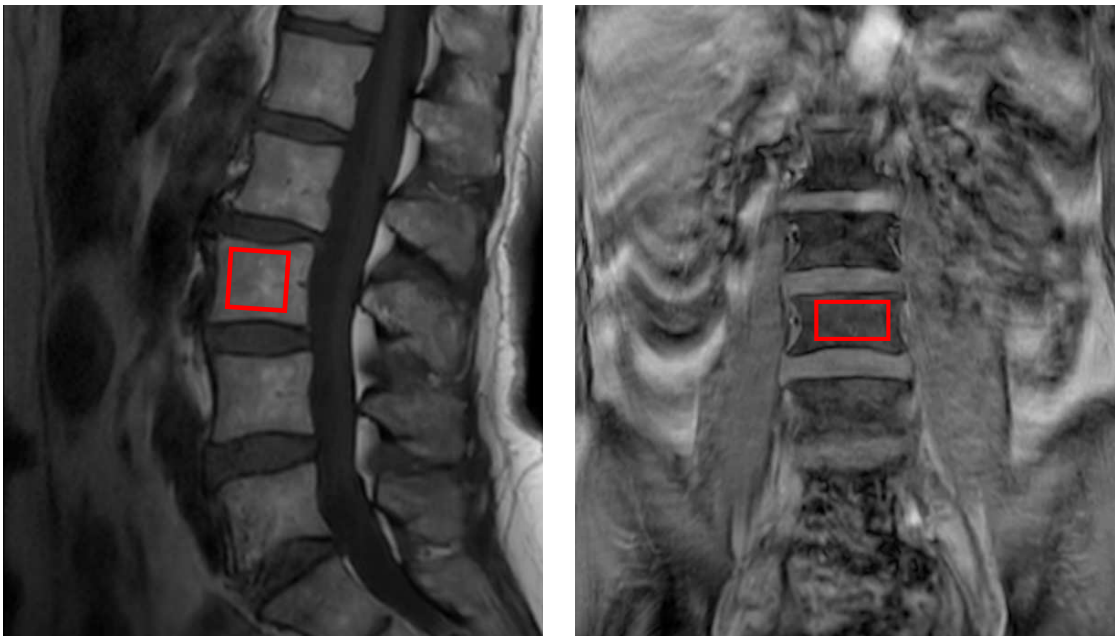

Figure 4.1: Placement of the volume of interest (red) during an MRS experiment within the bone marrow of the L3 vertebral body. For this purpose acquired sagittal (left) and coronal (right) images were used.

4.1 STEAM

Stimulated echo acquisition mode (STEAM) applies three consecutive 90° pulses, each one with a slice-selective gradient in one of the three directions (x, y and z) (Fig. 4.2). Of the multiple echoes that are generated the stimulated echo is the one being acquired. It is only formed in the cuboid-shaped VOI since it is the intersection of the three perpendicular slices the 90° pulses were applied in. Between the first and second pulse and between the third pulse and the stimulated echo the magnetization is in the transverse plane and hence subject to T_2 decay but not to T_2^* decay because dephasing occurring after the first pulse gets refocused after the third pulse. Between the second and third pulse the magnetization is aligned along the longitudinal axis and hence subject to T_1 relaxation. A representative in-vivo vertebral bone marrow STEAM spectrum from JP-1 is shown in figure 4.3.

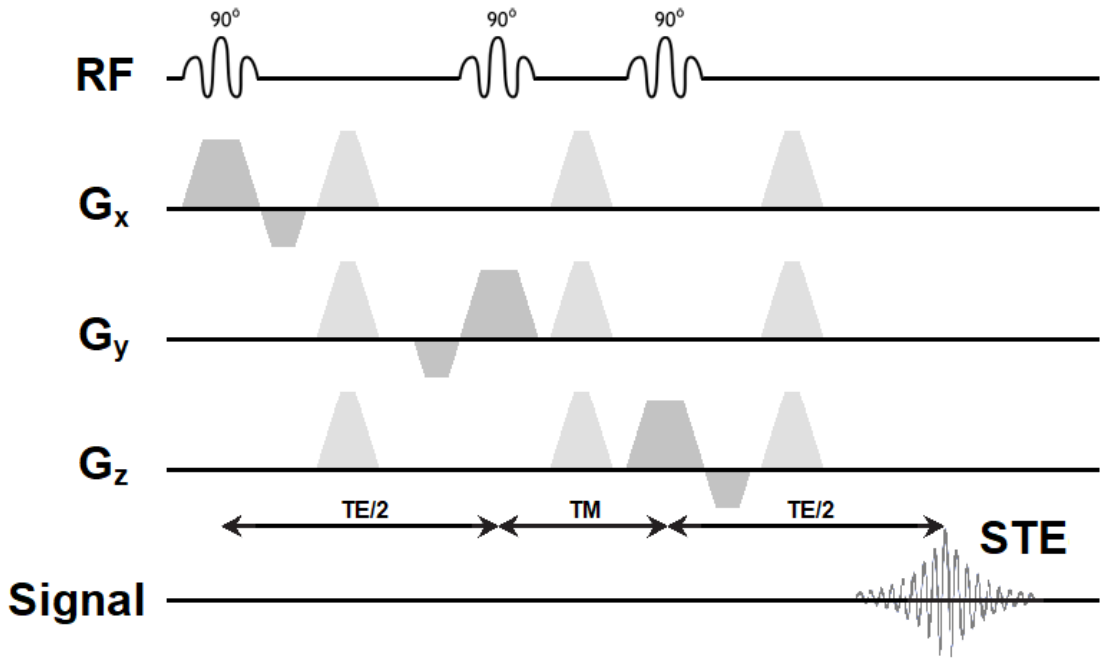

Figure 4.2: STEAM sequence diagram. The light gray trapezoids represent crusher gradients to eliminate spurious signals from contaminating the desired STEAM spectrum. TE: Echo time, TM: Mixing time, STE: Stimulated echo, $G_{x/y/z}$: Gradient in x- y- and z-direction, respectively.

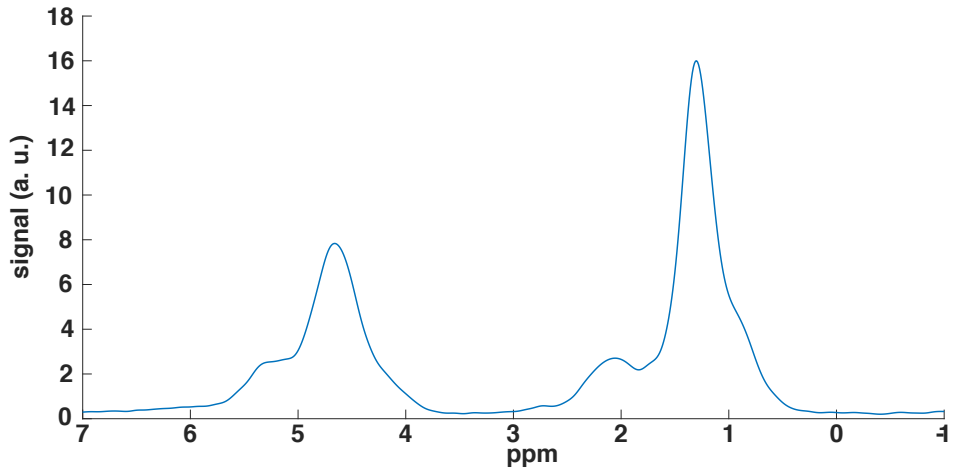

Figure 4.3: Sample in-vivo vertebral bone marrow STEAM spectrum, TE = 11 ms, TM = 16 ms, TR = 6000 ms. ppm: parts per million, a.u.: arbitrary units.

4.2 PRESS

Point-resolved spectroscopy (PRESS) uses a 90° pulse for excitation that is followed by two 180° refocusing pulses (Fig. 4.4). Again, each pulse is accompanied by a slice-selective gradient in one of the three directions. After a certain slice is excited by the 90° pulse it gets refocused by the first 180° pulse only in a perpendicular slice resulting in a primary spin echo that is generated in a well-defined slab. The second 180° pulse refocuses the primary echo and is only applied in a slice perpendicular to this slab resulting in the generation of a second spin echo within the cuboid-shaped intersection of the three perpendicular slices that finally is acquired. Since the magnetization is in the transverse plane at all times it is only subject to T_2 decay. PRESS has the advantage of an intrinsically higher SNR than STEAM. However, STEAM can achieve shorter minimal echo times. Therefore it depends on the application, the properties of the tissue being analyzed, the hardware and software conditions as well as the experience of the user which localization technique is best.

4.3 Diffusion Weighted STEAM

By inserting diffusion encoding gradients after the first and third RF pulse in a STEAM sequence (Fig. 4.5) diffusion weighted MRS was achieved in JP-2 [40]. A representative spectrum acquired at multiple b-values is shown in figure 4.6.

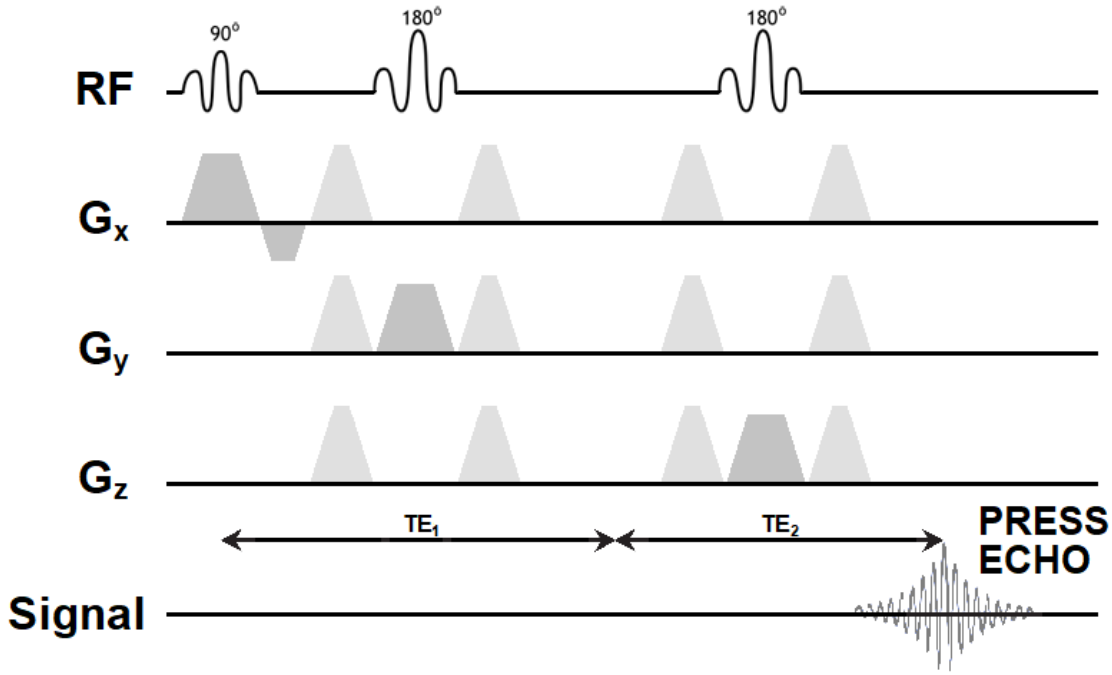

Figure 4.4: PRESS sequence diagram. The light gray trapezoids represent crusher gradients to eliminate spurious signals from contaminating the desired PRESS spectrum. The total echo times equals the sum of TE_1 and TE_2. $TE_{1/2}$: Echo time 1 and 2, $G_{x/y/z}$: Gradient in x- y- and z-direction, respectively.

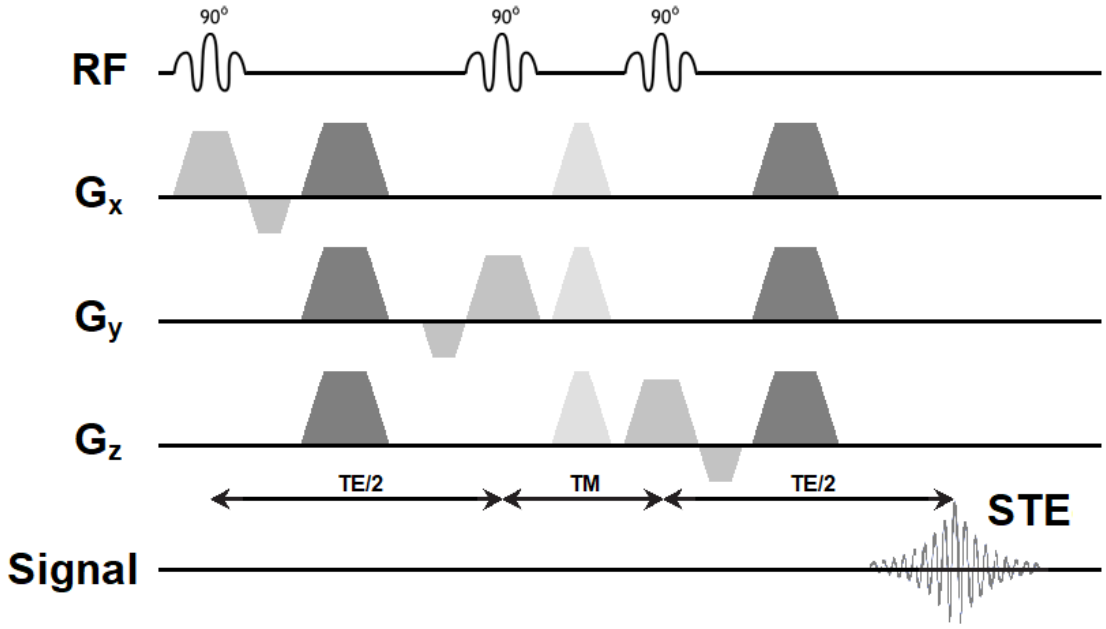

Figure 4.5: DW-STEAM sequence diagram. The dark gray trapezoids represent diffusion encoding gradients. TE: Echo time, TM: Mixing time, STE: Stimulated echo, $G_{x,y,z}$: Gradient in x- y- and z-direction, respectively.

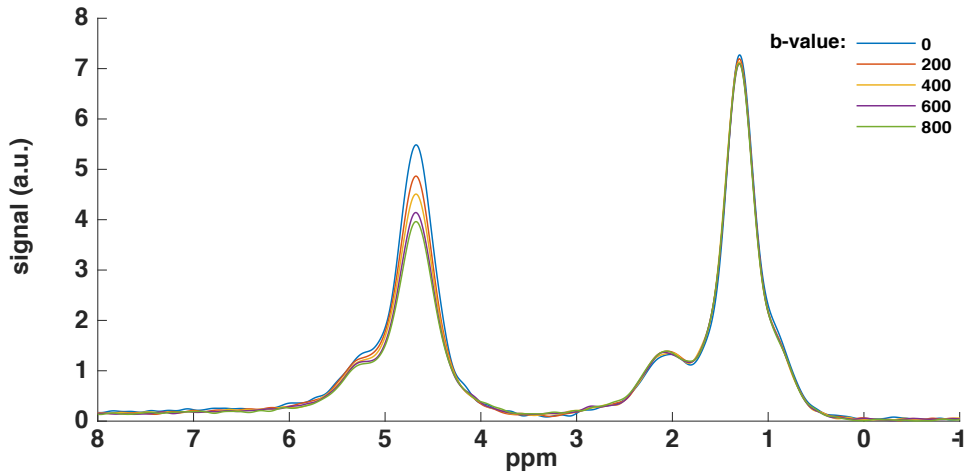

Figure 4.6: Sample in-vivo multi-b-value DW-STEAM spectrum. The difference in diffusion-dependent signal decay of the main fat component (at 1.3 ppm) and the water component (at 4.7 ppm) can be appreciated. ppm: parts per million, a.u.: arbitrary units.

5 MR-based Fat Quantification

5.1 Characterization of the Vertebral Bone Marrow MR Spectrum

For the MR-based in vivo quantification of fat one can utilize knowledge about its chemical structure. Triglycerides are the building blocks of human adipose tissue and consist of three fatty acids esterified with a glycerol backbone. Depending on their number of double bonds fatty acids can be further classified into saturated, monounsaturated and polyunsaturated, exhibiting none, one or more double bonds, respectively (Figure 5.1). Each proton within the triglyceride has a certain chemical environment and can therefore be assigned a proton type giving rise to a characteristic chemical shift and corresponding peak in the MR spectrum (Figure 5.2). The letters A - J label the distinct fat peaks. Table 5.1 displays the different proton types of a triglyceride together with the corresponding chemical shift.

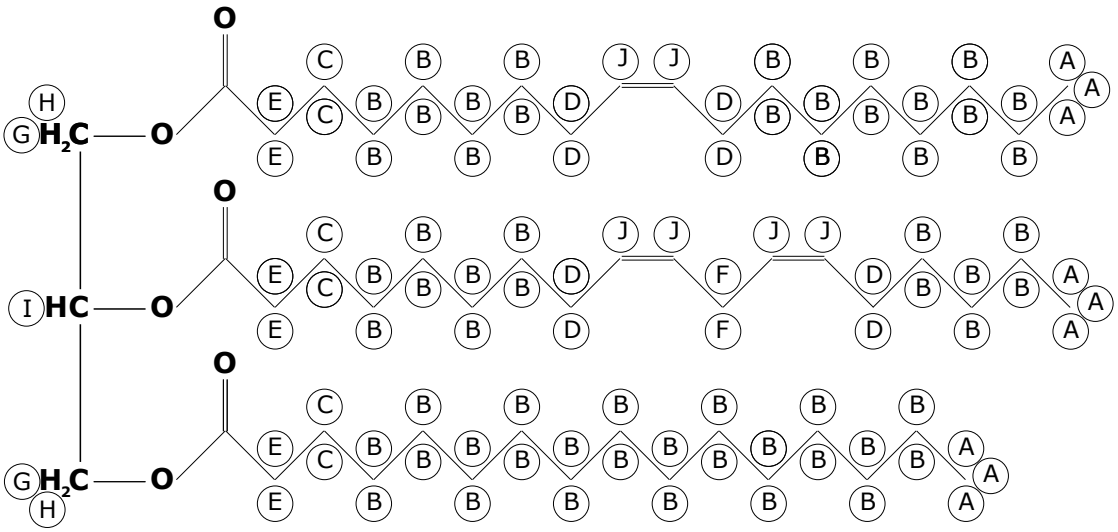

Figure 5.1: Sample triglyeride structure consisting of oleic acid (18:1, 9*c*; top row), linoleic acid (18:2, 9*c*, 12*c*; centre row) and palmitic acid (16:0; bottom row). The labels A - J group the protons according to their characteristic resonance frequency and corresponding peak in the MR spectrum.

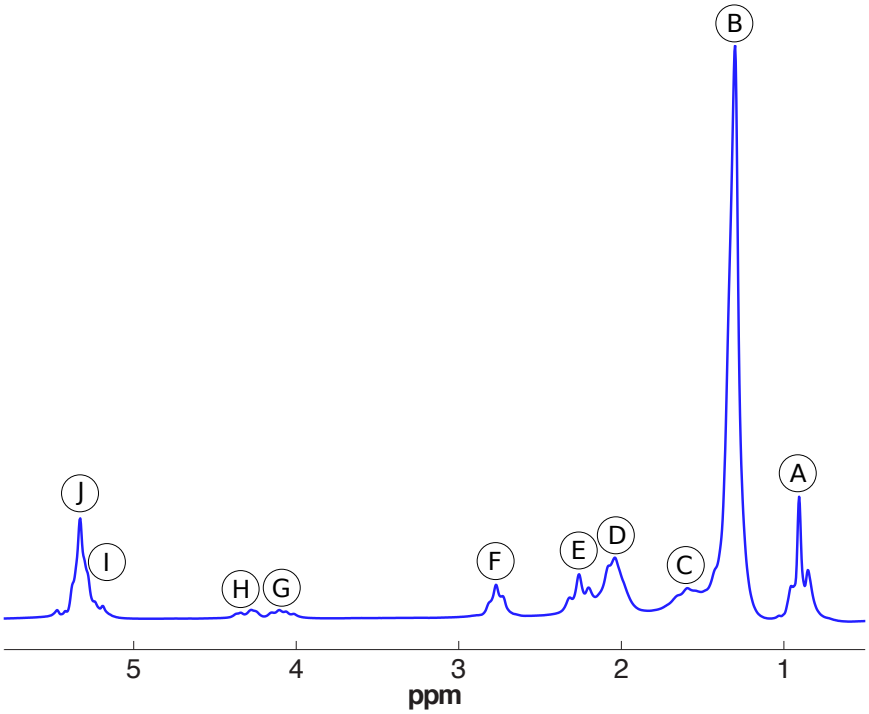

Figure 5.2: Sample triglyceride spectrum of corn oil acquired on a 3 T clinical MR system. The different peaks of the fat spectrum are labeled A - J according to the protons in figure 5.1

In vivo quantification of bone marrow fat is complicated by the presence of water as well as peak broadening caused by short T_2^*. In order to achieve a robust quantification of the fat components a fixed triglyceride structure with constant values of the characteristic parameters *ndb* (number of double bonds), *nmidb* (number of methylene-interrupted double bonds) and *CL* (mean fatty acid chain length) is assumed. In JP-I, these values were determined for the mean vertebral bone marrow spectrum inspired by an approach described by Hamilton et al. [41] for liver fat spectrum characterization. They are displayed in table 5.1 together with the resulting relative amplitudes of the different fat peaks. These relative amplitudes were also used for water-fat imaging-based PDFF quantification in JP-II where the spectral model consisted of six fat peaks and a single water peak.

peak	chemical shift (ppm)	type	relative amplitudes	relative amplitudes of used vertebral bone marrow model [42]
A	0.90	methyl	9	9
B	1.30	methylene	(CL - 4) × 6 - ndb × 8 + nmidb × 2	56.16
C	1.60	β-carboxyl	6	6
D	2.02	α-olefinic	(ndb - nmidb) × 2	9.72
E	2.24	alpha-carboxyl	6	6
F	2.75	diallylic	nmidb × 2	1.4
G	4.10	glycerol	2	2
H	4.30	glycerol	2	2
I	5.19	glycerol	1	1
J	5.29	olefinic	ndb × 2	6.26

Table 5.1: Parameters of triglyceride modeling used in MRS-based and water-fat imaging-based quantification of vertebral bone marrow fat. Peaks A - J of the fat spectrum are displayed in figure 5.2 as well as the corresponding protons of a sample triglyceride structure in figure 5.1.

5.2 Vertebral Bone Marrow PDFF Quantification

To account for differences in T_2 relaxation between the water and fat component of vertebral bone marrow data is acquired at multiple echo times and the T_2 relaxation times of water (T_{2w}) and fat (T_{2f}) were included as additional model parameters. After extracting the different peaks by fitting the acquired data to the described spectral model (Figure 5.3) the PDFF is calculated as the ratio of the combined energy of all fat peaks and the combined energy of all peaks of the proton density spectrum:

$$\text{PDFF} = \frac{\int_{-\infty}^{\infty} \sum_{i=\text{A}}^{\text{J}} S_i(f) df}{\int_{-\infty}^{\infty} \sum_{i=\text{A}}^{\text{J}} S_i(f) + S_w(f) df}, \tag{5.2.1}$$

S_i: fitted i-th fat peak, S_w: fitted water peak, f: resonance frequency.

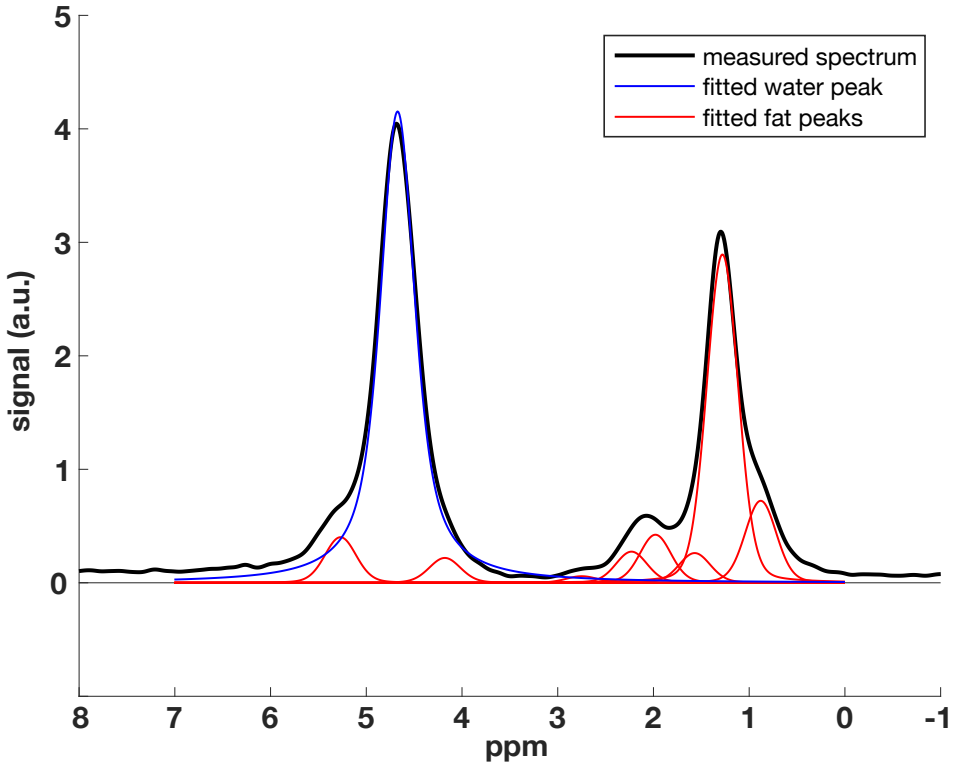

Figure 5.3: Sample vertebral bone marrow STEAM spectrum at TE = 11 ms (black). and superimposed fitted water peak (blue) and fat peaks (red). ppm: parts per million, a. u.: arbitrary units

6 Bone Marrow Anatomy and Physiology

Bone marrow represents one of the largest organs in the human body. An average adult person has 2600 g of bone marrow which is equivalent to 4.5 % of its body weight. It is located in the central cavities of the bones and can be interspersed with trabecular bone matrix. It is the most important hematopoietic organ as well as a primary lymphatic organ and plays a major role in a variety of pathologies affecting either its own components, i.e. blood cells and adipocytes, or the bone tissue surrounding it.

Depending on its cellular and chemical composition two types of bone marrow are distinguished. The main component of yellow bone marrow are adipocytes and its chemical composition is approximately equivalent to 80 % fat, 15 % water and 5 % protein. Yellow bone marrow has only scarce vasculature and its main location is the appendicular skeleton. Red bone marrow contains both hematopoietic cells and adipocytes and its chemical composition can vary but is within the range of 40 - 60 % fat, 30 - 40 % water and 10 - 20 % protein arising from the higher relative water and protein content of hematopoietic cells. Due to its hematopoietic and lymphatic function red bone marrow has an abundant vasculature, being formed by an extensive network of sinusoids.

Bone marrow is a dynamic tissue which constantly undergoes changes depending on the varying demands and conditions the organism is facing throughout its lifetime. In adults red bone marrow can be encountered almost exclusively in the sternum, ribs, skull, clavicles, vertebral bodies, pelvic bones as well as proximal femur and humerus whereas in newborns it is found in almost all bones. This adult state of red and yellow bone marrow distribution where red marrow can only be found in the axial skeleton is usually reached around the age of 25 years. However, the conversion from red to yellow marrow continues throughout life and results in a heterogeneous spatial distribution of red bone marrow.

In addition to the traditional classification based on the presence of hematopoietic cells, Scheller et al. introduced the distinction of regulated bone marrow adipose tissue (rMAT) and constitutive bone marrow adipose tissue (cMAT). The primarily in the axial and proximal skeleton located rMAT is defined as single adipocytes interspersed with active hematopoiesis, whereas distal cMAT has low hematopoiesis, contains larger adipocytes, develops earlier and remains preserved upon systemic challenges [43]. Categorizing bone marrow based on subpopulations of its adipocytes aims at a classification based on its biology, physiology and metabolic function rather than its cellular and chemical composition and may therefore be more suitable for emerging research and upcoming studies.

7 Compliance with Ethical Standards

All investigations performed in studies involving human participants were in accordance with the ethical standards of the institutional and national research committee as well as the 1964 Helsinki declaration and its later amendments or comparable ethical standards. Informed consent was obtained from all individual participants included in the studies.

8 Journal Publications

8.1 Journal Publication I: The need for T_2 correction on MRS-based vertebral bone marrow fat quantification: implications for bone marrow fat fraction age dependence.

The publication entitled *The need for T_2 correction on MRS-based vertebral bone marrow fat quantification: implications for bone marrow fat fraction age dependence.* was published in NMR in Biomedicine (ISSN: 1099-1492). The manuscript was authored by Michael Dieckmeyer, Stefan Ruschke, Christian Cordes, Samuel P. Yap, Hendrik Kooijman, Hans Hauner, Ernst J. Rummeny, Jan S. Kirschke, Thomas Baum and Dimitrios C. Karampinos.

8.1.1 Abstract

Vertebral bone marrow fat quantification using single-voxel MRS is confounded by overlapping water-fat peaks and the difference in T_2 relaxation time between water and fat components. The purposes of the present study were: (i) to determine the proton density fat fraction (PDFF) of vertebral bone marrow using single-voxel multi-TE MRS, addressing these confounding effects; and (ii) to investigate the implications of these corrections with respect to the age dependence of the PDFF. Single-voxel MRS was performed in the L5 vertebral body of 86 subjects (54 women and 32 men). To reliably extract the water peak from the overlying fat peaks, the mean bone marrow fat spectrum was characterized based on the area of measurable fat peaks and an a priori knowledge of the chemical triglyceride structure. MRS measurements were performed at multiple TEs. The T_2-weighted fat fraction was calculated at each TE. In addition, a T_2 correction was performed to obtain the PDFF and the T_2 value of water (T_{2w}) was calculated. The implications of the T_2 correction were investigated by studying the age dependence of the T_2-weighted fat fractions and the PDFF. Compared with the PDFF, all T_2-weighted fat fractions significantly overestimated the fat fraction. Compared with the age dependence of the PDFF, the age dependence of the T_2-weighted fat fraction showed an increased slope and intercept as TE increased for women and a strongly increased intercept as TE increased for men. For women, a negative association between the T_2 value of bone marrow water and PDFF was found. Single-voxel MRS-based vertebral bone marrow fat

quantification should be based on a multi-TE MRS measurement to minimize confounding effects on PDFF determination, and also to allow the simultaneous calculation of T_{2w}, which might be considered as an additional parameter sensitive to the composition of the water compartment.

8.1.2 Author contributions

I performed the postprocessing, quantification and statistical analysis of the magnetic resonance spectroscopy data using MATLAB (Mathworks, Natick, MA). In collaboration with the coauthors I designed the MRI protocol and performed the recruitment and MRI examinations of the study participants, implemented the MRS post-processing framework using MATLAB, analyzed and interpreted the data and drafted the publication manuscript.

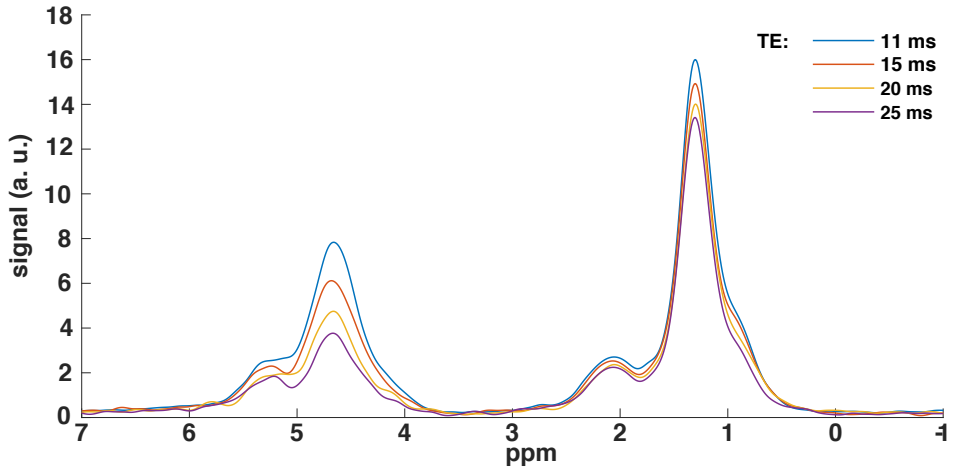

Figure 8.1: Sample multi-TE STEAM spectrum of one of the subjects. The difference in T_2 decay of the main fat component (at 1.3 ppm) and the water component (at 4.7 ppm) can be appreciated. ppm: parts per million, a.u.: arbitrary units.

Research article

NMR IN BIOMEDICINE

Received: 3 November 2014, Revised: 9 January 2015, Accepted: 12 January 2015, Published online in Wiley Online Library: 13 February 2015

(wileyonlinelibrary.com) DOI: 10.1002/nbm.3267

The need for T_2 correction on MRS-based vertebral bone marrow fat quantification: implications for bone marrow fat fraction age dependence

Michael Dieckmeyer[a]*, Stefan Ruschke[a], Christian Cordes[a], Samuel P. Yap[a], Hendrik Kooijman[b], Hans Hauner[c], Ernst J. Rummeny[a], Jan S. Bauer[d], Thomas Baum[a] and Dimitrios C. Karampinos[a]

Vertebral bone marrow fat quantification using single-voxel MRS is confounded by overlapping water–fat peaks and the difference in T_2 relaxation time between water and fat components. The purposes of the present study were: (i) to determine the proton density fat fraction (PDFF) of vertebral bone marrow using single-voxel multi-TE MRS, addressing these confounding effects; and (ii) to investigate the implications of these corrections with respect to the age dependence of the PDFF. Single-voxel MRS was performed in the L5 vertebral body of 86 subjects (54 women and 32 men). To reliably extract the water peak from the overlying fat peaks, the mean bone marrow fat spectrum was characterized based on the area of measurable fat peaks and an a priori knowledge of the chemical triglyceride structure. MRS measurements were performed at multiple TEs. The T_2-weighted fat fraction was calculated at each TE. In addition, a T_2 correction was performed to obtain the PDFF and the T_2 value of water (T_{2w}) was calculated. The implications of the T_2 correction were investigated by studying the age dependence of the T_2-weighted fat fractions and the PDFF. Compared with the PDFF, all T_2-weighted fat fractions significantly overestimated the fat fraction. Compared with the age dependence of the PDFF, the age dependence of the T_2-weighted fat fraction showed an increased slope and intercept as TE increased for women and a strongly increased intercept as TE increased for men. For women, a negative association between the T_2 value of bone marrow water and PDFF was found. Single-voxel MRS-based vertebral bone marrow fat quantification should be based on a multi-TE MRS measurement to minimize confounding effects on PDFF determination, and also to allow the simultaneous calculation of T_{2w}, which might be considered as an additional parameter sensitive to the composition of the water compartment. Copyright © 2015 John Wiley & Sons, Ltd.

Keywords: bone marrow; fat quantification; MRS; T_2 correction; spine

INTRODUCTION

The quantification of the bone marrow fat fraction (FF) is becoming a useful tool in the investigation of the relationship between bone marrow adiposity and bone health (1–6), in the study of the connection between bone marrow adiposity and metabolic syndrome (7,8) and in the assessment of bone marrow composition changes in patients receiving chemotherapy and radiotherapy (9,10). Recent studies have reported the use of chemical shift encoding-based MRI techniques for the measurement of bone marrow FF in the proximal femur (11) and the spine (9,12), enabling the examination of both intra-individual as well as inter-individual differences. However, single-voxel MRS has been the technique most frequently applied in the past for the measurement of bone marrow FF in the most clinically relevant red marrow region, i.e. the lumbar vertebrae (2–7,13–22). Despite the wide use of vertebral bone marrow MRS in the research setting, different studies have

* Correspondence to: M. Dieckmeyer, Department of Diagnostic and Interventional Radiology, Klinikum rechts der Isar, Ismaninger Str. 22, 81675 Munich, Germany.
E-mail: michael.dieckmeyer@mytum.de

a M. Dieckmeyer, S. Ruschke, C. Cordes, S. P. Yap, E. J. Rummeny, T. Baum, D. C. Karampinos
Department of Diagnostic and Interventional Radiology, Klinikum rechts der Isar, Technische Universität München, Munich, Germany

b H. Kooijman
Philips Healthcare, Hamburg, Germany

c H. Hauner
Else Kröner Fresenius Center for Nutritional Medicine, Klinikum rechts der Isar, Technische Universität München, Munich, Germany

d J. S. Bauer
Department of Diagnostic and Interventional Neuroradiology, Klinikum rechts der Isar, Technische Universität München, Munich, Germany

Abbreviations used: *CV, coefficient of variation; FF, fat fraction; MUFA, monounsaturated fatty acid; ndb, number of double bonds; nmidb, number of methylene-interrupted double bonds; PDFF, proton density fat fraction; PUFA, polyunsaturated fatty acid; SNR, signal-to-noise ratio; STEAM, stimulated echo acquisition mode; T_{2f}, T_2 value of fat; T_{2w}, T_2 value of water; VOI, volume of interest.*

reported different ranges of bone marrow FF values for different male and female age groups (13).

The most important technical consideration in establishing MRS-based FF as a standardized bone marrow biomarker is that the measured property should be equal to the proton density fat fraction (PDFF), independent of the effects of any confounding factors (23). Previously, single-voxel MRS has been extensively used to measure PDFF in the liver, considering the multiple peaks of the fat spectrum (24), correcting the differences in T_2 relaxation times between water and fat (25), and aiming to minimize J couplings using a stimulated echo acquisition mode (STEAM) MRS sequence (26).

Bone marrow contains water and fat components with different T_2 relaxation times (19,20) and is surrounded by the trabecular bone matrix. The presence of the trabecular bone matrix broadens the linewidths of all peaks in the bone marrow spectrum, complicating the robust extraction of the water peak next to the neighboring fat peaks (11). In order to robustly extract the overlapping water and fat peaks in vertebral bone marrow MRS, the spectrum should be characterized on the basis of the magnitude of measurable fat peaks, and an a priori knowledge of the chemical structure of triglycerides should be employed in the MRS peak extraction, as proposed previously for the liver (24) and the proximal femur (11).

The difference in T_2 relaxation times between water and fat components can also induce a bias in the quantification of bone marrow fat with significant implications when comparing FF values with a reference database. Specifically, several studies have shown a gradual physiological increase in bone marrow FF with advancing years, starting at a mean vertebral body bone marrow fat content of between 20% and 25% in the 11–20-year age group and rising to 65%–75% in the 81–90-year age group (13). Furthermore, there is evidence for a sex dependence of the bone marrow FF, suggesting that males under 50 years of age have an FF that is about 10% higher than that in females of comparable age, with a reversal of this difference in subjects over 60 years of age (14–16). However, most of the previous studies performing MRS in the lumbar vertebrae and studying the age dependence of the bone marrow FF employed a single-TE MRS measurement and did not use any T_2 correction, thus yielding the T_2-weighted FF rather than the PDFF. Therefore, the previously reported rates of increase in bone marrow FF with age could be dependent on the TE and T_2 relaxation values used, and could thus become dependent on the parameters of the MRS experiment and the field strength.

The purpose of this study was to address the most important effects confounding vertebral bone marrow PDFF quantification using single-voxel MRS. The specific aims were thus two-fold: (i) to characterize the mean fat spectrum of vertebral bone marrow fat in order to robustly extract the water peak from the overlapping fat peaks in the spectrum; and (ii) to perform a T_2 correction of the MRS data in order to remove T_2 decay effects and demonstrate the importance of the consideration of T_2 decay effects in bone marrow fat quantification in the context of the analysis of the age dependence of the bone marrow FF.

MATERIALS AND METHODS

Subjects

The lumbar spine region of 86 healthy volunteers (54 women; age, 45.3 ± 13.7 years; 32 men; age, 38.3 ± 14.7 years) was scanned on a 3-T whole-body scanner (Ingenia 3.0T, Philips Healthcare, Best, the Netherlands) using the built-in 12-channel posterior coil array. Inclusion criteria were no history of fracture and no pathological bone changes, such as bone metastases or hematological or metabolic bone disorders. Women had the following age distribution: n = 11, 9, 9, 19 and 6 subjects for the age ranges 18–30, 31–40, 41–50, 51–60 and 61–75 years, respectively. Men had the following age distribution: n = 14, 5, 5, 5 and 2 subjects for the age ranges 20–30, 31–40, 41–50, 51–60 and 61–75 years, respectively. The study was approved by the local institutional committee for human research. All subjects gave written informed consent before participation in the study.

MR measurements

Following the acquisition of survey images in all three planes, T_2-weighted sagittal images of the lumbar spine were obtained to verify the absence of any vertebral fractures, metastases and anatomical abnormalities, and to guide the positioning of the MRS voxel within the vertebral body. The MRS examination consisted of an MRS sequence, applied in the L5 vertebral body. The L5 vertebral body was selected because it usually has the largest volume of all vertebral bodies. This maximizes the size of the prescribable volume of interest (VOI) and hence the signal-to-noise ratio (SNR) of the MRS measurement. The MRS voxel was positioned on the basis of the survey images and T_2-weighted sagittal images. The size of the VOI was 15 × 15 × 15 mm^3. If necessary, the size of the VOI was reduced in order to fit into the vertebral body. Moreover, chemical shift displacement effects were considered during the positioning of the VOI. A STEAM sequence with the following parameters was used: TR = 6 s (to minimize any T_1-weighting effects); TM = 16 ms; TE = 11/15/20/25 ms [STEAM with short TE to reduce J-coupling effects (26)]; eight averages per TE; 4096 sampling points; acquisition bandwidth, 5 kHz; no water suppression; no regional saturation bands.

Characterization of the mean fat spectrum

Spectra were fitted using frequency-based methods based on in-house built routines written in MATLAB (Mathworks, Natick, MA, USA). Pseudo-Voigt lineshapes (27) with a 0.8 × Gauss + 0.2 × Lorentzian lineshape for the fat peaks and a 0.2 × Gauss + 0.8 × Lorentzian lineshape for the water peak were employed. Figure 1a shows a typical vertebral bone marrow fat spectrum with fat peaks observed at spectral locations 0.90, 1.30, 1.59, 2.00, 2.25, 2.77, 4.20 and 5.31 ppm. The letters A, D, E and F were assigned to peaks at 0.90 ppm (methyl: $-(CH_2)_n-\mathbf{CH_3}-$), 2.77 ppm (diacyl: $-CH=CH-\mathbf{CH_2}-CH=CH-$), 4.20 ppm (glycerol: $-\mathbf{CH_2}-O-CO-$) and 5.31 ppm (olefinic: $-\mathbf{CH}=\mathbf{CH}-$), respectively. The letter B was assigned to the superposition of peaks at 1.30 ppm (methylene: $-(\mathbf{CH_2})_n-$) and 1.59 ppm (β-carboxyl: $-CO-CH_2-\mathbf{CH_2}-$), and the letter C to the superposition of peaks at 2.00 ppm (α-olefinic: $-\mathbf{CH_2}-CH=CH-\mathbf{CH_2}-$) and 2.25 ppm (α-carboxyl: $-CO-\mathbf{CH_2}-CH_2-$).

In a first step, all peaks contributing to the fat peaks A, B, C and D were fitted assuming a common linewidth. The fat spectrum peak fitting was performed for the shortest TE of 11 ms only, because a common T_2 relaxation time for all fat peaks was assumed. The relationships between the computed fat peaks A, B and C were studied for the bone marrow spectra of all 86 subjects using linear correlation analysis. Specifically, the

relationship between the combined areas of peaks A and B and the area of peak C (Fig. 1b) and the relationship between the area of peak B and the area of peak C (Fig. 1c) were studied using linear regression analysis. The slopes of the two linear regression models were determined and two-sided *t*-tests at a significance level of $p = 0.05$ were used to determine whether the estimated intercept was statistically significantly different from zero. In a second step, the slopes of the two linear regression models were inserted into the triglyceride structure model to estimate the number of double bonds (ndb) and number of methylene-interrupted double bonds (nmidb) following the formulation introduced by Hamilton *et al.* (24). A common triglyceride chain length of 17.3 was assumed. Based on the estimated ndb and nmidb, the relative areas of fat peaks E and F were determined. The described approach makes the assumption that the unsaturation level of the vertebral bone marrow is independent of age. This may not be valid for younger ages when a conversion from red to yellow marrow is occurring. However, changes in the fatty acid composition of the evaluated region should be considered subtle compared with changes in fat content. Therefore, the assumption of a common fatty acid composition should constitute an acceptable simplification with regard to the measured quantity, i.e. PDFF.

Fat quantification

To allow a good fit of the entire spectrum, peak fitting was performed by constraining the areas of peaks E and F at a given ratio of peaks A + B, determined as described in the fat spectrum characterization step. A common linewidth, constrained below 0.50 ppm, was assumed for all fat peaks, and an independent linewidth, constrained below 1.50 ppm, was assumed for the water peak, resulting in two different linewidths as free variables. The spectral locations of the fat peaks were allowed to vary by ±0.03 ppm, and the water peak location was allowed to vary by ±0.10 ppm. However, the distance between the spectral locations of the fat peaks was not allowed to change, resulting in two free variables for the peak locations. Peak fitting was performed first independently for every individual TE (TE-independent fitting) and then jointly incorporating the measurements of all four TEs (TE-joint fitting). The T_2 relaxation times were introduced again as free variables, assuming a mono-exponential T_2 decay for each component with a common T_2 relaxation time for all fat peaks (T_{2f}) and a different T_2 relaxation time for the water peak (T_{2w}). Initial values for T_{2f} and T_{2w} were set to 75 and 20 ms, respectively. Based on the results of the TE-independent fitting, the T_2-weighted FF was computed as the ratio of the T_2-weighted fat peak area over the sum of the T_2-weighted fat peak area and T_2-weighted water peak area at every TE. Based on the results of the TE-joint fitting, the PDFF was computed as the ratio of the T_2-corrected fat peak area over the sum of the T_2-corrected fat peak area and T_2-corrected water peak area.

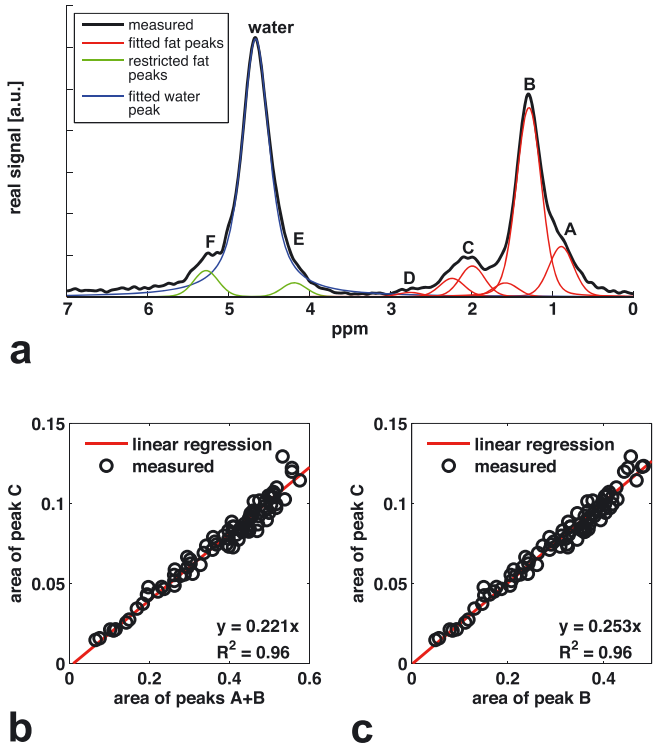

Figure 1. Model of vertebral bone marrow triglyceride structure. (a) Typical vertebral bone marrow MR spectrum with fitted fat peaks (red), fitted water peak (blue) and fat peaks whose peak areas were restricted to the main fat peak area (green). (b) Relationship between area of peaks A + B and area of peak C. (c) Relationship between area of peak B and area of peak C. Data from all subjects were included ($n = 86$).

Statistical analysis

The statistical analyses were performed with MATLAB (Mathworks). All tests were performed using a two-sided 0.05 level of significance. Linear regression analysis using least-squares fitting was performed to determine correlation coefficients (R^2), slope and intercept between age and the different FF measures (PDFF and T_2-weighted FFs). Simple and multiple linear regression model analyses were performed to test the significance of the dependence of PDFF on age and T_{2w} effects.

RESULTS

The results of the linear regression used for the mean fat spectrum characterization step are shown in Figure 1b, c. The ratio of the area of peak C to the area of peaks A + B was determined to be 0.221, with the intercept not found to be statistically significantly different from zero ($p > 0.05$). The ratio of the area of peak C to the area of peak B was determined to be 0.253, with the intercept not found to be statistically significantly different from zero ($p > 0.05$). Adopting the triglyceride structure model of Hamilton *et al.* (24), assuming a triglyceride chain length of 17.3 (28), and based on the measured ratio of the area of peaks A + B to the area of peak C, and the measured ratio of the area of peak B to the area of peak C, ndb and nmidb were computed to be 3.13 and 0.70, respectively. The derived triglyceride structure parameters were used to determine the area of peaks E and F relative to the area of peaks A + B as 5.62% and 10.20%, respectively.

In order to highlight the effects of T_2 decay on the extraction of PDFF, the spectra from two different subjects of different age, but with similar PDFF, were plotted (Fig. 2). The spectra in the top row of Figure 2 correspond to a 53-year-old woman (Fig. 2a, b) and the spectra in the bottom row of Figure 2 correspond to a 27-year-old woman (Fig. 2c, d). A comparison of the

NMR IN BIOMEDICINE

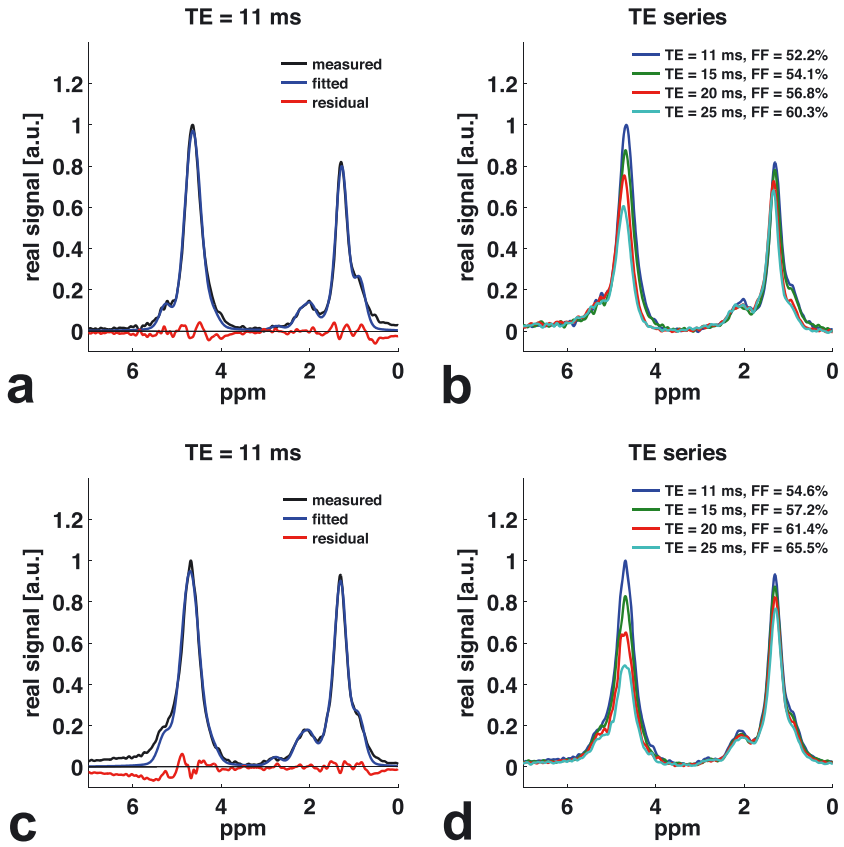

Figure 2. Comparison of vertebral bone marrow spectra in two women of different ages showing similar proton density fat fraction (PDFF) but different T_2 of water (T_{2w}). (a, c) Measured and fitted spectra at TE = 11 ms. (b, d) Measured spectra at different TEs. Spectra (a) and (b) correspond to a 53-year-old woman with PDFF = 45.6% and T_{2w} = 26.8 ms. Spectra (c) and (d) correspond to a 27-year-old woman with PDFF = 45.6% and T_{2w} = 21.7 ms. The maximum signal has been set to 1.0 arbitrary unit to facilitate visual comparison. T_2-weighted fat fraction values at each TE are also given in the key in (b) and (d).

spectra from the two subjects at the shortest TE of 11 ms shows a clear difference in the signal amplitude of the main fat peak of the two subjects, when the spectra are scaled so that the water signal amplitudes are equal (Fig. 2a, c). Therefore, the short-TE spectra show a lower T_2-weighted FF at TE = 11 ms for the 53-year-old woman than for the 27-year-old woman. However, the 53-year-old woman had a slower T_2 decay for the water peak than the 27-year-old woman, whereas the T_2 decay of the fat peak was almost identical in the two women (Fig. 2b, d). Taking into consideration T_2 effects, the same PDFF value of 45.6% was determined for both subjects.

Taking into account all 86 subjects, the means and standard deviations of the T_2 relaxation time for the water component were determined to be 22.5 ± 5.1 ms (range, 14.5–35.0 ms) and for the fat component 72.3 ± 6.2 ms (range, 58.3–89.2 ms). Considering the women only, the corresponding values were determined to be T_{2w} = 24.6 ± 5.1 ms (range, 16.8–35.0 ms) and T_{2f} = 72.6 ± 6.0 ms (range, 58.3–86.9 ms). Considering men only, the corresponding values were determined to be T_{2w} = 18.6 ± 2.4 ms (range, 14.5–24.7 ms) and T_{2f} = 71.8 ± 6.5 ms (range, 60.1–89.2 ms).

Both T_2-weighted FF values at different TEs and PDFF values were positively correlated with age ($0.46 < R^2 < 0.50$, $p < 0.001$). The results of the linear regression between age and T_2-weighted FF at different TEs, as well as the PDFFs for women and men, are shown in Tables 1 and 2, respectively. As the TE increased from 11 to 25 ms, the age dependence of the T_2-weighted FF showed a slope increasing from 0.773 to 0.835 and an intercept increasing from 12.3% to 18.5% for women. As the TE increased from 11 to 25 ms, the age dependence of the T_2-weighted FF showed a fairly constant slope in the range 0.526–0.562 and a strongly increasing intercept from 28.4% to 42.8% for men. In women, the age dependence of the PDFF revealed slope and intercept values of 0.657 and 9.4%, respectively, which are both lower than the equivalent values for the T_2-weighted FF at the shortest TE. In men, the age dependence of the PDFF revealed a slope of 0.530, which is within the range of the T_2-weighted measurements, and an intercept value of 19.3%, which is considerably lower than the corresponding value for the shortest TE measurement.

Figure 3 depicts the linear correlation between PDFF and the T_2-weighted FF at the longest TE of 25 ms for both men and women. For women, the overestimation of FF as a result of T_2 weighting with regard to PDFF clearly increased with age. For men, the discrepancy between PDFF and the T_2-weighted FF is larger than for women, but it stays effectively constant with age.

Figure 4a, b shows the PDFF as a function of age for women and men. Figure 4c shows a negative association of PDFF with T_{2w} with R^2 = 0.21 ($p < 0.001$), which could only be found for women (men: $p > 0.05$). In addition, when the effects of both age and T_{2w} were considered, a multiple linear regression indicated that PDFF variation was dependent on both the effects of age ($p < 0.001$) and T_{2w} ($p = 0.028$) with R^2 = 0.55. Finally,

Table 1. Linear regression analysis results: bone marrow fat fraction (%) as a function of age (years) for women (n = 54)

	Slope	Intercept	R^2	p
Proton density fat fraction	0.690	8.9	0.49	<0.001
T_2-weighted fat fraction at TE = 11 ms	0.773	12.3	0.48	<0.001
T_2-weighted fat fraction at TE = 15 ms	0.796	13.9	0.47	<0.001
T_2-weighted fat fraction at TE = 20 ms	0.819	16.1	0.46	<0.001
T_2-weighted fat fraction at TE = 25 ms	0.835	18.5	0.46	<0.001

Table 2. Linear regression analysis results: bone marrow fat fraction (%) as a function of age (years) for men (n = 32)

	Slope	Intercept	R^2	p
Proton density fat fraction	0.530	19.3	0.46	<0.001
T_2-weighted fat fraction at TE = 11 ms	0.562	28.4	0.47	<0.001
T_2-weighted fat fraction at TE = 15 ms	0.560	32.3	0.47	<0.001
T_2-weighted fat fraction at TE = 20 ms	0.548	37.4	0.47	<0.001
T_2-weighted fat fraction at TE = 25 ms	0.526	42.8	0.46	<0.001

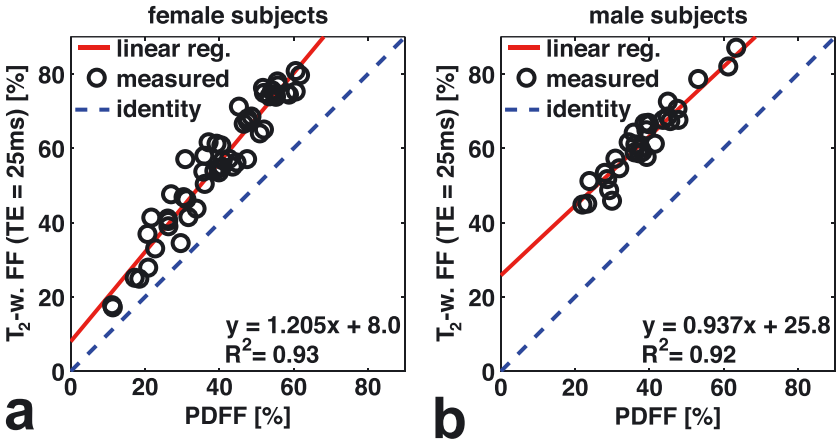

Figure 3. Linear regression analysis results between the proton density fat fraction (PDFF) and T_2-weighted fat fraction (T_2-w.FF) at TE = 25 ms for women (n = 54) (a) and men (n = 32) (b). The broken line represents the identity line to highlight the overestimation of the fat fraction without T_2 correction.

PDFF showed no statistically significant correlation with body mass index.

DISCUSSION

Vertebral bone marrow fat quantification using single-voxel MRS can be biased because of the confounding effects of overlapping water–fat peaks and differences in the T_2 relaxation times of the water and fat peaks. First, the presence of trabecular bone shortens the T_2* relaxation time of all bone marrow compartments. The shortened T_2* relaxation time induces broad peaks and causes severe overlap of the different water–fat peaks. Second, the two components of the bone marrow spectrum, water and fat, differ in their T_2 relaxation time, leading to T_2-weighted FF if measurements at only a single TE are considered. To enable a quantification of the fat spectrum which takes into account all fat peaks, even fat peaks E and F that overlap with the water peak, the present study incorporated a priori knowledge and used linear regression analysis in a first step to characterize the vertebral bone marrow fat spectrum. To remove any T_2 decay effects, the present study acquired spectra at four different TEs and performed T_2 correction, also enabling the reliable derivation of T_{2w} and T_{2f}.

The presently derived bone marrow ndb and nmidb values are higher than those reported in the liver (ndb = 1.92 and nmidb = 0.32) (24), but are comparable with the results of previous studies in bone marrow. Specifically, based on the present fat spectrum characterization results (ndb = 3.13, nmidb = 0.70), the fractions of monounsaturated fatty acids (f_{MUFA}) and polyunsaturated fatty acids (f_{PUFA}) were determined, as described previously in ref. (29). The derived values of f_{MUFA} = 0.59 and f_{PUFA} = 0.23 were then compared with the values obtained by measurements of bone marrow samples with gas chromatography or high-resolution NMR. The presently determined f_{MUFA} and f_{PUFA} values are slightly higher, but comparable with, the values measured for

NMR IN BIOMEDICINE

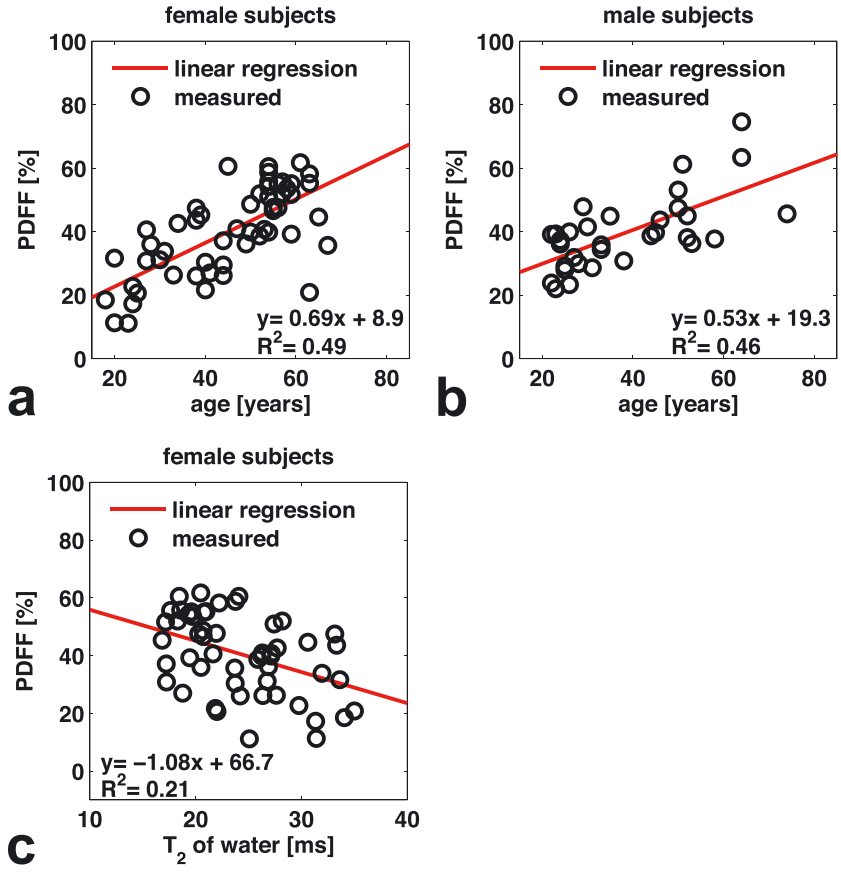

Figure 4. Linear regression analysis results between age and proton density fat fraction (PDFF) for women (a) and men (b). (c) Linear regression analysis results between T_2 of water (T_{2w}) and PDFF for women.

bone marrow fat in the proximal femur and tibia in ref. (30) and vertebral bone marrow fat in ref. (6). In addition, the computed area of peak F relative to the area of peaks A + B is 10.36%, and the computed area of peak F relative to the area of all fat peaks is 7.38%, which are both within the range of the values reported in previous studies (6,7,17,18).

The present results show that the vertebral bone marrow water component has a significantly shorter T_2 relaxation time than the fat component (mean values: T_{2w} = 22.5 ms, T_{2f} = 72.3 ms). Therefore, an FF measured from a single-TE MRS experiment will depend on the TE of that experiment. T_{2f} does not show large variations across subjects. However, the T_{2w} relaxation time shows a much higher coefficient of variation (CV) than the T_{2f} relaxation time (CV_{T2w} = 0.23, CV_{T2f} = 0.09), which is in agreement with results reported previously at 1.5 T (19). Therefore, a T_2 correction using reference T_2 values (16) will not totally remove T_2 weighting effects. Instead, a T_2 correction based on the measured T_2 values in a multi-TE MRS experiment is necessary in order to totally remove T_2 weighting effects.

An example of the T_2 weighting effect is shown in the investigation of the age dependence of the vertebral bone marrow FF. As TE increases, the age dependence of the FF follows a different linear relationship if T_2 weighting effects are not removed. Therefore, a T_2-weighted FF depends on the experimental parameters, and PDFF should be used instead when forming a bone marrow FF reference database and when comparing bone marrow FF values in disease (e.g. osteoporosis) with the reference database. The present results show a different overestimation of FF between women and men, when T_2 weighting effects are not considered. On the one hand, the reported differences between women and men are consistent with previous findings that there is a sex dependence of the bone marrow FF. As already mentioned in the Introduction, men tend to have a higher bone marrow FF than women at younger ages, with a reversal of this difference in older subjects (14–16). On the other, the reported difference in the T_2 weighting effect between men and women is partially related to the presently reported difference in T_2 relaxation times, particularly T_{2w} (women: T_{2w} = 24.6 ± 5.1 ms, T_{2f} = 72.6 ± 6.0 ms; men: T_{2w} = 18.6 ± 2.4 ms, T_{2f} = 71.8 ± 6.5 ms). This difference in T_2 relaxation times remains, even when only subjects younger than 41 years are considered, in order to yield a more comparable age distribution in the presently studied female and male cohorts (women, age $<$ 41 years, n = 20: T_{2w} = 26.7 ± 5.5 ms, T_{2f} = 77.0 ± 12.5 ms; men, age $<$ 41 years, n = 19: T_{2w} = 19.3 ± 2.5 ms, T_{2f} = 74.5 ± 6.7 ms). A possible explanation for this gender-dependent difference in T_{2w} may be the different contribution of fluid or hematopoietic blood cells to the water bone marrow component in women relative to men.

The present results also show a negative association between T_{2w} and PDFF in the scanned women, verifying the results of a preliminary study by Machann *et al.* (31). The dependence of PDFF on T_{2w} also remained statistically significant after correction for age effects. This negative association between T_{2w} and PDFF has two important implications. First, not employing the T_2 correction shows a dependence of the T_2-weighted FF on age with a slope that increases with the TE employed, and thus exaggerates the well-known age dependence of the bone marrow fat content. Second, the present results suggest that

differences in water–fat composition may also be associated with changes in water composition. For this purpose, T_{2w} could be considered as a marker of the bone marrow water compartment including hematopoietic marrow cells and fluid. Therefore, further studies are needed to investigate changes in both PDFF and T_{2w} in disease and to analyze their relationship.

The present study has some limitations. First, a common fat spectrum was assumed in all subjects independent of age and gender. Despite the previously documented inter-individual variations in vertebral bone marrow FF unsaturation (6,7,18), the assumption of a constant triglyceride model across subjects can be considered adequate for the purpose of the fitting of fat peaks E and F for a robust FF quantification. Second, a common T_2 relaxation time was assumed for all fat peaks to improve the robustness of the fat T_2 extraction, as most fat peaks in the vertebral bone marrow exhibit strong overlap with other fat peaks. Although there are significant differences in T_2 relaxation times between the different components of the fat signal, the assumption of a common T_2 relaxation time for all fat peaks is necessary to allow a reasonable fitting. When fitting with individual T_2 relaxation times for each fat peak, the resulting T_2 values exhibit very high inter-individual standard deviations, even showing standard deviations three or four times as high as the mean value for some fat peaks. In addition, the main fat peak contributes the most to the common T_{2f} and its T_2 should therefore be affected the least by this simplifying assumption. As the main fat peak is also the peak representing the largest portion of the fat signal, the assumption of a common T_2 for all fat peaks should not induce significant bias on the calculated PDFF. Third, the number of men in the present study was smaller than the number of women and they had a non-uniform age distribution. Further studies are needed to better address the relationship between PDFF, age and T_{2w} in larger scale male populations.

CONCLUSIONS

Vertebral bone marrow fat quantification using single-voxel MRS should be based on a multi-TE MRS measurement and should aim to quantify both PDFF and T_{2w}. The extraction of the bone marrow PDFF, instead of a T_2-weighted FF, is essential in order to standardize MRS-based bone marrow fat quantification, but can also simultaneously provide T_{2w}, which might be considered as an additional parameter potentially sensitive to the composition of the water compartment.

Acknowledgements

The present study was supported by Philips Healthcare.

REFERENCES

1. Blake GM, Griffith JF, Yeung DK, Leung PC, Fogelman I. Effect of increasing vertebral marrow fat content on BMD measurement, T-Score status and fracture risk prediction by DXA. Bone 2009; 44(3): 495–501.
2. Griffith JF, Yeung DKW, Antonio GE, Lee FKH, Hong AWL, Wong SYS, Lau EMC, Leung PC. Vertebral bone mineral density, marrow perfusion, and fat content in healthy men and men with osteoporosis: dynamic contrast-enhanced MR imaging and MR spectroscopy. Radiology 2005; 236(3): 945–951.
3. Griffith JF, Yeung DKW, Antonio GE, Wong SYS, Kwok TCY, Woo J, Leung PC. Vertebral marrow fat content and diffusion and perfusion indexes in women with varying bone density: MR evaluation. Radiology 2006; 241(3): 831–838.
4. Schellinger D, Lin CS, Hatipoglu HG, Fertikh D. Potential value of vertebral proton MR spectroscopy in determining bone weakness. Am. J. Neuroradiol. 2001; 22(8): 1620–1627.
5. Schwartz AV, Sigurdsson S, Hue TF, Lang TF, Harris TB, Rosen CJ, Vittinghoff E, Siggeirsdottir K, Sigurdsson G, Oskarsdottir D, Shet K, Palermo L, Gudnason V, Li X. Vertebral bone marrow fat associated with lower trabecular BMD and prevalent vertebral fracture in older adults. J. Clin. Endocr. Metab. 2013; 98(6): 2294–2300.
6. Yeung DKW, Griffith JF, Antonio GE, Lee FKH, Woo J, Leung PC. Osteoporosis is associated with increased marrow fat content and decreased marrow fat unsaturation: a proton MR spectroscopy study. J. Magn. Reson. Imaging 2005; 22(2): 279–285.
7. Baum T, Yap SP, Karampinos DC, Nardo L, Kuo D, Burghardt AJ, Masharani UB, Schwartz AV, Li X, Link TM. Does vertebral bone marrow fat content correlate with abdominal adipose tissue, lumbar spine bone mineral density, and blood biomarkers in women with type 2 diabetes mellitus? J. Magn. Reson. Imaging 2012; 35(1): 117–124.
8. Bredella MA, Torriani M, Ghomi RH, Thomas BJ, Brick DJ, Gerweck AV, Rosen CJ, Klibanski A, Miller KK. Vertebral bone marrow fat is positively associated with visceral fat and inversely associated with IGF-1 in obese women. Obesity 2011; 19(1): 49–53.
9. Bolan PJ, Arentsen L, Sueblinvong T, Zhang Y, Moeller S, Carter JS, Downs LS, Ghebre R, Yee D, Froelich J, Hui S. Water–fat MRI for assessing changes in bone marrow composition due to radiation and chemotherapy in gynecologic cancer patients. J. Magn. Reson. Imaging 2013; 38(6): 1578–1584.
10. Carmona R, Pritz J, Bydder M, Gulaya S, Zhu H, Williamson CW, Welch CS, Vaida F, Bydder G, Mell LK. Fat composition changes in bone marrow during chemotherapy and radiation therapy. Int. J. Radiat. Oncol. Biol. Phys. 2014; 90(1): 155–163.
11. Karampinos DC, Melkus G, Baum T, Bauer JS, Rummeny EJ, Krug R. Bone marrow fat quantification in the presence of trabecular bone: initial comparison between water–fat imaging and single-voxel MRS. Magn. Reson. Med. 2013; 71(3): 1158–1165
12. Kuhn JP, Hernando D, Meffert PJ, Reeder S, Hosten N, Laqua R, Steveling A, Ender S, Schroder H, Pillich DT. Proton-density fat fraction and simultaneous R2* estimation as an MRI tool for assessment of osteoporosis. Eur. Radiol. 2013; 23(12): 3432–3439.
13. Griffith JF. *Bone Marrow Changes in Osteoporosis. Osteoporosis and Bone Densitometry Measurements*. Springer-Verlag: Berlin, Heidelberg; 2013.
14. Griffith JF, Yeung DK, Ma HT, Leung JC, Kwok TC, Leung PC. Bone marrow fat content in the elderly: a reversal of sex difference seen in younger subjects. J. Magn. Reson. Imaging 2012; 36(1): 225–230.
15. Ishijima H, Ishizaka H, Horikoshi H, Sakurai M. Water fraction of lumbar vertebral bone marrow estimated from chemical shift misregistration on MR imaging: normal variations with age and sex. Am. J. Roentgenol. 1996; 167(2): 355–358.
16. Kugel H, Jung C, Schulte O, Heindel W. Age- and sex-specific differences in the ^{1}H-spectrum of vertebral bone marrow. J. Magn. Reson. Imaging 2001; 13(2): 263–268.
17. Li X, Kuo D, Schafer AL, Porzig A, Link TM, Black D, Schwartz AV. Quantification of vertebral bone marrow fat content using 3 Tesla MR spectroscopy: reproducibility, vertebral variation, and applications in osteoporosis. J. Magn. Reson. Imaging 2011; 33(4): 974–979.
18. Patsch JM, Li X, Baum T, Yap SP, Karampinos DC, Schwartz AV, Link TM. Bone marrow fat composition as a novel imaging biomarker in postmenopausal women with prevalent fragility fractures. J. Bone Miner. Res. 2013; 28(8): 1721–1728.
19. Schick F, Bongers H, Jung W-I, Eismann B, Skalej M, Einsele H, Lutz O, Claussen CD. Proton relaxation times in human red bone marrow by volume selective magnetic resonance spectroscopy. Appl. Magn. Reson. 1992; 3: 947–963.
20. Schick F, Bongers H, Jung WI, Skalej M, Lutz O, Claussen CD. Volume-selective proton MRS in vertebral bodies. Magn. Reson. Med. 1992; 26(2): 207–217.
21. Shen W, Gong X, Weiss J, Jin Y. Comparison among T1-weighted magnetic resonance imaging, modified Dixon method, and magnetic resonance spectroscopy in measuring bone marrow fat. J. Obesity 2013; 2013: 298675 doi: 10.1155/2013/298675
22. Roldan-Valadez E, Pina-Jimenez C, Favila R, Rios C. Gender and age groups interactions in the quantification of bone marrow fat content in lumbar spine using 3T MR spectroscopy: a multivariate analysis of covariance (Mancova). Eur. J. Radiol. 2013; 82(11): e697–e702.

23. Reeder SB, Cruite I, Hamilton G, Sirlin CB. Quantitative assessment of liver fat with magnetic resonance imaging and spectroscopy. J. Magn. Reson. Imaging 2011; 34(4): 729–749.
24. Hamilton G, Yokoo T, Bydder M, Cruite I, Schroeder ME, Sirlin CB, Middleton MS. In vivo characterization of the liver fat ^{1}H MR spectrum. NMR Biomed. 2011; 24(7): 784–790.
25. Sharma P, Martin DR, Pineda N, Xu Q, Vos M, Anania F, Hu X. Quantitative analysis of T2-correction in single-voxel magnetic resonance spectroscopy of hepatic lipid fraction. J. Magn. Reson. Imaging 2009; 29(3): 629–635.
26. Hamilton G, Middleton MS, Bydder M, Yokoo T, Schwimmer JB, Kono Y, Patton HM, Lavine JE, Sirlin CB. Effect of PRESS and STEAM sequences on magnetic resonance spectroscopic liver fat quantification. J. Magn. Reson. Imaging 2009; 30(1): 145–152.
27. Marshall I, Higinbotham J, Bruce S, Freise A. Use of Voigt lineshape for quantification of in vivo ^{1}H spectra. Magn. Reson. Med. 1997; 37 (5): 651–657.
28. Ren J, Dimitrov I, Sherry AD, Malloy CR. Composition of adipose tissue and marrow fat in humans by ^{1}H NMR at 7 Tesla. J. Lipid Res. 2008; 49(9): 2055–2062.
29. Peterson P, Mansson S. Simultaneous quantification of fat content and fatty acid composition using MR imaging. Magn. Reson. Med. 2013; 69(3): 688–697.
30. Griffith JF, Yeung DK, Ahuja AT, Choy CW, Mei WY, Lam SS, Lam TP, Chen ZY, Leung PC. A study of bone marrow and subcutaneous fatty acid composition in subjects of varying bone mineral density. Bone 2009; 44(6): 1092–1096.
31. Machann J, Brechtel IK, Duda SH, Lutz O, Claussen CD, Schick F. Correlation between water content, transverse relaxation, and magnetization transfer in red bone marrow of healthy young subjects. *Proceedings of the ISMRM 8th Scientific Meeting & Exhibition in Denver, Colorado, USA*, 2000; 1945.

8.2 Journal Publication II: ADC Quantification of the Vertebral Bone Marrow Water Component: Removing the Confounding Effect of Residual Fat.

The publication entitled *ADC Quantification of the Vertebral Bone Marrow Water Component: Removing the Confounding Effect of Residual Fat* was published in Magnetic Resonance in Medicine (ISSN: 1522-2594). The manuscript was authored by Michael Dieckmeyer, Stefan Ruschke, Holger Eggers, Hendrik Kooijman, Ernst J. Rummeny, Jan S. Kirschke, Thomas Baum and Dimitrios C. Karampinos.

8.2.1 Abstract

Purpose To remove the confounding effect of unsuppressed fat on the imaging-based apparent diffusion coefficient (ADC) of the vertebral bone marrow water component when using spectrally selective fat suppression and to compare and validate the proposed quantification strategy against diffusion-weighted magnetic resonance spectroscopy (DW-MRS).

Methods Twelve subjects underwent diffusion-weighted imaging (DWI) and DW-MRS of the vertebral bone marrow. A theoretical model was developed to take into account and correct the effects of residual fat on ADC, incorporating additional measurements for proton density fat fraction (PDFF) and water T_2 (T_{2w}). Uncorrected and corrected DWI-based ADC was compared with DW-MRS-based ADC using the Bland-Altman method.

Results There was a systematic bias equal to $0.118 \pm 0.116 \cdot 10^{-3}$ mm/s between DWI and DW-MRS when no correction was performed. Taking into account measured PDFF and constant T_{2w} reduced the bias to $0.006 \pm 0.128 \cdot 10^{-3}$ mm/s. Using the proposed approach with both individually measured PDFF and T_{2w} reduced both the bias and the limits of agreement between DWI and DW-MRS ($0.018 \pm 0.065 \cdot 10^{-3}$ mm/s).

Conclusion By taking into account the presence of residual fat in a modified signal model that incorporates additional individual measurements of PDFF and T_{2w}, good agreement of imaging-based ADC with MRS-based ADC can be achieved in vertebral bone marrow.

8.2.2 Author contributions

I performed the recruitment and MRI examinations of the study participants, manual segmentation of ROIs within the vertebral bone marrow as well as the simulation, post-processing, quantification and statistical analysis of the MRS and MRI ROI data using

MATLAB (Mathworks, Natick, MA). In collaboration with the coauthors I designed the MRI protocol, implemented the MRS postprocessing framework using MATLAB, analyzed and interpreted the data and drafted the publication manuscript.

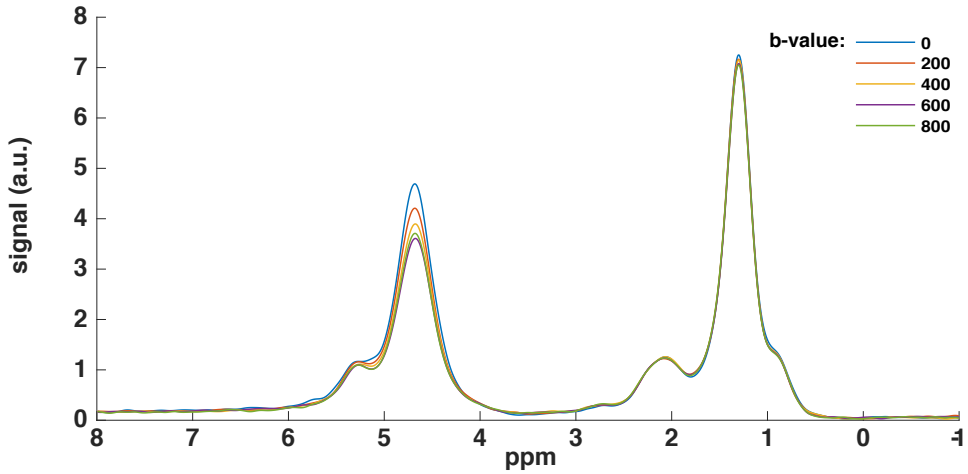

Figure 8.2: Sample multi-b-value DW-STEAM spectrum of one of the subjects. The difference in diffusion-dependent signal decay of the main fat component (at 1.3 ppm) and the water component (at 4.7 ppm) can be appreciated. ppm: parts per million, a.u.: arbitrary units.

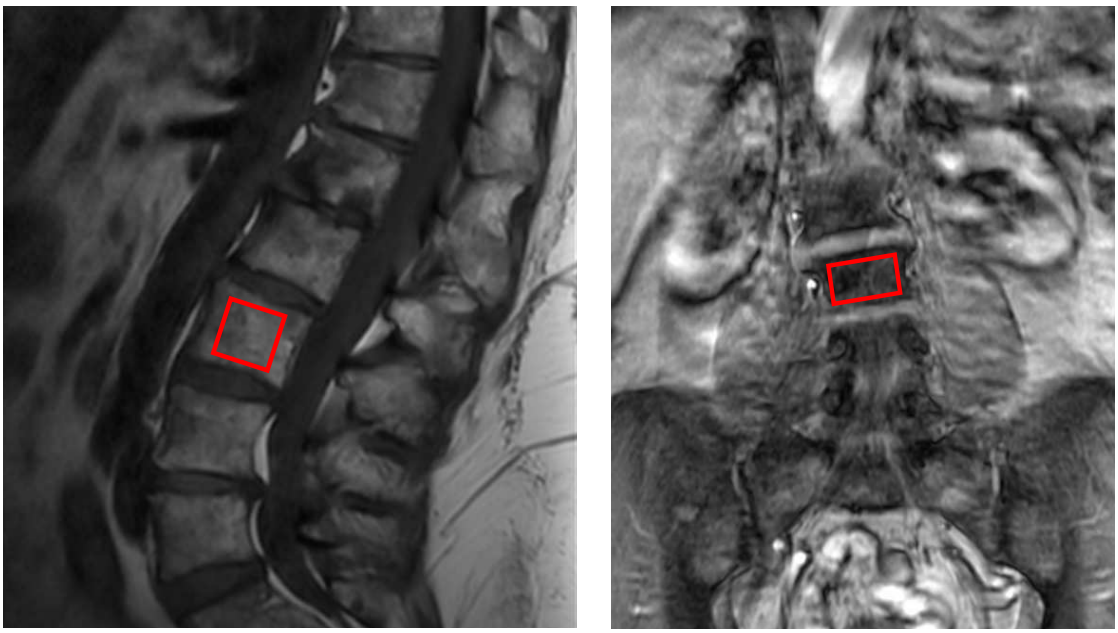

Figure 8.3: Placement of the volume of interest (red) during an MRS experiment within the bone marrow of the L3 vertebral body. For this purpose the acquired sagittal (left) and coronal (right) images were used. Note that the VOI was placed slightly anterior within the vertebral body to avoid the venous plexus in the posterior part.

ADC Quantification of the Vertebral Bone Marrow Water Component: Removing the Confounding Effect of Residual Fat

Michael Dieckmeyer,[1]* Stefan Ruschke,[1] Holger Eggers,[2] Hendrik Kooijman,[3] Ernst J. Rummeny,[1] Jan S. Kirschke,[4] Thomas Baum,[1] and Dimitrios C. Karampinos[1]

Purpose: To remove the confounding effect of unsuppressed fat on the imaging-based apparent diffusion coefficient (ADC) of the vertebral bone marrow water component when using spectrally selective fat suppression and to compare and validate the proposed quantification strategy against diffusion-weighted magnetic resonance spectroscopy (DW-MRS).
Methods: Twelve subjects underwent diffusion-weighted imaging (DWI) and DW-MRS of the vertebral bone marrow. A theoretical model was developed to take into account and correct the effects of residual fat on ADC, incorporating additional measurements for proton density fat fraction (PDFF) and water T_2 (T_{2w}). Uncorrected and corrected DWI-based ADC was compared with DW-MRS–based ADC using the Bland–Altman method.
Results: There was a systematic bias equal to $0.118 \pm 0.116 \times 10^{-3}$ mm^2/s between DWI and DW-MRS when no correction was performed. Taking into account measured PDFF and constant T_{2w} reduced the bias to $0.006 \pm 0.128 \times 10^{-3}$ mm^2/s. Using the proposed approach with both individually measured PDFF and T_{2w} reduced both the bias and the limits of agreement between DWI and DW-MRS ($0.018 \pm 0.065 \times 10^{-3}$ mm^2/s).
Conclusion: By taking into account the presence of residual fat in a modified signal model that incorporates additional individual measurements of PDFF and T_{2w}, good agreement of imaging-based ADC with MRS-based ADC can be achieved in vertebral bone marrow. **Magn Reson Med 78:1432–1441, 2017. © 2016 International Society for Magnetic Resonance in Medicine.**

Key words: bone marrow; ADC quantification; magnetic resonance spectroscopy (MRS); diffusion-weighted imaging (DWI); spine

INTRODUCTION

Healthy vertebral bone marrow consists of two main MR-sensitive components: hematopoietic red blood cells (containing primarily water) and adipocytes (containing primarily fat). The apparent diffusion coefficient of the bone marrow water component (ADC_w) has been measured through quantitative analysis of diffusion-weighted imaging (DWI) data in numerous previous studies (1–6) and has been proposed as a biomarker for differentiating between benign and malignant vertebral fractures (7). Previous works have also investigated the relationship between ADC_w and anatomical location (4,6,8), age (5) and bone mineral density (9–12).

DWI of the spine has traditionally been performed in axial or sagittal orientation using in most cases a single-shot echo planar imaging (EPI) sequence. In order to reduce chemical shift artifacts and the confounding of the water diffusion quantification induced by lipid signal, some previous studies measuring vertebral ADC_w have used fat suppression (2). The employed fat suppression has been based primarily on spectrally selective pulses (chemical saturation) or combination of spectral selection and inversion recovery (spectral inversion recovery). Figure 1 shows typical in vivo vertebral bone marrow diffusion-weighted spectra in a healthy volunteer at different b-values. By using spectrally selective pulses, the signal of the main fat peaks (in the spectral region between 0 and 3 ppm; Fig. 1) is nulled without affecting signal located around the water peak location (4.7 ppm). However, since the NMR spectrum of triglycerides has a nonnegligible amount of signal located close to the water peak (labeled as olefinic and glycerol fat signal), the fat signal close to the water peak does not get suppressed (13). Taking into account the large difference in the diffusion coefficient between bone marrow water and fat (13,14) (Fig. 1), we hypothesize that the residual unsuppressed fat can bias ADC_w quantification toward lower values. Such bias can be of particular importance for longitudinal as well as cross-sectional studies of vertebral bone marrow, where the marrow fat fraction also exhibits strong interindividual and age-related variation (15–18).

In 2013, Hansmann et al. (14) investigated a comparable problem in the context of liver ADC quantification in the presence of hepatic steatosis. The investigators developed a modified model for the diffusion signal taking into account the presence of unsuppressed fat signal, based on a measurement of proton density fat fraction (PDFF). Multiple echo time (TE) magnetic resonance spectroscopy (MRS) was used to measure PDFF needed as an input to the modified model. However, Hansmann et al. measured PDFF in a single location, neglecting any

[1]Department of Diagnostic and Interventional Radiology, Klinikum rechts der Isar, Technische Universität München, Munich, Germany.
[2]Philips Research Laboratory, Hamburg, Germany.
[3]Philips Healthcare, Hamburg, Germany.
[4]Section of Diagnostic and Interventional Neuroradiology, Klinikum rechts der Isar, Technische Universität München, Munich, Germany.

Grant sponsor: Philips Healthcare.

*Correspondence to: Michael Dieckmeyer, Dipl.-math. (German equivalent to MSc in Mathematics), Department of Diagnostic and Interventional Radiology, Klinikum rechts der Isar, Ismaninger Str. 22, 81675 Munich, Germany. E-mail: michael.dieckmeyer@mytum.de

Received 19 July 2016; revised 5 October 2016; accepted 18 October 2016
DOI 10.1002/mrm.26550
Published online 8 November 2016 in Wiley Online Library (wileyonlinelibrary.com).

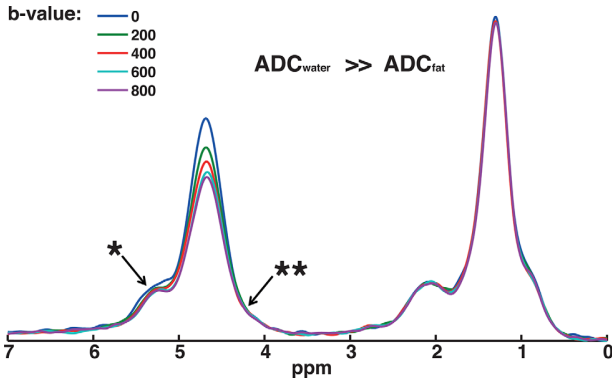

FIG. 1. Bone marrow DW-MRS spectra at increasing b-values. The different signal decay of the water and the main fat peak indicates the difference between the ADCs of water and fat. The olefinic fat peak (*) and glycerol (**) fat peak exhibit strong overlap with the water peak.

intrasubject variation in PDFF, and used average a priori known values for T_2 of the water and fat components, neglecting any intersubject or intrasubject variation in T_2 of water. Using a chemical shift encoding-based water–fat separation technique for PDFF mapping and additionally measuring the T_2 of the water (T_{2w}) have the potential to achieve a more accurate ADC correction on an individual basis and allow the simultaneous analysis of multiple vertebrae. In addition, Hansmann et al. did not compare the corrected ADC_w with a reference value. Single voxel diffusion-weighted MRS (DW-MRS) constitutes an alternative method to measure ADC_w (19,20) and can be used as a reference. The inherently high spectral resolution of DW-MRS enables good differentiation of the water and fat peaks and reliable extraction of ADC_w.

Therefore, the purpose of the present work was to analyze the ADC of the vertebral bone marrow water component using a modified signal model in order to remove the confounding effect of unsuppressed fat and to compare and validate the proposed quantification strategy against DW-MRS.

METHODS

Theory

In the presence of imperfectly suppressed fat, the diffusion-weighted signal of a SE-EPI sequence as a function of b-value can be modeled as

$$S(b,TE) = S_0\left[\alpha PDFFe^{-\frac{TE}{T_{2f}}}e^{-b\,ADC_f} + (1-PDFF)e^{-\frac{TE}{T_{2w}}}e^{-bA\,DC_w}\right]. \quad [1]$$

where S_0 is the proton density; α is the fraction of unsuppressed fat spectrum energy; *PDFF* is the proton density fat fraction; *TE* is the echo time; T_{2f} and T_{2w} are the T_2 relaxation times of the residual fat and the water component, respectively; and ADC_f and ADC_w are the apparent diffusion coefficients of the residual fat and the water component, respectively. The above expression assumes that all unsuppressed fat peaks have equal T_{2f} and ADC_f.

Given that ADC_f is much lower than ADC_w, and hence the fat signal is only decaying minimally at the employed b-values, it was assumed that $ADC_f = 0\,mm^2/s$. For simplifying the notation ADC is used from now on instead of ADC_w.

$$S(b,TE) = S_0\left[\alpha PDFFe^{-\frac{TE}{T_{2f}}} + (1-PDFF)e^{-\frac{TE}{T_{2w}}}e^{-b\,ADC}\right] \quad [2]$$

In the quantitative analysis of the DWI data, the following methods are compared.

Method 1: monoexponential model

Method 1 relies on the fitting of a b-series signal at a constant $TE = TE_{b\text{-series}}$ to the conventional monoexponential model neglecting the presence of unsuppressed fat:

$$S(b,TE = TE_{b-series}) = S_{0_1}e^{-b\,ADC_1}, \quad [3]$$

where S_{01} and ADC_1 are the fitted parameters.

Method 2: model proposed by Hansmann et al

As mentioned above, a signal model has been previously proposed considering the presence of unsuppressed fat (α and PDFF are known) and assuming constant a priori known values for $T_{2w} = T_{2w_{priori}}$ and $T_{2f} = T_{2f_{priori}}$ (14). Therefore, method 2 relies on the fitting of a b-series signal at a constant $TE = TE_{b\text{-series}}$ to the expression

$$S(b,TE = TE_{b-series}) = S_{0_2}\left[\alpha PDFFe^{-\frac{TE}{T_{2f_{priori}}}} + (1-PDFF)e^{-\frac{TE}{T_{2w_{priori}}}}e^{-b\,ADC_2}\right], \quad [4]$$

where S_{02} and ADC_2 are the fitted parameters.

Method 3: proposed model

T_2-weighthing effects in Equation [2] are different across subjects and spatial locations due to intersubject variability in T_{2w} and T_{2f} (18). Given that for a typical DW spin echo at 3T $TE > T_{2w}$ and $TE < T_{2f}$, intersubject variability in the relative T_2-weighting is much higher for the water component than for the fat component. This can be showed by computing the ratio of T_2-weighting factors for water and fat, based on the minimum and maximum T_2 values from Dieckmeyer et al. (18) and $TE_{b\text{-series}} = 56$ ms (value used for in vivo imaging):

$$\frac{exp\left(-\frac{TE_{b-series}}{T_{2w,max}}\right)}{exp\left(-\frac{TE_{b-series}}{T_{2w,min}}\right)} = 9.7, \quad \frac{exp\left(-\frac{TE_{b-series}}{T_{2f,max}}\right)}{exp\left(-\frac{TE_{b-series}}{T_{2f,min}}\right)} = 1.4\,.$$

A considerable limitation of method 2 is thus the assumption of constant T_{2w} across subjects and spatial locations. Specifically, in a recent study, a significant interindividual variation was reported in bone marrow T_{2w} (18). To overcome the above limitation, we propose method 3, which relies first on the fitting of a TE-series signal at a constant b-value ($b = 0$) to the expression

$$S(b,TE) = S_{0_{3a}}\left[\alpha PDFFe^{-\frac{TE}{T_{2f_{priori}}}} + (1-PDFF)e^{-\frac{TE}{T_{2w_3}}}\right], \quad [5]$$

where $S_{0_{3a}}$ and T_{2w_3} are the fitted parameters.

Taking into account the estimated T_{2w_3}, method 3 considers then the presence of unsuppressed fat by the fitting of a b-series signal at a constant $TE = TE_{b\text{-series}}$ to the expression

$$S(b, TE = TE_{b-series}) = S_{0_{3b}}\left[\alpha PDFFe^{-\frac{TE}{T_{2f_{priori}}}} + (1-PDFF)e^{-\frac{TE}{T_{2w_3}}}e^{-b\,ADC_3}\right], \quad [6]$$

where $S_{0_{3b}}$ and ADC_3 are the fitted parameters.

Simulations

In order to show the sensitivity of accurate ADC extraction with respect to T_{2w} and PDFF, a simulation analysis was performed comparing the aforementioned methods. It was assumed that the true ADC of water was equal to 0.4×10^{-3} mm^2/s. The parameters α and T_{2f} were assumed to be constant across subjects and determined equal to $\alpha = 0.1131$ and $T_{2f_{\text{priori}}} = 72.3$ ms based on a previous bone marrow MRS study (18). Specifically, α was determined based on the expression $\alpha = (2\ \text{ndb} + 5)/(3\ \text{CL} - \text{ndb} + 1)$ introduced by Hamilton et al. (21), where ndb and CL refer to the number of double bonds and chain length, respectively, of the mean bone marrow triglyceride spectrum as determined in (18) (ndb = 3.13 and CL = 17.3). Constant values were assumed for the other parameters related to the residual fat signal.

The signal as a function of b-value was simulated according to Equation [1] at TE = 56 ms and b = 200/400/600/800 s/mm^2, for a set of values of PDFF varying between 0% and 60% and T_{2w} varying between 15 ms and 35 ms. Method 1 was first used to extract ADC_1 assuming the conventional monoexponential model not accounting for residual fat signal (Eq. [3]). Method 2 was used to extract ADC_2 with the correct PDFF but constant $T_{2w_{\text{priori}}} = 22.5$ ms (18), therefore considering the presence of residual fat but assuming a constant T_{2w}. The deviation of the estimated ADC_1 and ADC_2 values from the correct ADC value was then computed using the relative error formula

$$\Delta ADC_i = \frac{ADC_i - ADC}{ADC}, \quad i = 1, 2. \quad [7]$$

Another important aspect of the proposed method is the sensitivity of the ADC results with respect to the accuracy in α, since α is assumed to be constant across subjects and not determined individually. For this purpose, a simulation analysis was performed making following assumptions: TE = 56 ms, $ADC_0 = 0.4 \times 10^{-3}$ mm^2/s, $\alpha_0 = 0.1131$, $T_{2f_{\text{priori}}} = 72.3$ ms, $T_{2w_{\text{priori}}} = 22.5$ ms. The relative ADC error was calculated as a function of α and PDFF. For this purpose, the parameters PDFF and α were varied from 10% to 60% and from $\alpha_0 - 0.03$ to $\alpha_0 + 0.03$, respectively, to generate S(b,TE) according to Equation [4]. The same equation was then used to fit for ADC_2 using $\alpha = \alpha_0$ and the according correct PDFF. The relative ADC error was then calculated according to

$$\Delta ADC = \frac{ADC_2 - ADC_0}{ADC_0}. \quad [8]$$

In Vivo Measurements

Subjects

The lumbar spine of 12 healthy subjects (women, n = 6; men, n = 6; age, 26.9 ± 4.0 y) was examined in a 3T scanner (Ingenia; Philips Healthcare, Best, Netherlands). Informed written consent was obtained from all subjects, and the study was approved by and performed in accordance with the rules and regulations of the Committee for Human Research at our institution.

MRI Measurements

Sagittal diffusion-weighted images at multiple b-values (b-series) were obtained using a spin echo single-shot EPI sequence (DW-EPI) combined with a reduced field of view (rFOV) technique (22) to reduce geometric distortions. Sequence parameters for the rFOV DW-EPI included repetition time (TR) = 6000 ms, echo time (TE) = 56 ms, b = 0/200/400/600/800 s/mm^2 applied in a single direction (F/H), spectral adiabatic inversion recovery (SPAIR) fat suppression (inversion time [TI] = 198 ms), FOV = 220 × 86 × 80 mm^3, PE direction = AP, 10 averages per b-value, voxel size = 3.0 × 3.0 × 8.0 mm^3, and scan time = 12 min. A spectrally selective inversion pulse is applied to flip the main fat peak spins by 180°. After a TI, the excitation pulse of the imaging sequence is applied. Adiabatic inversion pulses were used to reduce the sensitivity of the technique to B_1 inhomogeneity effects. The DW-EPI sequence was also run in a single subject at both b = 0 and b = 800 s/mm^2 with the RF power switched off to obtain noise images. ROIs were then drawn within the vertebral bodies, and the signal-to-noise ratio (SNR) was estimated using the National Electrical Manufacturers Association method (23,24).

The same EPI sequence without diffusion sensitizing but applying four different TEs was used for T_{2w} estimation (TE series). Sequence parameters for the rFOV multi–TE-EPI included TR = 6000 ms, TE = 26/36/46/56 ms, SPAIR fat suppression (TI = 198 ms), FOV = 220 × 86 × 80 mm^3, PE direction = AP, four averages per TE, voxel size = 3.0 × 3.0 × 8.0 mm^3, and scan time = 4 min.

For the generation of PDFF maps, an eight-echo gradient echo sequence (Dixon sequence) was used with sequence parameters: eight echoes per TR with non-flyback (alternating) read-out gradients, $TR/TE_{min}/\Delta TE = 15/1.47/1.05$ ms, FOV = 220 × 220 × 80 mm^3, voxel size = 1.8 × 1.8 × 4.0 mm^3, acquisition time = 117 s. A flip angle of flip 3° was used to minimize T_1 bias in the PDFF quantification.

MRS Measurements

The DW-MRS measurements were obtained using a single voxel Stimulated Echo Acquisition Mode (STEAM) acquisition with sequence parameters: TR/TM/TE = 6000/32/25 ms, b = 0/200/400/600/800 s/mm^2, voxel size = 15 ×

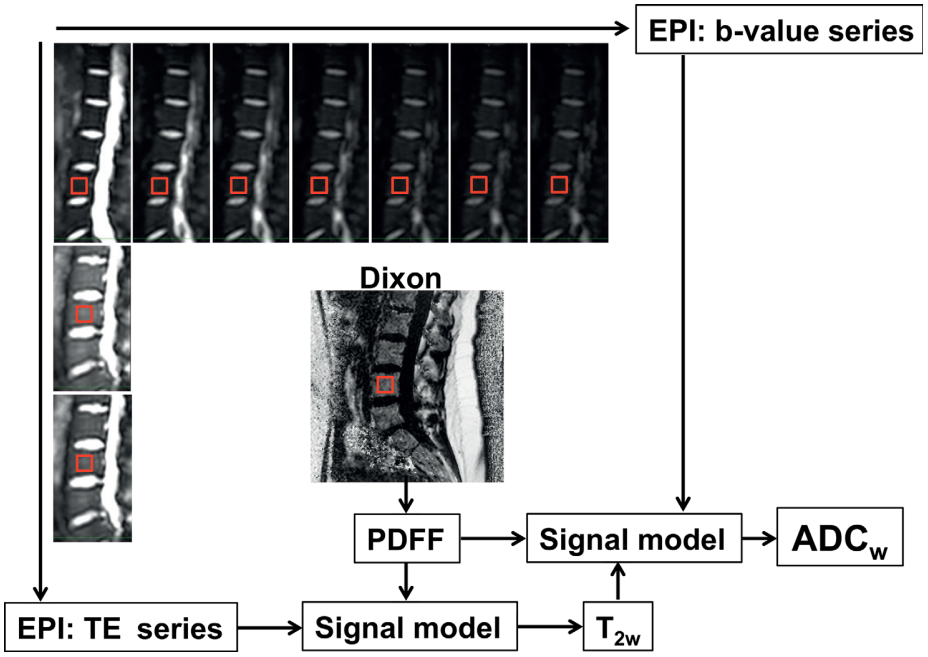

FIG. 2. Schematic of the proposed MRI protocol and postprocessing framework to remove the confounding effect of unsuppressed bone marrow fat. PDFF and T_{2w} are measured with a Dixon and TE series sequence, respectively, and used as input for the fitting routine that yields the corrected ADC_w.

$15 \times 15\,mm^3$, eight averages, RF pulse bandwidth = 2277 Hz (inducing a chemical shift displacement error of 5.6 % per ppm). The diffusion gradients switched to the opposite polarity for half of the acquired averages for eddy current phase correction (20). The voxel was placed within the L5 vertebral body taking into account chemical shift displacement effects and avoiding blood vessels.

Data Analysis

MRI Data

PDFF maps were generated online on the scanner based on the eight-echo gradient echo data by using a water–fat separation algorithm accounting for T_2* effects and the presence of multiple fat peaks (25).

To obtain individual values of S(b,TE) and PDFF at the vertebral bodies of each subject, the corresponding imaging data was averaged over a cuboid or prism shaped region of interest. ROIs were manually drawn by an experienced operator within the L2, L3, and L4 vertebral bodies of each subject based on the water-separated images generated by the Dixon sequence. The L5 ROI was generated automatically based on geometrical information of the MRS-voxel to assure maximum agreement of the tissue volume compared between DWI and DW-MRS.

The performance of the three methods currently under investigation was then compared. To avoid perfusion effects that affect the signal behavior at low b-values, only measurements at b-values $\geq 200\ s/mm^2$ were considered in the data fitting. First, a monoexponential fitting following Equation [3] using diffusion data acquired at multiple b-values was employed to estimate ADC_1 of each vertebral body (method 1). Second, a fitting following Equation [4] using experimentally measured PDFF values, $\alpha = 0.1131$, $T_{2f} = T_{2f_{priori}} = 72.3$ ms, $T_{2w} = T_{2w_{priori}} = 22.5$ ms, and diffusion data at multiple b-values was employed to estimate ADC_2 of each vertebral body (method 2).

Our proposed method (i.e., method 3) was then applied. A fitting following Equation [5] using experimentally measured PDFF values and T_2-weighted data at multiple TEs was employed to estimate $T_{2w} = T_{2w_3}$ of each vertebral body. An additional fitting following Equation [6] using experimentally measured PDFF values, experimentally measured $T_{2w} = T_{2w_3}$ and diffusion data at multiple b-values was employed to estimate ADC_3 of each vertebral body. Figure 2 shows a flow diagram of the proposed MRI acquisition and postprocessing routine.

MRS Data

MRS data processing was performed using in-house built software written in MATLAB (MathWorks, Natick, Massachusetts, USA). Assuming that the additional eddy current–induced phase term had an opposite sign between acquisitions with opposite DW gradient polarity, the eddy current–induced phase term was compensated for by combining the time-domain signals as described previously (20). Spectra were fitted using frequency-based methods. Pseudo-Voigt line shapes (26) with a $0.8 \cdot G + 0.2 \cdot L$ line shape for the fat peaks and a $0.2 \cdot G + 0.8 \cdot L$ line shape (G = Gauss, L = Lorentzian) for the water peak were employed. A mean bone marrow fat spectrum established by Dieckmeyer et al. (18) was used to reliably extract the water peak from the overlaying fat peaks. ADC_w was obtained by jointly fitting the spectral data at all b-values $\geq 200\ s/mm^2$ acquired with the DW-STEAM sequence. Eight fat peaks, located at 0.90, 1.30, 1.59, 2.00, 2.25, 2.77, 4.20, and 5.29 ppm, respectively, and one water peak, located at 4.67 ppm, were fitted.

Methods Comparison

The relative difference in the estimated DWI-based ADC between the proposed method 3 and the conventional

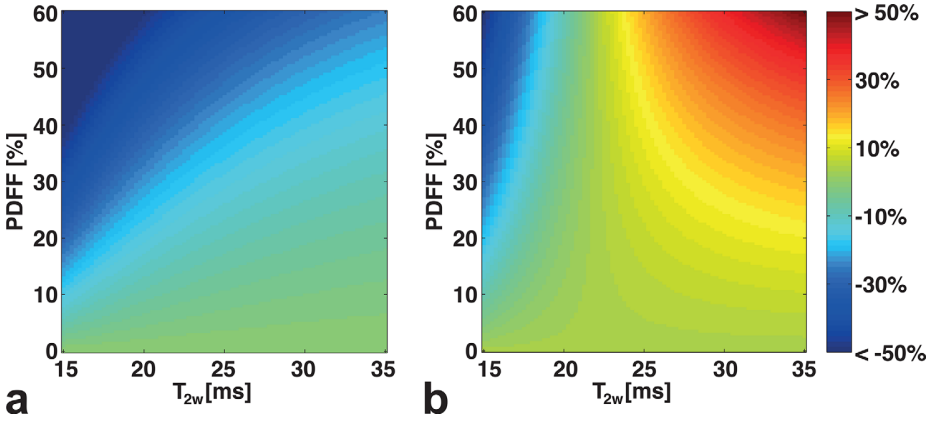

FIG. 3. Simulated relative error in ADC_w as a function of PDFF and T_{2w} when (**a**) no correction is performed (method 1) and (**b**) a correction is performed taking into account measured PDFF and constant T_{2w} (method 2).

method 1 and between the proposed method 3 and the previously proposed method 2 was examined against experimentally measured PDFF and T_{2w} in all imaged nondegenerated vertebrae (47 ROIs covering L2, L3, L4, and L5 in all subjects), using a linear regression analysis. The agreement of the ADC estimated by DW-MRS and DWI-based method 1, method 2, method 3, respectively, was analyzed in the L5 vertebrae using the Bland–Altman method (27).

RESULTS

Figure 3 shows the simulated relative difference of the ADC as a result of method 1 and method 2 in comparison with method 3 as a function of PDFF and T_{2w}. When the confounding effect of the residual fat signal was not considered (method 1), the relative ADC difference increased both with an increasing PDFF and a decreasing T_{2w} (Fig. 3a). Accounting for the residual fat with the previously proposed method by Hansmann et al. (14) using measured PDFF but constant average T_{2w} (method 2) reduced the ADC relative difference but still resulted in significant deviations in subjects exhibiting high PDFF and a strong disparity in T_{2w} compared with the assumed constant average T_{2w} (Fig. 3b).

Figure 4 show the simulation results of the relative ADC error as a function of α for increasing PDFF. Even at a high PDFF of 60% the relative ADC error is below 10% or 8% for an absolute inaccuracy in α of -0.02 or 0.02, respectively.

Figure 5 shows representative in vivo spine images with increasing diffusion weighting (Fig. 5a) and T_2-weighting (Fig. 5b). It is worth to notice the absence of any serious chemical shift artifacts due to any incomplete suppression of the main fat peak. The measured SNR over the five vertebral bodies of the spine was for the $b = 0$ image equal to 33.4 ± 5.1 (range, 25.8–37.8) and for the $b = 800$ s/mm^2 image equal to 17.3 ± 0.7 (range, 16.3–18.1).

Figure 6 shows examples of the logarithm of the experimentally measured DW signal as a function of the b-value and compares the performance of the three studied ADC quantification methods for a subject with $T_{2w} = 20.1$ ms and a subject with $T_{2w} = 32.5$ ms. The logarithm of the experimental data can be fitted by a linear fit for the range of the employed b-values (between 200 and 800 s/mm^2). A brief mathematical derivation of the association between the slope of the above linear relationship and ADC can be found in the Discussion section. Differences can be observed between the three fitted lines from the three employed methods only for $b > 2000$ s/mm^2.

Table 1 reports all mean and standard deviation values from the measured parameters in the in vivo experiments. The measured T_{2w} values were 24.0 ± 5.0 ms with a minimum value of 15 ms and a maximum value of 32.3 ms.

Figure 7 plots the relative difference in the experimentally estimated ADC between method 1 and method 3 (Figs. 7a and 7b) and between method 2 and method 3 (Fig. 7c and 7d). The relative ADC differences are plotted as a function of the measured PDFF (Figs. 7a and 7c) and T_{2w} (Fig. 7b and 7d). The relative ADC difference between method 1 and method 3 showed statistically significant linear correlations with both PDFF (Fig. 7a, $R^2 = 0.74$, $P < 0.001$) and T_{2w} (Fig. 7b, $R^2 = 0.81$, $P < 0.001$). The relative ADC difference between method 2 and method 3 showed a high, statistically significant linear correlation with T_{2w} (Fig. 7d, $R^2 = 0.83$, $P < 0.001$)

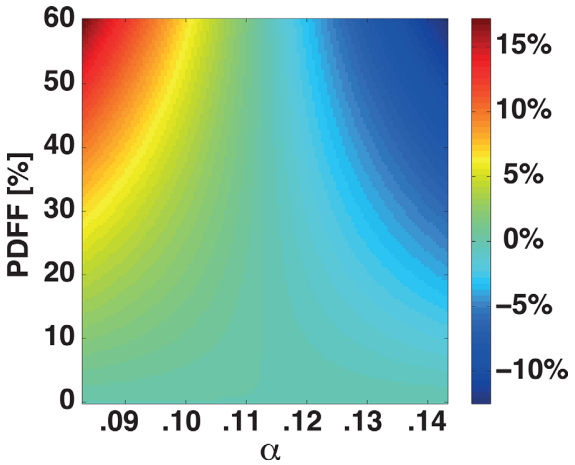

FIG. 4. Relative ADC_w error as result of simulation analysis to visualize the sensitivity of the proposed method to inaccuracy in α using Equation [8].

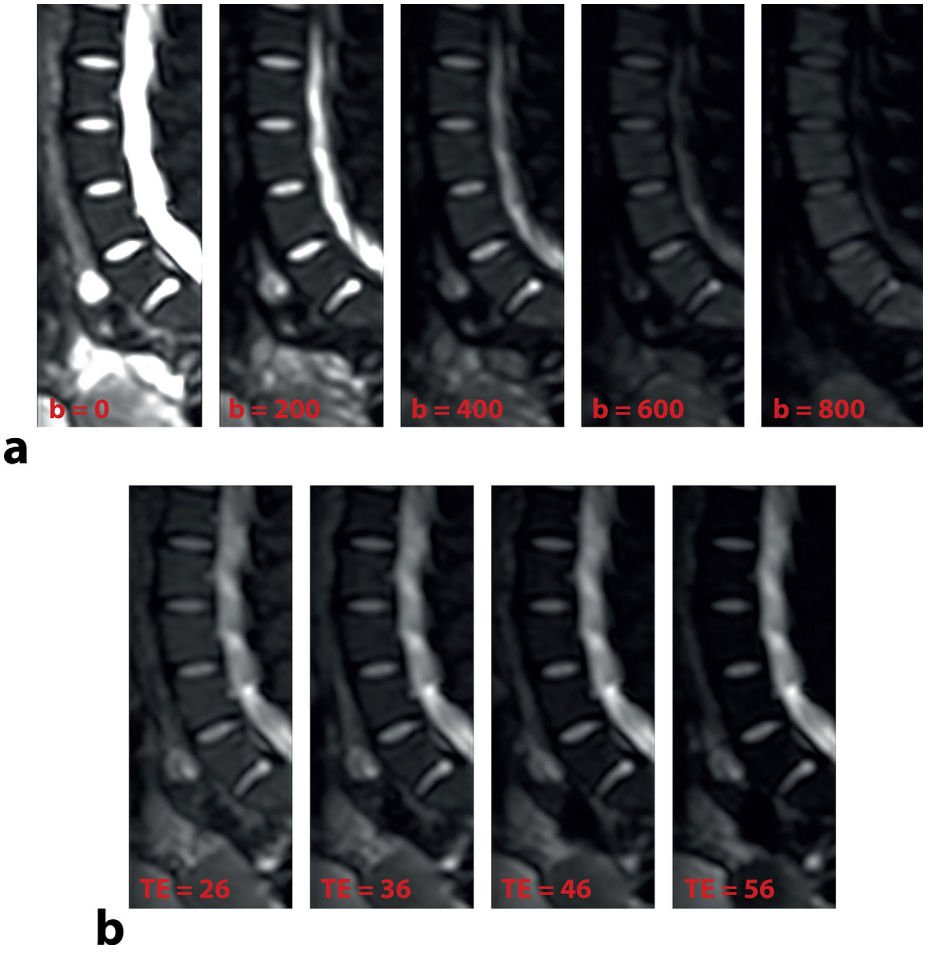

FIG. 5. (**a**) Sample images of the rFOV DW-EPI sequence using SPAIR fat suppression at increasing b-values and (**b**) sample images of the rFOV EPI sequence using SPAIR fat suppression at increasing echo times.

but a low, statistically significant linear correlation with PDFF (Fig. 7c, $R^2 = 0.21$, $P = 0.001$).

Figure 8 compares the MRI-based results using the three methods currently under investigation with the MRS-based results. The mean values over the L5 vertebral body of the 12 scanned subjects were $0.412 \pm 0.050 \times 10^{-3}$ mm^2/s using DW-MRS, $0.296 \pm 0.072 \times 10^{-3}$ mm^2/s using DWI with method 1, $0.406 \pm 0.083 \times 10^{-3}$ mm^2/s using DWI with method 2, and $0.394 \pm 0.057 \times 10^{-3}$ mm^2/s using DWI with method 3 (Fig. 8a). Bland–Altman plots in Fig. 8b, 8c, and 8d show the agreement of ADC measured by DW-MRS and

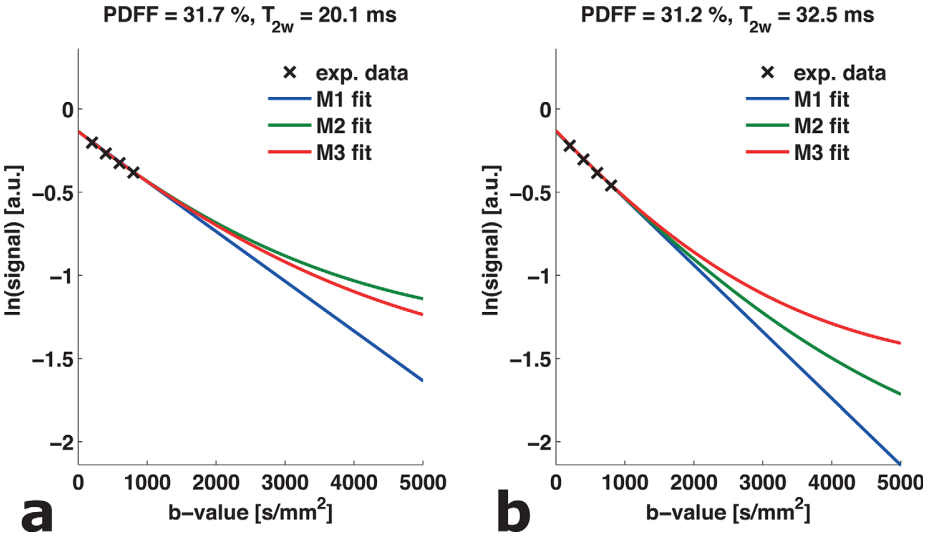

FIG. 6. Plot of the logarithm of the DW signal as a function of b-value: experimental data points and fitted lines using the three signal models for (**a**) a subject with $T_{2w} = 20.1$ ms and (**b**) a subject with $T_{2w} = 32.5$ ms.

Table 1
Quantitative Parameters

	PDFF	T_{2w} (ms)	ADC_{M1} (10^{-3} mm^2/s)	ADC_{M2} (10^{-3} mm^2/s)	ADC_{M3} (10^{-3} mm^2/s)	ADC_{MRS} (10^{-3} mm^2/s)
Mean	0.33	24.0	0.30	0.41	0.39	0.41
Standard deviation	0.12	5.0	0.07	0.09	0.06	0.05
Minimum	0.14	15.0	0.19	0.27	0.28	0.34
Maximum	0.55	32.3	0.40	0.58	0.49	0.50

DWI using method 1, method 2 and method 3, respectively. Bias and limits of agreement were $0.118 \pm 0.116 \times 10^{-3}$ mm^2/s for method 1, $0.006 \pm 0.126 \times 10^{-3}$ mm^2/s for method 2, and $0.018 \pm 0.065 \times 10^{-3}$ mm^2/s for method 3, respectively.

DISCUSSION

Residual fat signal has been shown to confound ADC measurements using spectrally selective fat suppression in different tissues including liver (14) and skeletal muscle (13,28,29). The confounding effect of residual fat on ADC measurements becomes of particular importance in bone marrow, where large PDFF values are observed. The present work quantifies the confounding effect of residual fat on bone marrow ADC using the conventional approach not considering the residual fat (method 1) and a previously proposed approach considering the presence of residual fat (method 2) using PDFF values from a separate water–fat acquisition (14). However, the residual fat signal in a diffusion-weighted acquisition is both dependent on the PDFF and the individual local T_2 value in conjunction with the amount of T_2-weighting. Therefore, we propose a new method for modeling the presence of residual fat (method 3) using PDFF and T_2 values from separate acquisitions.

When no correction is performed (method 1), the presented correlation analysis suggests a strong underestimation of ADC that increases with PDFF (Fig. 7a). In addition, the ADC underestimation introduced by residual fat signal increases as T_{2w} decreases (Fig. 7b). This is plausible because the residual fat signal responsible for the underestimation is proportional to the PDFF and is affected by T_2-weighting: a lower T_{2w} implies a higher

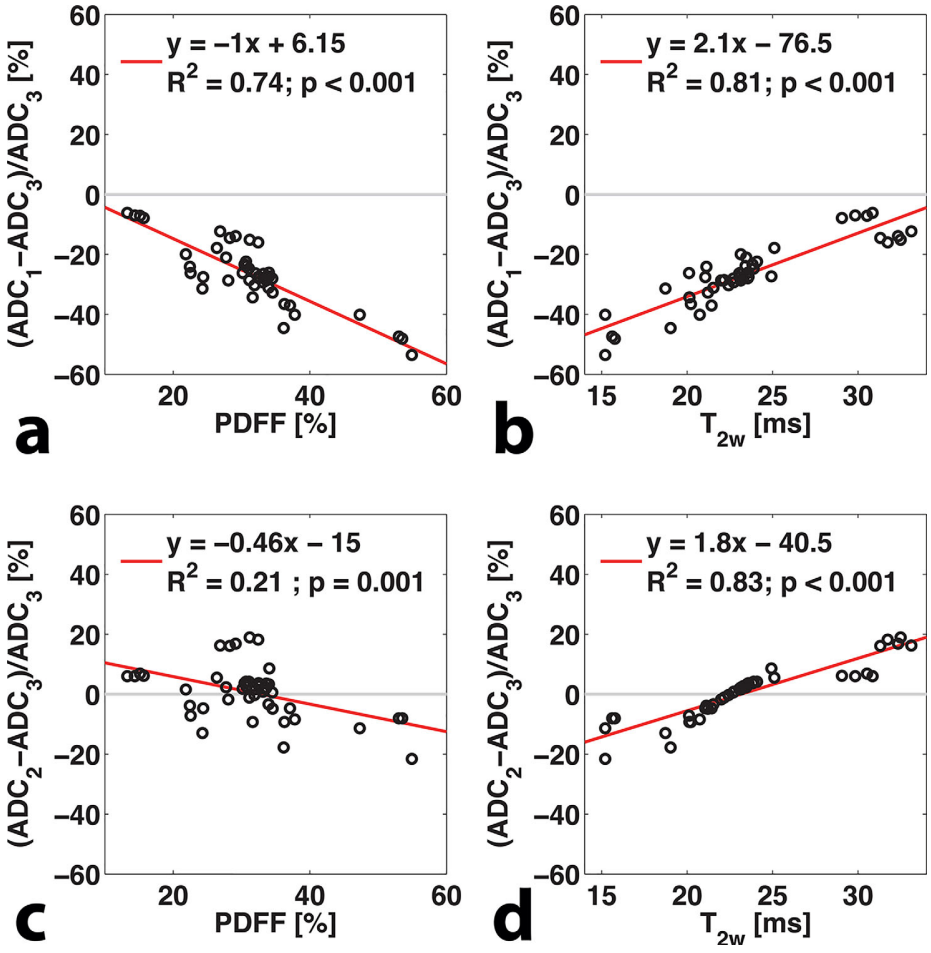

FIG. 7. Linear correlation analysis. (**a** ,**b**) Relative error of method 1 compared with method 3. (**c, d**) Relative error of method 2 compared with method 3 as a function of PDFF (a, c) and T_{2w} (b, d), respectively.

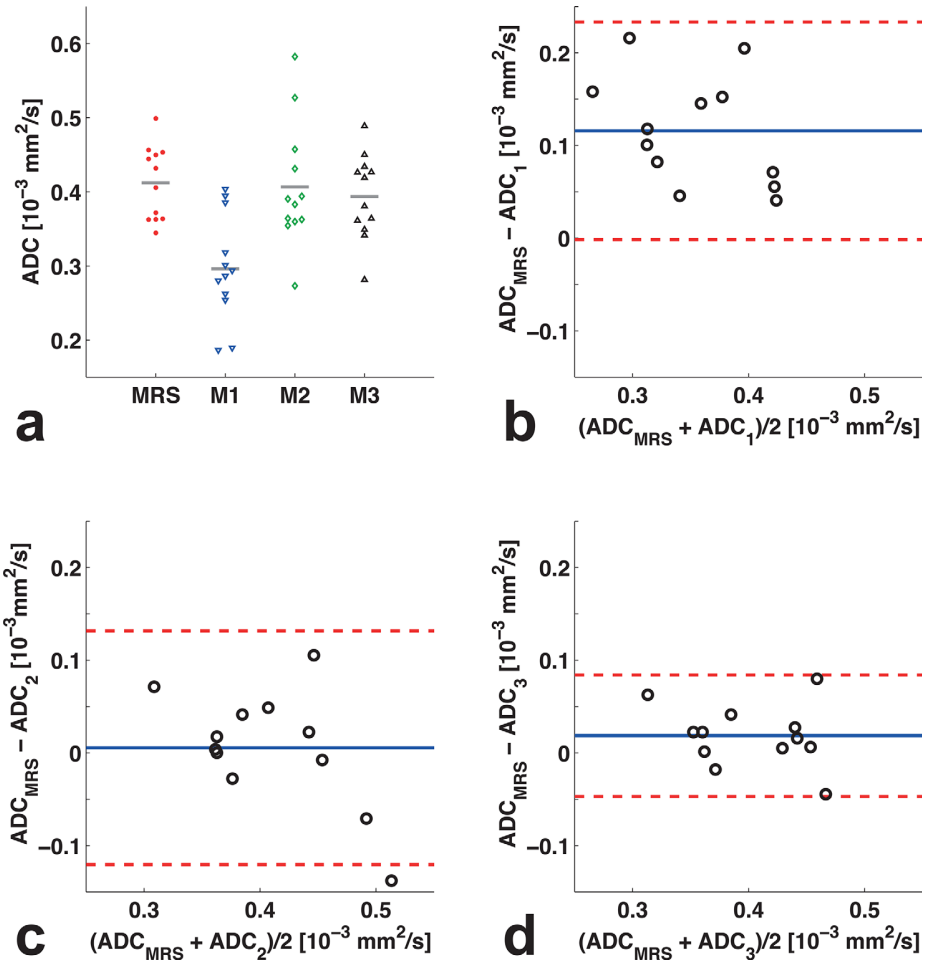

FIG. 8. (**a**) ADC grouped by quantification method: DW-MRS (red); DW-MRI, method 1 (blue); DW-MRI, method 2 (green); DW-MRI, method 3 (black); and (**b–d**) Bland–Altman plots showing the agreement of ADC quantification between MRS and DWI method 1 (b), method 2 (c), and method 3 (d), respectively (solid blue line, bias; dashed red line, limits of agreement).

difference in T_2 between water and fat. A higher difference in T_2 between water and fat increases the T_2-weighted fat signal relative to the T_2-weighted water signal and increases the ADC underestimation (Fig. 7b). When the previously proposed correction (14) is performed accounting for residual fat using measured PDFF but constant T_{2w}, the PDFF-dependent error is removed, but a residual error remains, presumably due to error in T_{2w} (Fig. 7c and 7d).

When comparing the imaging results with the spectroscopy results, it is shown that there is a significant bias between DW-MRS–based and DWI-based ADC if residual fat signal is not taken into account. Method 2 and method 3 are able to correct for the bias introduced by the residual fat signal and yield mean ADC values that are comparable to the MRS-based value. However, Figure 8d clearly illustrates that the confidence interval between DW-MRS–based ADC and DWI-based ADC using method 3 is smaller than the confidence interval between DW-MRS–based ADC and DWI-based ADC using method 2. Therefore, on an individual basis, the agreement with the DW-MRS–based ADC is better for method 3 than for method 2.

The proposed model in method 3 is valid for any range of b-values. A three-parameter fit on the DW data would be an alternative method to correct for the effect of unsuppressed fat, without the need to separately measure PDFF and T_2 relaxation times. A three-parameter fit would require sampling b-values higher than 2000 s/mm^2 (Fig. 6) with sufficiently high SNR and therefore significantly longer scan times. As highlighted in Figure 6, the dependence of the logarithm of experimental data on the b-value is linear in the presently employed range of b between 200 and 800 s/mm^2. Denoting $S_w = (1 - PDFF)e^{-\frac{TE}{T_{2w}}}$ and $S_f = \alpha PDFF\, e^{-\frac{TE}{T_{2f}}}$, and assuming $ADC_f = 0$, Equation [1] yields $S(b) = S_w e^{-bADC_w} + S_f$. Taking the derivative of the logarithm of the signal, we can derive the linear slope of the dependence of the logarithm of signal on the b-value around a b-value b_0:

$$\frac{d}{db}[\ln(S(b))](b_0) = -\frac{S_w}{S_w + S_f e^{b_0 ADC_w}} ADC_w. \qquad [9]$$

According to Equation [9], ADC_w depends on the above slope, the PDFF, and T_2 relaxation times. Therefore, separate measurements of PDFF and T_2 relaxation times are necessary to correct for the bias in ADC for the employed range of b between 200 and 800 s/mm^2.

The above results have significant implications for studies trying to investigate the relationship between bone marrow water ADC and trabecular bone health. Some previous studies have suggested that the bone

marrow water ADC decreases as the bone mineral density decreases. However, it is also well established that vertebral bone mineral density is inversely correlated with vertebral bone marrow PDFF (10,30). In addition, large inter- and intra-individual differences in both PDFF and T_{2w} have been reported. Specifically, a recent study has shown a strong variation of the vertebral bone marrow PDFF with anatomical location within the same subject. Both PDFF and T_{2w} have also been shown to vary significantly with age (17,18). The well-known correlation between age and vertebral bone marrow PDFF (15,17) makes it very likely that the observed effects are more severe in older subjects. Therefore, the bias in the water ADC estimation due to the inclusion of the unsuppressed fat signal should be considered in the investigation of the association between water bone marrow ADC and bone health.

The present study has some limitations. First, the parameters α and T_{2f} were considered constant which represents a simplification of the real conditions. Although interindividual variations in vertebral bone marrow fat unsaturation have been documented previously (30–32), the assumption of a constant α seems to be a sufficient approximation for the purpose of correction for residual fat. The error that results from inaccuracy in α [based on the physiological variability reported in Yeung et al. (30)] was analyzed in a simulation (Fig. 4) and was considered sufficiently small to justify the simplifying assumption of predefined constant α. Despite the absence of visually detectable chemical shift artifacts in the entire set of images that were acquired, imperfect suppression of the main fat peaks (in the range of 0–3 ppm) could have a substantial impact on the ADC measurement for both method 2 and method 3 but was not considered in the present study. Because the residual fat peaks (olefinic and glycerol) exhibit a strong overlap with the water peak in the vertebral bone marrow spectrum and there are significant differences in T_2 between the different components of the triglyceride spectrum, it is also difficult to directly measure the T_2 relaxation time of the residual fat. Therefore, a previously reported value for T_{2f} was used. Maximal expected variation in T_{2f} based on values reported by Dieckmeyer et al. (18) would lead to a relative error of only 4.7% in ADC_w, evaluated at mean PDFF and T_{2w} values. Second, the number of subjects was small, and only healthy young subjects were examined. Further study is needed to investigate the present results in larger-scale groups of higher age and/or pathological vertebral bone marrow status that are associated with different ranges of PDFF and ADC. Finally, the present study only considered the effect of residual fat when a spectrally selective fat suppression method was employed. However, similar arguments should be also valid when employing exclusively inversion recovery-based fat suppression, given that all different fat peaks do not have equal T_1 relaxation times.

In conclusion, ADC quantification of the vertebral bone marrow water component using DWI with spectral inversion recovery fat suppression can be significantly confounded by residual fat signal located close to the water peak. By taking into account this residual fat signal in a modified fitting model that incorporates additionally measured PDFF and T_{2w} parameters, good agreement with MRS-based ADC can be achieved. Using individual T_{2w} rather than a constant average T_{2w} increases the individual agreement of DWI-based and MRS-based ADC.

REFERENCES

1. Biffar A, Baur-Melnyk A, Schmidt GP, Reiser MF, Dietrich O. Quantitative analysis of the diffusion-weighted steady-state free precession signal in vertebral bone marrow lesions. Invest Radiol 2011;46:601–609.
2. Dietrich O, Geith T, Reiser MF, Baur-Melnyk A. Diffusion imaging of the vertebral bone marrow. NMR Biomed 2017;30. doi: 10.1002/nbm.3333.
3. Dietrich O, Herlihy A, Dannels WR, Fiebach J, Heiland S, Hajnal JV, Sartor K. Diffusion-weighted imaging of the spine using radial k-space trajectories. MAGMA 2001;12:23–31.
4. Eguchi Y, Ohtori S, Yamashita M, et al. Diffusion magnetic resonance imaging to differentiate degenerative from infectious endplate abnormalities in the lumbar spine. Spine (Phila Pa 1976) 2011;36:E198–E202.
5. Herrmann J, Krstin N, Schoennagel BP, Sornsakrin M, Derlin T, Busch JD, Petersen KU, Graessner J, Adam G, Habermann CR. Age-related distribution of vertebral bone-marrow diffusivity. Eur J Radiol 2012;81:4046–4049.
6. Hillengass J, Stieltjes B, Bauerle T, et al. Dynamic contrast-enhanced magnetic resonance imaging (DCE-MRI) and diffusion-weighted imaging of bone marrow in healthy individuals. Acta Radiol 2011;52:324–330.
7. Biffar A, Sourbron S, Dietrich O, Schmidt G, Ingrisch M, Reiser MF, Baur-Melnyk A. Combined diffusion-weighted and dynamic contrast-enhanced imaging of patients with acute osteoporotic vertebral fractures. Eur J Radiol 2010;76:298–303.
8. Dutoit JC, Vanderkerken MA, Anthonissen J, Dochy F, Verstraete KL. The diagnostic value of SE MRI and DWI of the spine in patients with monoclonal gammopathy of undetermined significance, smouldering myeloma and multiple myeloma. Eur Radiol 2014;24:2754–2765.
9. Yeung DK, Wong SY, Griffith JF, Lau EM. Bone marrow diffusion in osteoporosis: evaluation with quantitative MR diffusion imaging. J Magn Reson Imaging 2004;19:222–228.
10. Griffith JF, Yeung DK, Antonio GE, Wong SY, Kwok TC, Woo J, Leung PC. Vertebral marrow fat content and diffusion and perfusion indexes in women with varying bone density: MR evaluation. Radiology 2006;241:831–838.
11. Hatipoglu HG, Selvi A, Ciliz D, Yuksel E. Quantitative and diffusion MR imaging as a new method to assess osteoporosis. AJNR Am J Neuroradiol 2007;28:1934–1937.
12. Tang GY, Lv ZW, Tang RB, Liu Y, Peng YF, Li W, Cheng YS. Evaluation of MR spectroscopy and diffusion-weighted MRI in detecting bone marrow changes in postmenopausal women with osteoporosis. Clin Radiol 2010;65:377–381.
13. Hernando D, Karampinos DC, King KF, Haldar JP, Majumdar S, Georgiadis JG, Liang ZP. Removal of olefinic fat chemical shift artifact in diffusion MRI. Magn Reson Med 2011;65:692–701.
14. Hansmann J, Hernando D, Reeder SB. Fat confounds the observed apparent diffusion coefficient in patients with hepatic steatosis. Magn Reson Med 2013;69:545–552.
15. Kugel H, Jung C, Schulte O, Heindel W. Age- and sex-specific differences in the 1H-spectrum of vertebral bone marrow. J Magn Reson Imaging 2001;13:263–268.
16. Ishijima H, Ishizaka H, Horikoshi H, Sakurai M. Water fraction of lumbar vertebral bone marrow estimated from chemical shift misregistration on MR imaging: normal variations with age and sex. AJR Am J Roentgenol 1996;167:355–358.
17. Griffith JF, Yeung DK, Ma HT, Leung JC, Kwok TC, Leung PC. Bone marrow fat content in the elderly: a reversal of sex difference seen in younger subjects. J Magn Reson Imaging 2012;36:225–230.
18. Dieckmeyer M, Ruschke S, Cordes C, Yap SP, Kooijman H, Hauner H, Rummeny EJ, Bauer JS, Baum T, Karampinos DC. The need for T(2) correction on MRS-based vertebral bone marrow fat quantification: implications for bone marrow fat fraction age dependence. NMR Biomed 2015;28:432–439.

19. Corum CA, McIntosh AD, Bolan PJ, et al. Feasibility of single-voxel MRS measurement of apparent diffusion coefficient of water in breast tumors. Magn Reson Med 2009;61:1232–1237.
20. Ruschke S, Kienberger H, Baum T, Kooijman H, Settles M, Haase A, Rychlik M, Rummeny EJ, Karampinos DC. Diffusion-weighted stimulated echo acquisition mode (DW-STEAM) MR spectroscopy to measure fat unsaturation in regions with low proton-density fat fraction. Magn Reson Med 2016;75:32–41.
21. Hamilton G, Yokoo T, Bydder M, Cruite I, Schroeder ME, Sirlin CB, Middleton MS. In vivo characterization of the liver fat (1)H MR spectrum. NMR Biomed 2011;24:784–790.
22. Wilm BJ, Gamper U, Henning A, Pruessmann KP, Kollias SS, Boesiger P. Diffusion-weighted imaging of the entire spinal cord. NMR Biomed 2009;22:174–181.
23. Dietrich O, Raya JG, Reeder SB, Reiser MF, Schoenberg SO. Measurement of signal-to-noise ratios in MR images: influence of multichannel coils, parallel imaging, and reconstruction filters. J Magn Reson Imaging 2007;26:375–385.
24. National Electrical Manufacturers Association. Determination of signal-to-noise ratio (SNR) in diagnostic magnetic resonance imaging. NEMA Standards Publication MS 1-2001. Arlington, VA: National Electrical Manufacturers Association; 2001. 15 p.
25. Yu H, Shimakawa A, McKenzie CA, Brodsky E, Brittain JH, Reeder SB. Multiecho water-fat separation and simultaneous R2* estimation with multifrequency fat spectrum modeling. Magn Reson Med 2008; 60:1122–1134.
26. Marshall I, Higinbotham J, Bruce S, Freise A. Use of Voigt lineshape for quantification of in vivo 1H spectra. Magn Reson Med 1997;37: 651–657.
27. Bland JM, Altman DG. Statistical methods for assessing agreement between two methods of clinical measurement. Lancet 1986;1:307–310.
28. Hooijmans MT, Damon BM, Froeling M, Versluis MJ, Burakiewicz J, Verschuuren JJ, Niks EH, Webb AG, Kan HE. Evaluation of skeletal muscle DTI in patients with Duchenne muscular dystrophy. NMR Biomed 2015;28:1589–1597.
29. Williams SE, Heemskerk AM, Welch EB, Li K, Damon BM, Park JH. Quantitative effects of inclusion of fat on muscle diffusion tensor MRI measurements. J Magn Reson Imaging 2013;38:1292–1297.
30. Yeung DK, Griffith JF, Antonio GE, Lee FK, Woo J, Leung PC. Osteoporosis is associated with increased marrow fat content and decreased marrow fat unsaturation: a proton MR spectroscopy study. J Magn Reson Imaging 2005;22:279–285.
31. Baum T, Yap SP, Karampinos DC, Nardo L, Kuo D, Burghardt AJ, Masharani UB, Schwartz AV, Li X, Link TM. Does vertebral bone marrow fat content correlate with abdominal adipose tissue, lumbar spine bone mineral density, and blood biomarkers in women with type 2 diabetes mellitus? J Magn Reson Imaging 2012;35:117–124.
32. Patsch JM, Li X, Baum T, Yap SP, Karampinos DC, Schwartz AV, Link TM. Bone marrow fat composition as a novel imaging biomarker in postmenopausal women with prevalent fragility fractures. J Bone Miner Res 2013;28:1721–1728.

9 Discussion

9.1 Review of Existing Literature

One exceptional feature of bone marrow tissue is that both water and fat components can be equally present. This gives rise to MR-based measurements of the fat fraction and characterization of the bone marrow water-fat composition. However, the existence of two significant signal components also implies that when measuring individual properties of one component the other component must be sufficiently suppressed or at least taken into account. This is important because bone marrow water and fat exhibit different relaxation times and diffusion constants: the water component has shorter T_2, longer T_1 and faster diffusion constant than the fat component [44].

The anatomical properties of vertebral bone marrow represent an additional challenge for quantitative measurements. The trabecular bone matrix within the vertebral bodies leads to shortening of the T_2^* relaxation times of both components and broad peaks in the MR spectrum of the bone marrow causing a significant overlap of the water peak with the adjacent olefinic and glycerol fat peaks. This has implications for the quantification of both fat fraction and diffusion constant. On the one hand fat fraction is underestimated if fat signal resonating at a frequency close to the one of water is not taken into account. On the other hand the overlapping fat peaks are not easily suppressible without affecting the water signal and thus bias the ADC quantification of the water component towards lower values. To overcome this problem an indirect method of extracting the overlapping water-fat peaks was proposed by Hamilton et al. [41]. By using data of the measurable fat peaks that are not overlapped by the water peak and incorporating it into a theoretical triglyceride model one can characterize the complete fat spectrum of fatty tissue. In the liver, good agreement of the derived fat spectrum with MRS measurements in water-fat phantoms was shown [41]. Karampinos et al. translated this approach to the bone marrow and demonstrated its feasibility in the proximal femur [45].

In the following, the literature regarding MR-based quantification of vertebral bone marrow fat fraction and ADC, with an emphasis on the confounding effect of the fat component, will be briefly reviewed.

9.1.1 Vertebral Bone Marrow Fat Fraction Quantification

Variations in vertebral bone marrow fat fraction in healthy subjects have been investigated in relation to aging, gender and anatomical location, using both single-voxel ^{1}H

MRS [46, 47, 48, 49, 50] and chemical shift encoding-based water–fat imaging [51, 52]. In a water-fat imaging study of the entire spine in 28 subjects (age: 26 ± 4 years) Baum et al. reported an increase of bone marrow PDFF from cervical to lumbar vertebral bodies [51].

Multiple large-scale single-voxel ^{1}H MRS studies verified an age-dependent increase of vertebral bone marrow fat fraction [47, 49, 50]. Additionally, a gender-dependence was observed in all studies, with higher fat fraction values in males compared to females. More specifically, Griffith et al. observed a reversal of this gender-dependence in the age group over 60 years, i.e. higher fat fraction values in females compared to males [49]. This is due to a sharp rise of vertebral bone marrow fat fraction in female subjects between 55 and 65 years of age, an observation the authors potentially attribute to an altered fat distribution pattern in postmenopausal women. However, in all of these studies measurements were based on single-TE MRS experiments resulting in a signal-weighted fat fraction instead of the PDFF. Since the signal-weighted fat fraction is dependent on the employed data acquisition and analysis care has to be taken when comparing results from different studies.

In the context of osteoporosis vertebral bone marrow fat fraction has been extensively investigated. In 2005, Griffith et al. compared subjects with normal BMD to osteopenic and osteoporotic subjects [10] in a large-scale in-vivo study. According to this work, vertebral bone marrow fat fraction based on single-voxel ^{1}H MRS was significantly increased in osteoporotic and osteopenic subjects. This negative association of vertebral bone marrow fat fraction and BMD was then confirmed by several other studies employing both single-voxel ^{1}H MRS [9, 11, 12, 13, 14, 53] and chemical shift encoding-based water–fat imaging [8, 54, 55, 53].

Furthermore, vertebral bone marrow fat fraction was also investigated in the context of vertebral fractures. Schwartz et al. found that higher marrow fat content was associated with prevalent vertebral fracture in men, even after adjustment for BMD [13]. Karampinos et al. reported a negative association with failure load assessed by destructive biomechanical testing of vertebral specimens [14].

However, only two of the MRS-based studies quantified the PDFF by employing a multi-TE approach: one in vivo [53] and one in vitro [14].

9.1.2 Vertebral Bone Marrow ADC Quantification

ADC quantification has traditionally been based upon diffusion weighted imaging (DWI), mostly using a single-shot echo planar imaging (ssEPI) or single-shot fast spin echo (ssFSE) sequence [34]. Studies using ssEPI employ fat suppression in order to reduce chemical shift artifacts and the confounding of the water diffusion quantification caused by lipid signal [56, 16, 57, 11, 17, 58, 59, 60, 61, 62, 63, 64]. Of the studies using an ssFSE sequence only one employed fat suppression [65].

There are only few studies on age-dependent variations in vertebral bone marrow

diffusion, with different results. While Hillengass et al. did not observe a significant correlation of vertebral bone marrow ADC with age [66], Yeung et al. found reduced ADC values in healthy older women compared to younger controls [16].

Studies investigating vertebral bone marrow diffusion in the context of osteoporosis found significantly lower ADC values in subjects with reduced BMD compared to subjects with normal BMD [16, 17, 59]. One study reported a negative association of ADC and fat fraction [11]. All these studies used a single-shot DW-EPI sequence at 1.5 T.

DWI-based ADC measurements using spectrally selective fat suppression techniques have been shown to be biased by residual fat signal in the liver [67] and skeletal muscle [68, 69, 70]. However, only in the liver this bias has been quantified and corrected by means of a theoretical model and additional quantitative MRI measurements [67].

An alternative method to measure ADC is single-voxel diffusion-weighted MRS (DW-MRS). In the majority of measurements, its inherent spectral resolution allows the extraction of the water ADC that is not confounded by residual fat signal. DW-MRS has been previously applied in breast tumors [71] and skeletal muscle [40].

9.2 Present Work

Several contributions to the field of quantitative MR of vertebral bone marrow were made within the scope of the present dissertation. The focus was put on confounding effects on parameter quantification arising from the different MR properties of the two main tissue components: water and fat. JP-I emphasizes the importance of measuring the PDFF in order to standardize MRS-based bone marrow fat quantification. JP-II highlights the confounding effect of unsuppressed fat signal on DWI-based ADC quantification of vertebral bone marrow water and proposes a correction method.

9.2.1 Novelty

Both journal publications bring innovations to the field of quantitative MR of bone marrow. Concretely, in JP-I the mean fat spectrum of vertebral bone marrow fat was characterized, inspired by an approach previously described in the liver [41]. This enables robust extraction of the water peak from the overlapping neighboring fat peaks. Furthermore, for the first time a direct comparison of PDFF and T_2-weighted fat fraction was performed and the impact of T_2 decay effects in the context of the age dependence of vertebral bone marrow fat content was investigated. T_2 of water was identified as an additional biomarker potentially sensitive to the composition of the bone marrow water compartment.

Again, JP-II took a similar approach as previously described in the liver [67] but significantly advanced the proposed method. For the first time, in vivo DW-MRS was performed as a reference measurement in order to validate the newly developed method correcting the confounding effect of residual fat on ADC quantification in vertebral bone

marrow. It was demonstrated that individual measurements of water T_2 outperform the approach assuming a constant water T_2 in the correction process.

9.2.2 Impact

The present dissertation advances quantitative MR of bone marrow. In JP-I the mean vertebral bone marrow fat spectrum was characterized. This mean spectrum can be of great utility in future studies quantifying vertebral bone marrow fat content and fat composition. A significant difference in the T_2 relaxation time between men and women was found. This implies that sex-dependent variations in water-fat composition of vertebral bone marrow found in previous studies measuring T_2-weighted fat fraction should be reconsidered [49]. In light of the present findings, the reported sex-dependent fat fraction variations can, at least partially, be explained by sex-dependent differences in T_2. Similar considerations apply to the age-dependence of the bone marrow fat content. Since in JP-I there was found a negative association between T_2 of water and PDFF, not employing a T_2 correction results in an overestimation of the age-dependence. In conclusion, the results of JP-I are of high relevance for the investigation of MRS-based fat fraction of vertebral bone marrow in relation to sex and age and suggest that the same holds true in the context of bone health, e.g., osteoporosis. It is also emphasized that MRS-based bone marrow fat quantification should be based on a multi-TE experiment yielding the PDFF as a fundamental tissue property. This should be considered a guideline for the design of future studies.

JP-II quantifies the confounding effect of residual fat on bone marrow water ADC measurements. This is particularly important in vertebral bone marrow because it is a tissue exhibiting a high fat content. A strong underestimation of ADC is demonstrated when residual fat is not taken into account which increases with PDFF. The positive correlations of PDFF with BMD and age, respectively, are well-established. Therefore, these results of JP-II have significant implications for the investigation of bone marrow water ADC in the context of bone health and aging. They suggest that the bias in water ADC estimation caused by residual fat signal should be taken into account when the association between water ADC and bone health is investigated. Analogously, the same arguments apply to the investigation of the ADC of vertebral bone marrow water in relation to anatomical location and age, respectively. Furthermore, the proposed method to analyze and correct the confounding effect of unsuppressed fat can be used as a blueprint for quantitative MR in other fatty tissues. Of course, specific customization of the method to the respective tissue properties would be necessary for this purpose. Lastly, the application of DW-MRS as a validation tool for MRI-based ADC quantification could be of high interest in the research setting.

Both journal publications prove that additional quantitative measurements, requiring reasonable additional effort, can significantly improve the accuracy of MR-based quantification of vertebral bone marrow parameters. The proposed methods have been developed

in close collaboration with clinical scientists and are being applied in currently running clinical studies.

9.2.3 Limitations

The publications this dissertation is based upon are not without limitations regarding methodology and study cohorts.

In order to achieve a robust extraction of overlapping water and fat peaks a mean vertebral bone marrow fat spectrum was utilized (in JP-I). This implies the assumption of a common fat spectrum for all subjects independent of age and sex although inter-individual variations in vertebral bone marrow fat composition have been reported [9, 29, 15]. However, for the purpose of robust PDFF quantification this simplification can be considered reasonable since, except for extreme cases, the overall improvement in fat fraction quantification accuracy easily exceeds inaccuracies due to individual deviations from the mean fat spectrum. Another simplification was the assumption of a common T_2 relaxation time for all fat peaks whereas in reality the different fat components exhibit significant differences in this regard. This step was necessary to guarantee a robust extraction of the fat T_2 and allow a reasonable fitting. Attempts trying to fit for the T_2 of each fat component individually proved to be unstable and yielded highly implausible T_2 values. However, the biasing effect of this simplification on PDFF estimation can be considered insignificant. The final limitation of JP-I regards the study cohort. The number of male subjects was smaller than the number of females and had a non-uniform age distribution. Therefore, further studies are necessary to investigate the relation between PDFF, age and water T_2 in male populations.

Similar to JP-I, the methodology described in JP-II relies on a mean vertebral bone marrow fat spectrum. This makes the simplifying assumption that the fraction of unsuppressed fat spectrum energy α is constant across subjects despite previously reported inter-individual variations in vertebral bone marrow fat unsaturation [9, 29, 15]. A simulation analysis was performed to estimate the error resulting from inaccuracies in α which was considered acceptably small to justify the simplifying assumption of a common α for all subjects. Moreover, the T_2 relaxation time of the residual fat was again assumed to be constant across subjects using a previously reported value. To analyze the impact of this simplification the relative ADC error resulting from maximal expected variation in the T_2 of fat [42] was estimated. The calculated maximal relative error of 4.7 % was considered sufficiently small. Another limitation which was not closer addressed could be the imperfect suppression of the main fat peaks. It would result in additional bias of water ADC quantification. However, the absence of visible chemical shift artifacts in the acquired DWI images indicates that the implied effect, if at all, would be very small. The study cohort examined in JP-II was relatively small and did not include older subjects or patients suffering from conditions affecting the bone marrow. Therefore, further studies in older subjects and patients with bone marrow pathologies are needed to extend

the present results to, firstly, a larger range of ADC and PDFF values and, secondly, a clinically more relevant subpopulation. Lastly, the effect of unsuppressed fat on ADC quantification was only analyzed in presence of a spectrally selective fat suppression technique. However, the proposed approach could be readily translated to inversion-recovery based fat suppression techniques. In this case, residual fat signal would arise from variations in T_1 relaxation times of the different fat spectrum components and the method proposed in JP-II would have to be modified accordingly.

9.3 Perspective

There is still some room for further technical development and refinement of the methods presented in this dissertation. In addition, advancements in MRI technology will further reduce the cost of adding sequences to the examination protocol in order to employ the methods proposed in JP-I and JP-II. This could help to facilitate their application in the clinical setting. The application in future clinical studies could contribute to gain more insight into the role of bone marrow in health and disease, such as osteoporosis and metabolic syndrome.

The results from JP-I suggest that marrow fat quantification should aim at measuring the PDFF rather than a signal weighted fat fraction. In future studies this could be realized more efficiently by quantitative water-fat imaging since recent publications demonstrated excellent agreement with MRS-based measurements [45, 72, 53]. By modification of the data acquisition and analysis parameters the proposed method could be translated to other tissues with significant water and fat components.

The methodology developed in JP-II is currently applied in a clinical study of postmenopausal breast cancer patients receiving aromatase inhibitor therapy. The study aims at the cross-sectional and longitudinal analysis of vertebral bone marrow parameters including water ADC. This will reveal the performance of the proposed method in a larger cohort exhibiting a different age distribution as well as potentially altered bone marrow conditions. Furthermore, results of JP-II might assist in raising the awareness for the potentially confounding effect of residual fat signal in future quantitative MR studies. Some of them could also adopt MRS as a validation tool.

Acknowledgements

First of all, I want to thank my supervisors, Dimitrios Karampinos and Thomas Baum. Dimitrios introduced me to the world of MR and more than once helped me to overcome my mental blockades in understanding the physics of magnetic resonance. With his exceptional dedication and work ethic he is the heart and soul of the research group I am glad to be part of. I am really grateful for his efforts in realizing this research project. Thomas was an outstanding mentor on the clinical side of this thesis. As a future clinician I consider him a role-model, professionally as well as personally. The willingness of both of my supervisors to discuss emerging problems at any given time as well as the teamwork among our group was a key factor to the success of the project. Furthermore, I thank Ernst J. Rummeny for his support and providing the necessary infrastructure as head of the department.

I owe special thanks to Stefan Ruschke who did significant ground-work for the technical aspects of this dissertation and helped me understanding the involved physics, software and hardware whenever I asked him.

I would like to express my gratitude to Barbara, Christian, Dominik and Max for filling in for me as MR technician when my medical school schedule prevented me from examining study subjects. Together with Sarah, Sophia and Jan you have been a great team of colleagues.

Lastly, but most importantly, my dearest thanks go to my beloved girlfriend Ana Alicia. You were my greatest source of support and motivation throughout the last four years.

List of Symbols and Abbreviations

δ_{ppm}	chemical shift [ppm]
γ	gyromagnetic ratio [Hz T^{-1}]
ω	precession frequency [Hz]
ω_0	Larmor frequency [Hz]
ρ	spin density [m^{-3}]
τ	magnetic torque [N m]
^1H	hydrogen atom (proton)
A	intrinsic angular moment [kg m^2 s^{-1}]
B	magnetic field [T]
b	b-value (b-factor) [s m^{-2}]
B_0	static main magnetic field [T]
D	diffusion coefficient [m^2 s^{-1}]
f	resonance frequency [Hz]
f_{TMS}	resonance frequency of tetramethylsilane [Hz]
G	gradient strength [T m^{-1}]
G_{FE}	frequency-encoding gradient field [T m^{-1}]
G_{PE}	phase-encoding gradient field [T m^{-1}]
G_{SS}	slice-selection gradient field [T m^{-1}]
G_x	magnetic gradient field along x-dimension [T m^{-1}]
G_y	magnetic gradient field along y-dimension [T m^{-1}]
G_z	magnetic gradient field along z-dimension [T m^{-1}]

k	k-space vector [cycles/m]
k_x	component along x-dimension of k [cycles/m]
k_y	component along y-dimension of k [cycles/m]
k_z	component along z-dimension of k [cycles/m]
k_{FE}	component along frequency-encoding direction of k [cycles/m]
k_{PE}	component along phase-encoding direction of k [cycles/m]
M	magnetic moment [N m T^{-1}]
M_0	amplitude of the magnetization vector [-]
M_{xy}	transverse component of the magnetization vector [-]
M_z	longitudinal component of the magnetization vector [-]
R_1	longitudinal relaxation rate [s^{-1}]
R_2	transverse relaxation rate [s^{-1}]
R'_2	reversible transverse relaxation rate [s^{-1}]
R^*_2	effective transverse relaxation rate [s^{-1}]
S	signal intensity [-]
S_0	non-weighted signal intensity [-]
t	time [s]
T_1	spin-lattice (longitudinal) relaxation time [s]
T_2	spin-spin (transverse) relaxation time [s]
T'_2	reversible transverse relaxation time [s]
T^*_2	effective transverse relaxation time [s]
T_{2f}	spin-spin (transverse) relaxation time of the fat component [s]
T_{2w}	spin-spin (transverse) relaxation time of the water component [s]
1D	one-dimensional
2D	two-dimensional

3D	three-dimensional
ADC	apparent diffusion coefficient
BMD	bone mineral density
cMAT	constitutive bone marrow adipose tissue
DEXA	dual energy X-ray absorptiometry
DW-MRS	diffusion-weighted magnetic resonance spectroscopy
DWI	diffusion-weighted imaging
FID	free induction decay
FOV	field of view
GE	gradient echo
MR	magnetic resonance
MRI	magnetic resonance imaging
MRS	magnetic resonance spectroscopy
NMR	nuclear magnetic resonance
PDFF	proton density fat fraction
ppm	parts per million
PRESS	point-resolved spectroscopy
RF	radio frequency
rMAT	regulated bone marrow adipose tissue
ROI	region of interest
SAT	subcutaneous adipose tissue
SE	spin echo
SNR	signal-to-noise ratio
ssEPI	single-shot echo planar imaging
ssFSE	single-shot fast spin echo

STEAM	stimulated echo acquisition mode
T/R	transmit/receive
TE	echo time
TM	mixing time
TMS	tetramethylsilane
TR	repetition time
VAT	visceral adipose tissue
VOI	volume of interest

List of Figures

List of Tables

Bibliography

[1] I. I. Rabi, J. R. Zacharias, S. Millman, and P. Kusch. "A New Method of Measuring Nuclear Magnetic Moment". In: *Phys. Rev.* 53 (Feb. 1938), p. 318.

[2] No authors listed. "NIH Consensus Development Panel on Osteoporosis Prevention, Diagnosis, and Therapy, March 7-29, 2000: highlights of the conference". In: *South. Med. J.* 94.6 (June 2001), pp. 569–573.

[3] T. Jalava, S. Sarna, L. Pylkkanen, B. Mawer, J. A. Kanis, P. Selby, M. Davies, J. Adams, R. M. Francis, J. Robinson, and E. McCloskey. "Association between vertebral fracture and increased mortality in osteoporotic patients". In: *J. Bone Miner. Res.* 18.7 (July 2003), pp. 1254–1260.

[4] F. Bleibler, A. Konnopka, P. Benzinger, K. Rapp, and H. H. Konig. "The health burden and costs of incident fractures attributable to osteoporosis from 2010 to 2050 in Germany–a demographic simulation model". In: *Osteoporos Int* 24.3 (Mar. 2013), pp. 835–847.

[5] S. C. Schuit, M. van der Klift, A. E. Weel, C. E. de Laet, H. Burger, E. Seeman, A. Hofman, A. G. Uitterlinden, J. P. van Leeuwen, and H. A. Pols. "Fracture incidence and association with bone mineral density in elderly men and women: the Rotterdam Study". In: *Bone* 34.1 (Jan. 2004), pp. 195–202.

[6] E. S. Siris, Y. T. Chen, T. A. Abbott, E. Barrett-Connor, P. D. Miller, L. E. Wehren, and M. L. Berger. "Bone mineral density thresholds for pharmacological intervention to prevent fractures". In: *Arch. Intern. Med.* 164.10 (May 2004), pp. 1108–1112.

[7] M. Janghorbani, R. M. Van Dam, W. C. Willett, and F. B. Hu. "Systematic review of type 1 and type 2 diabetes mellitus and risk of fracture". In: *Am. J. Epidemiol.* 166.5 (Sept. 2007), pp. 495–505.

[8] J. P. Kuhn, D. Hernando, P. J. Meffert, S. Reeder, N. Hosten, R. Laqua, A. Steveling, S. Ender, H. Schroder, and D. T. Pillich. "Proton-density fat fraction and simultaneous R2* estimation as an MRI tool for assessment of osteoporosis". In: *Eur Radiol* 23.12 (Dec. 2013), pp. 3432–3439.

[9] D. K. Yeung, J. F. Griffith, G. E. Antonio, F. K. Lee, J. Woo, and P. C. Leung. "Osteoporosis is associated with increased marrow fat content and decreased marrow fat unsaturation: a proton MR spectroscopy study". In: *J Magn Reson Imaging* 22.2 (Aug. 2005), pp. 279–285.

[10] J. F. Griffith, D. K. Yeung, G. E. Antonio, F. K. Lee, A. W. Hong, S. Y. Wong, E. M. Lau, and P. C. Leung. "Vertebral bone mineral density, marrow perfusion, and fat content in healthy men and men with osteoporosis: dynamic contrast-enhanced MR imaging and MR spectroscopy". In: *Radiology* 236.3 (Sept. 2005), pp. 945–951.

[11] J. F. Griffith, D. K. Yeung, G. E. Antonio, S. Y. Wong, T. C. Kwok, J. Woo, and P. C. Leung. "Vertebral marrow fat content and diffusion and perfusion indexes in women with varying bone density: MR evaluation". In: *Radiology* 241.3 (Dec. 2006), pp. 831–838.

[12] X. Li, D. Kuo, A. L. Schafer, A. Porzig, T. M. Link, D. Black, and A. V. Schwartz. "Quantification of vertebral bone marrow fat content using 3 Tesla MR spectroscopy: reproducibility, vertebral variation, and applications in osteoporosis". In: *J Magn Reson Imaging* 33.4 (Apr. 2011), pp. 974–979.

[13] A. V. Schwartz, S. Sigurdsson, T. F. Hue, T. F. Lang, T. B. Harris, C. J. Rosen, E. Vittinghoff, K. Siggeirsdottir, G. Sigurdsson, D. Oskarsdottir, K. Shet, L. Palermo, V. Gudnason, and X. Li. "Vertebral bone marrow fat associated with lower trabecular BMD and prevalent vertebral fracture in older adults". In: *J. Clin. Endocrinol. Metab.* 98.6 (June 2013), pp. 2294–2300.

[14] D. C. Karampinos, S. Ruschke, O. Gordijenko, E. Grande Garcia, H. Kooijman, R. Burgkart, E. J. Rummeny, J. S. Bauer, and T. Baum. "Association of MRS-Based Vertebral Bone Marrow Fat Fraction with Bone Strength in a Human In Vitro Model". In: *J Osteoporos* 2015 (2015), p. 152349.

[15] J. M. Patsch, X. Li, T. Baum, S. P. Yap, D. C. Karampinos, A. V. Schwartz, and T. M. Link. "Bone marrow fat composition as a novel imaging biomarker in postmenopausal women with prevalent fragility fractures". In: *J. Bone Miner. Res.* 28.8 (Aug. 2013), pp. 1721–1728.

[16] D. K. Yeung, S. Y. Wong, J. F. Griffith, and E. M. Lau. "Bone marrow diffusion in osteoporosis: evaluation with quantitative MR diffusion imaging". In: *J Magn Reson Imaging* 19.2 (Feb. 2004), pp. 222–228.

[17] H. G. Hatipoglu, A. Selvi, D. Ciliz, and E. Yuksel. "Quantitative and diffusion MR imaging as a new method to assess osteoporosis". In: *AJNR Am J Neuroradiol* 28.10 (2007), pp. 1934–1937.

[18] S. M. Grundy, H. B. Brewer, J. I. Cleeman, S. C. Smith, and C. Lenfant. "Definition of metabolic syndrome: report of the National Heart, Lung, and Blood Institute/American Heart Association conference on scientific issues related to definition". In: *Arterioscler. Thromb. Vasc. Biol.* 24.2 (Feb. 2004), e13–18.

[19] L. Hutley and J. B. Prins. "Fat as an endocrine organ: relationship to the metabolic syndrome". In: *Am. J. Med. Sci.* 330.6 (Dec. 2005), pp. 280–289.

[20] R. H. Eckel, K. G. Alberti, S. M. Grundy, and P. Z. Zimmet. "The metabolic syndrome". In: *Lancet* 375.9710 (Jan. 2010), pp. 181–183.

[21] J. M. Dekker, C. Girman, T. Rhodes, G. Nijpels, C. D. Stehouwer, L. M. Bouter, and R. J. Heine. "Metabolic syndrome and 10-year cardiovascular disease risk in the Hoorn Study". In: *Circulation* 112.5 (Aug. 2005), pp. 666–673.

[22] K. G. Alberti, R. H. Eckel, S. M. Grundy, P. Z. Zimmet, J. I. Cleeman, K. A. Donato, J. C. Fruchart, W. P. James, C. M. Loria, and S. C. Smith. "Harmonizing the metabolic syndrome: a joint interim statement of the International Diabetes Federation Task Force on Epidemiology and Prevention; National Heart, Lung, and Blood Institute; American Heart Association; World Heart Federation; International Atherosclerosis Society; and International Association for the Study of Obesity". In: *Circulation* 120.16 (Oct. 2009), pp. 1640–1645.

[23] K. N. Frayn. "Visceral fat and insulin resistance–causative or correlative?" In: *Br. J. Nutr.* 83 Suppl 1 (Mar. 2000), S71–77.

[24] J. Machann, C. Thamer, N. Stefan, N. F. Schwenzer, K. Kantartzis, H. U. Haring, C. D. Claussen, A. Fritsche, and F. Schick. "Follow-up whole-body assessment of adipose tissue compartments during a lifestyle intervention in a large cohort at increased risk for type 2 diabetes". In: *Radiology* 257.2 (Nov. 2010), pp. 353–363.

[25] S. Kim, B. Cho, H. Lee, K. Choi, S. S. Hwang, D. Kim, K. Kim, and H. Kwon. "Distribution of abdominal visceral and subcutaneous adipose tissue and metabolic syndrome in a Korean population". In: *Diabetes Care* 34.2 (Feb. 2011), pp. 504–506.

[26] K. E. Therkelsen, A. Pedley, E. K. Speliotes, J. M. Massaro, J. Murabito, U. Hoffmann, and C. S. Fox. "Intramuscular fat and associations with metabolic risk factors in the Framingham Heart Study". In: *Arterioscler. Thromb. Vasc. Biol.* 33.4 (Apr. 2013), pp. 863–870.

[27] G. Marchesini, M. Brizi, A. M. Morselli-Labate, G. Bianchi, E. Bugianesi, A. J. McCullough, G. Forlani, and N. Melchionda. "Association of nonalcoholic fatty liver disease with insulin resistance". In: *Am. J. Med.* 107.5 (Nov. 1999), pp. 450–455.

[28] S. B. Reeder, I. Cruite, G. Hamilton, and C. B. Sirlin. "Quantitative Assessment of Liver Fat with Magnetic Resonance Imaging and Spectroscopy". In: *J Magn Reson Imaging* 34.4 (Oct. 2011), spcone.

[29] T. Baum, S. P. Yap, D. C. Karampinos, L. Nardo, D. Kuo, A. J. Burghardt, U. B. Masharani, A. V. Schwartz, X. Li, and T. M. Link. "Does vertebral bone marrow fat content correlate with abdominal adipose tissue, lumbar spine bone mineral density, and blood biomarkers in women with type 2 diabetes mellitus?" In: *J Magn Reson Imaging* 35.1 (Jan. 2012), pp. 117–124.

[30] M. A. Bredella, M. Torriani, R. H. Ghomi, B. J. Thomas, D. J. Brick, A. V. Gerweck, C. J. Rosen, A. Klibanski, and K. K. Miller. "Vertebral bone marrow fat is positively associated with visceral fat and inversely associated with IGF-1 in obese women". In: *Obesity (Silver Spring)* 19.1 (Jan. 2011), pp. 49–53.

[31] M. A. Bredella, P. K. Fazeli, K. K. Miller, M. Misra, M. Torriani, B. J. Thomas, R. H. Ghomi, C. J. Rosen, and A. Klibanski. "Increased bone marrow fat in anorexia nervosa". In: *J. Clin. Endocrinol. Metab.* 94.6 (June 2009), pp. 2129–2136.

[32] H. J. Yoo, S. H. Hong, D. H. Kim, J. Y. Choi, H. D. Chae, B. M. Jeong, J. M. Ahn, and H. S. Kang. "Measurement of fat content in vertebral marrow using a modified dixon sequence to differentiate benign from malignant processes". In: *J Magn Reson Imaging* 45.5 (May 2017), pp. 1534–1544.

[33] F. C. Schmeel, J. A. Luetkens, S. J. Enkirch, A. Feisst, C. H. Endler, L. C. Schmeel, P. J. Wagenhauser, F. Traber, H. H. Schild, and G. M. Kukuk. "Proton density fat fraction (PDFF) MR imaging for differentiation of acute benign and neoplastic compression fractures of the spine". In: *Eur Radiol* (June 2018).

[34] O. Dietrich, T. Geith, M. F. Reiser, and A. Baur-Melnyk. "Diffusion imaging of the vertebral bone marrow". In: *NMR Biomed* 30.3 (Mar. 2017).

[35] J. Hillengass and O. Landgren. "Challenges and opportunities of novel imaging techniques in monoclonal plasma cell disorders: imaging early myeloma". In: *Leuk. Lymphoma* 54.7 (July 2013), pp. 1355–1363.

[36] A. R. Padhani, K. van Ree, D. J. Collins, S. D'Sa, and A. Makris. "Assessing the relation between bone marrow signal intensity and apparent diffusion coefficient in diffusion-weighted MRI". In: *AJR Am J Roentgenol* 200.1 (Jan. 2013), pp. 163–170.

[37] S. L. Giles, C. Messiou, D. J. Collins, V. A. Morgan, C. J. Simpkin, S. West, F. E. Davies, G. J. Morgan, and N. M. deSouza. "Whole-body diffusion-weighted MR imaging for assessment of treatment response in myeloma". In: *Radiology* 271.3 (June 2014), pp. 785–794.

[38] M. Horger, K. Weisel, W. Horger, A. Mroue, M. Fenchel, and M. Lichy. "Whole-body diffusion-weighted MRI with apparent diffusion coefficient mapping for early response monitoring in multiple myeloma: preliminary results". In: *AJR Am J Roentgenol* 196.6 (June 2011), W790–795.

[39] J. Caers, N. Withofs, J. Hillengass, P. Simoni, E. Zamagni, R. Hustinx, and Y. Beguin. "The role of positron emission tomography-computed tomography and magnetic resonance imaging in diagnosis and follow up of multiple myeloma". In: *Haematologica* 99.4 (Apr. 2014), pp. 629–637.

[40] S. Ruschke, H. Kienberger, T. Baum, H. Kooijman, M. Settles, A. Haase, M. Rychlik, E. J. Rummeny, and D. C. Karampinos. "Diffusion-weighted stimulated echo acquisition mode (DW-STEAM) MR spectroscopy to measure fat unsaturation in regions with low proton-density fat fraction". In: *Magn Reson Med* 75.1 (Jan. 2016), pp. 32–41.

[41] G. Hamilton, T. Yokoo, M. Bydder, I. Cruite, M. E. Schroeder, C. B. Sirlin, and M. S. Middleton. "In vivo characterization of the liver fat ^{1}H MR spectrum". In: *NMR Biomed* 24.7 (Aug. 2011), pp. 784–790.

[42] **M. Dieckmeyer**, S. Ruschke, C. Cordes, S. P. Yap, H. Kooijman, H. Hauner, E. J. Rummeny, J. S. Bauer, T. Baum, and D. C. Karampinos. "The need for T_2 correction on MRS-based vertebral bone marrow fat quantification: implications for bone marrow fat fraction age dependence". In: *NMR Biomed* 28.4 (Apr. 2015), pp. 432–439.

[43] E. L. Scheller, C. R. Doucette, B. S. Learman, W. P. Cawthorn, S. Khandaker, B. Schell, B. Wu, S. Y. Ding, M. A. Bredella, P. K. Fazeli, B. Khoury, K. J. Jepsen, P. F. Pilch, A. Klibanski, C. J. Rosen, and O. A. MacDougald. "Region-specific variation in the properties of skeletal adipocytes reveals regulated and constitutive marrow adipose tissues". In: *Nat Commun* 6 (Aug. 2015), p. 7808.

[44] F. Schick, H. Bongers, W. -I. Jung, B. Eismann, M. Skalej, H. Einsele, O. Lutz, and C. Claussen. "Proton relaxation times in human red bone marrow by volume selective magnetic resonance spectroscopy". In: *Applied Magnetic Resonance* 3.6 (Dec. 1992), pp. 947–963.

[45] D. C. Karampinos, G. Melkus, T. Baum, J. S. Bauer, E. J. Rummeny, and R. Krug. "Bone marrow fat quantification in the presence of trabecular bone: initial comparison between water-fat imaging and single-voxel MRS". In: *Magn Reson Med* 71.3 (Mar. 2014), pp. 1158–1165.

[46] D. Schellinger, C. S. Lin, D. Fertikh, J. S. Lee, W. C. Lauerman, F. Henderson, and B. Davis. "Normal lumbar vertebrae: anatomic, age, and sex variance in subjects at proton MR spectroscopy–initial experience". In: *Radiology* 215.3 (June 2000), pp. 910–916.

[47] H. Kugel, C. Jung, O. Schulte, and W. Heindel. "Age- and sex-specific differences in the 1H-spectrum of vertebral bone marrow". In: *J Magn Reson Imaging* 13.2 (Feb. 2001), pp. 263–268.

[48] G. P. Liney, C. P. Bernard, D. J. Manton, L. W. Turnbull, and C. M. Langton. "Age, gender, and skeletal variation in bone marrow composition: a preliminary study at 3.0 Tesla". In: *J Magn Reson Imaging* 26.3 (Sept. 2007), pp. 787–793.

[49] J. F. Griffith, D. K. Yeung, H. T. Ma, J. C. Leung, T. C. Kwok, and P. C. Leung. "Bone marrow fat content in the elderly: a reversal of sex difference seen in younger subjects". In: *J Magn Reson Imaging* 36.1 (July 2012), pp. 225–230.

[50] E. Roldan-Valadez, C. Pina-Jimenez, R. Favila, and C. Rios. "Gender and age groups interactions in the quantification of bone marrow fat content in lumbar spine using 3T MR spectroscopy: a multivariate analysis of covariance (Mancova)". In: *Eur J Radiol* 82.11 (Nov. 2013), pp. 697–702.

[51] T. Baum, S. P. Yap, M. Dieckmeyer, S. Ruschke, H. Eggers, H. Kooijman, E. J. Rummeny, J. S. Bauer, and D. C. Karampinos. "Assessment of whole spine vertebral bone marrow fat using chemical shift-encoding based water-fat MRI". In: *J Magn Reson Imaging* 42.4 (Oct. 2015), pp. 1018–1023.

[52] T. Aoki, S. Yamaguchi, S. Kinoshita, Y. Hayashida, and Y. Korogi. "Quantification of bone marrow fat content using iterative decomposition of water and fat with echo asymmetry and least-squares estimation (IDEAL): reproducibility, site variation and correlation with age and menopause". In: *Br J Radiol* 89.1065 (Sept. 2016), p. 20150538.

[53] G. Li, Z. Xu, H. Gu, X. Li, W. Yuan, S. Chang, J. Fan, H. Calimente, and J. Hu. "Comparison of chemical shift-encoded water-fat MRI and MR spectroscopy in quantification of marrow fat in postmenopausal females". In: *J Magn Reson Imaging* 45.1 (Jan. 2017), pp. 66–73.

[54] F. B. Ergen, G. Gulal, A. E. Yildiz, A. Celik, J. Karakaya, and U. Aydingoz. "Fat fraction estimation of the vertebrae in females using the T2*-IDEAL technique in detection of reduced bone mineralization level: comparison with bone mineral densitometry". In: *J Comput Assist Tomogr* 38.2 (2014), pp. 320–324.

[55] G. W. Li, Z. Xu, Q. W. Chen, Y. N. Tian, X. Y. Wang, L. Zhou, and S. X. Chang. "Quantitative evaluation of vertebral marrow adipose tissue in postmenopausal female using MRI chemical shift-based water-fat separation". In: *Clin Radiol* 69.3 (Mar. 2014), pp. 254–262.

[56] J. H. Chan, W. C. Peh, E. Y. Tsui, L. F. Chau, K. K. Cheung, K. B. Chan, M. K. Yuen, E. T. Wong, and K. P. Wong. "Acute vertebral body compression fractures: discrimination between benign and malignant causes using apparent diffusion coefficients". In: *Br J Radiol* 75.891 (Mar. 2002), pp. 207–214.

[57] M. H. Pui, A. Mitha, W. I. Rae, and P. Corr. "Diffusion-weighted magnetic resonance imaging of spinal infection and malignancy". In: *J Neuroimaging* 15.2 (Apr. 2005), pp. 164–170.

[58] A. Y. Oner, T. Tali, F. Celikyay, A. Celik, and P. Le Roux. "Diffusion-weighted imaging of the spine with a non-carr-purcell-meiboom-gill single-shot fast spin-echo sequence: initial experience". In: *AJNR Am J Neuroradiol* 28.3 (Mar. 2007), pp. 575–580.

[59] G. Y. Tang, Z. W. Lv, R. B. Tang, Y. Liu, Y. F. Peng, W. Li, and Y. S. Cheng. "Evaluation of MR spectroscopy and diffusion-weighted MRI in detecting bone marrow changes in postmenopausal women with osteoporosis". In: *Clin Radiol* 65.5 (May 2010), pp. 377–381.

[60] Y. Eguchi, S. Ohtori, M. Yamashita, K. Yamauchi, M. Suzuki, S. Orita, H. Kamoda, G. Arai, T. Ishikawa, M. Miyagi, N. Ochiai, S. Kishida, Y. Masuda, S. Ochi, T. Kikawa, M. Takaso, Y. Aoki, G. Inoue, T. Toyone, and K. Takahashi. "Diffusion magnetic resonance imaging to differentiate degenerative from infectious endplate abnormalities in the lumbar spine". In: *Spine* 36.3 (Feb. 2011), pp. 198–202.

[61] G. Pozzi, C. Garcia Parra, P. Stradiotti, T. V. Tien, A. Luzzati, and A. Zerbi. "Diffusion-weighted MR imaging in differentiation between osteoporotic and neoplastic vertebral fractures". In: *Eur Spine J* 21 Suppl 1 (May 2012), S123–127.

[62] J. Herrmann, N. Krstin, B. P. Schoennagel, M. Sornsakrin, T. Derlin, J. D. Busch, K. U. Petersen, J. Graessner, G. Adam, and C. R. Habermann. "Age-related distribution of vertebral bone-marrow diffusivity". In: *Eur J Radiol* 81.12 (Dec. 2012), pp. 4046–4049.

[63] J. K. Sung, W. H. Jee, J. Y. Jung, M. Choi, S. Y. Lee, Y. H. Kim, K. Y. Ha, and C. K. Park. "Differentiation of acute osteoporotic and malignant compression fractures of the spine: use of additive qualitative and quantitative axial diffusion-weighted MR imaging to conventional MR imaging at 3.0 T". In: *Radiology* 271.2 (May 2014), pp. 488–498.

[64] J. C. Dutoit, M. A. Vanderkerken, J. Anthonissen, F. Dochy, and K. L. Verstraete. "The diagnostic value of SE MRI and DWI of the spine in patients with monoclonal gammopathy of undetermined significance, smouldering myeloma and multiple myeloma". In: *Eur Radiol* 24.11 (Nov. 2014), pp. 2754–2765.

[65] A. Biffar, A. Baur-Melnyk, G. P. Schmidt, M. F. Reiser, and O. Dietrich. "Quantitative analysis of the diffusion-weighted steady-state free precession signal in vertebral bone marrow lesions". In: *Invest Radiol* 46.10 (Oct. 2011), pp. 601–609.

[66] J. Hillengass, B. Stieltjes, T. Bauerle, F. McClanahan, C. Heiss, T. Hielscher, B. Wagner-Gund, V. Habetler, H. Goldschmidt, H. P. Schlemmer, S. Delorme, and C. M. Zechmann. "Dynamic contrast-enhanced magnetic resonance imaging

(DCE-MRI) and diffusion-weighted imaging of bone marrow in healthy individuals". In: *Acta Radiol* 52.3 (Apr. 2011), pp. 324–330.

[67] J. Hansmann, D. Hernando, and S. B. Reeder. "Fat confounds the observed apparent diffusion coefficient in patients with hepatic steatosis". In: *Magn Reson Med* 69.2 (Feb. 2013), pp. 545–552.

[68] D. Hernando, D. C. Karampinos, K. F. King, J. P. Haldar, S. Majumdar, J. G. Georgiadis, and Z. P. Liang. "Removal of olefinic fat chemical shift artifact in diffusion MRI". In: *Magn Reson Med* 65.3 (Mar. 2011), pp. 692–701.

[69] S. E. Williams, A. M. Heemskerk, E. B. Welch, K. Li, B. M. Damon, and J. H. Park. "Quantitative effects of inclusion of fat on muscle diffusion tensor MRI measurements". In: *J Magn Reson Imaging* 38.5 (Nov. 2013), pp. 1292–1297.

[70] M. T. Hooijmans, B. M. Damon, M. Froeling, M. J. Versluis, J. Burakiewicz, J. J. Verschuuren, E. H. Niks, A. G. Webb, and H. E. Kan. "Evaluation of skeletal muscle DTI in patients with duchenne muscular dystrophy". In: *NMR Biomed* 28.11 (Nov. 2015), pp. 1589–1597.

[71] C. A. Corum, A. D. McIntosh, P. J. Bolan, M. Nelson, A. L. Snyder, N. J. Powell, J. Boyum, T. H. Emory, D. Yee, T. M. Tuttle, L. I. Everson, and M. Garwood. "Feasibility of single-voxel MRS measurement of apparent diffusion coefficient of water in breast tumors". In: *Magn Reson Med* 61.5 (May 2009), pp. 1232–1237.

[72] S. Ruschke, A. Pokorney, T. Baum, H. Eggers, J. H. Miller, H. H. Hu, and D. C. Karampinos. "Measurement of vertebral bone marrow proton density fat fraction in children using quantitative water-fat MRI". In: *MAGMA* 30.5 (Oct. 2017), pp. 449–460.